

University of New Hampshire

University of New Hampshire Scholars' Repository

Doctoral Dissertations

Student Scholarship

Winter 1994

Photoacoustic spectroscopy and heavy-atom overtone transitions in the near infrared

Xiaoke Yang

University of New Hampshire, Durham

Follow this and additional works at: <https://scholars.unh.edu/dissertation>

Recommended Citation

Yang, Xiaoke, "Photoacoustic spectroscopy and heavy-atom overtone transitions in the near infrared" (1994). *Doctoral Dissertations*. 1830.

<https://scholars.unh.edu/dissertation/1830>

This Dissertation is brought to you for free and open access by the Student Scholarship at University of New Hampshire Scholars' Repository. It has been accepted for inclusion in Doctoral Dissertations by an authorized administrator of University of New Hampshire Scholars' Repository. For more information, please contact Scholarly.Communication@unh.edu.

INFORMATION TO USERS

This manuscript has been reproduced from the microfilm master. UMI films the text directly from the original or copy submitted. Thus, some thesis and dissertation copies are in typewriter face, while others may be from any type of computer printer.

The quality of this reproduction is dependent upon the quality of the copy submitted. Broken or indistinct print, colored or poor quality illustrations and photographs, print bleedthrough, substandard margins, and improper alignment can adversely affect reproduction.

In the unlikely event that the author did not send UMI a complete manuscript and there are missing pages, these will be noted. Also, if unauthorized copyright material had to be removed, a note will indicate the deletion.

Oversize materials (e.g., maps, drawings, charts) are reproduced by sectioning the original, beginning at the upper left-hand corner and continuing from left to right in equal sections with small overlaps. Each original is also photographed in one exposure and is included in reduced form at the back of the book.

Photographs included in the original manuscript have been reproduced xerographically in this copy. Higher quality 6" x 9" black and white photographic prints are available for any photographs or illustrations appearing in this copy for an additional charge. Contact UMI directly to order.

UMI

A Bell & Howell Information Company
300 North Zeeb Road, Ann Arbor, MI 48106-1346 USA
313/761-4700 800/521-0600

Order Number 9518495

**Photoacoustic spectroscopy and heavy-atom overtone transitions
in the near infrared**

Yang, Xiaoke, Ph.D.

University of New Hampshire, 1994

U·M·I

300 N. Zeeb Rd.
Ann Arbor, MI 48106

PHOTOACOUSTIC SPECTROSCOPY AND HEAVY-ATOM OVERTONE
TRANSITIONS IN THE NEAR INFRARED

by

Xiaoke Yang

B.S. Beijing Normal University, 1982

DISSERTATION

Submitted to the University of New Hampshire
in Partial Fulfillment of
the Requirements for the Degree of

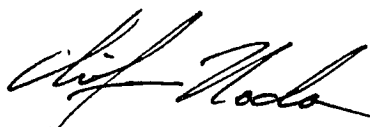
Doctor of Philosophy

in

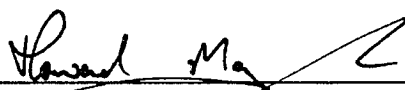
Chemistry

December, 1994

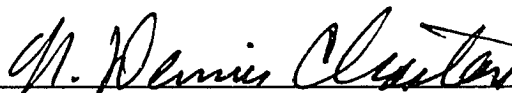
This dissertation has been examined and approved.



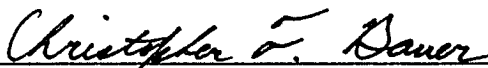
Dissertation Director, Chifuru Noda
Assistant Professor of Chemistry



Howard R. Mayne
Professor of Chemistry



N. Dennis Chasteen
Professor of Chemistry



Christopher F. Bauer
Associate Professor of Chemistry



Robert E. Leuchtner
Assistant Professor of Physics

December 16, 1994

DEDICATION

This work is dedicated to my parents, especially to my mother Peisheng Shi who insisted that I should finish high school during the difficult years in my family.

I would also like to mention my grandmother, Xiurong Gu, who brought me up and educated me in a special way in my childhood when my parents could not take care of me.

ACKNOWLEDGEMENTS

First I would like to express my appreciation to my research advisor, Dr. Chifuru Noda for the opportunity to work on this thesis project which I have enjoyed so much over my graduate years. I have also benefited from his deep understanding of chemistry and physics, as well as his wide knowledge in computer techniques. In addition, his great talents should be admired.

I also wish to thank Dr. Howard Mayne and his group present and past for their help during these past years, especially Dr. Mayne, for his influence on me with his zest for excellence in science and research. Discussions with his group members, such as John Niesse and James Barrett, were very helpful in my understanding of some fundamental questions.

Furthermore, I wish to thank every faculty and staff member in the Chemistry Department for their support and patience with students from foreign countries. Specially, I would like to mention our former Department Chairman, Dr. Frank Pilar whom I first met during his visit in China. I feel much in debt for his recommendation to the graduate committee on my behalf for admission.

Finally, I would like to thank the Town of Durham and her people for providing such a beautiful environment for me to fulfill my graduate education. I appreciate the foliage, the snow and the ocean, for they all add cheer and joy to my life as a graduate student.

TABLE OF CONTENTS

	DEDICATION.....	iii
	ACKNOWLEDGEMENTS.....	iv
	TABLE OF CONTENTS.....	v
	LIST OF TABLES.....	viii
	LIST OF FIGURES.....	x
	ABSTRACT.....	xii
CHAPTER I	INTRODUCTION.....	1
	References.....	8
CHAPTER II	A GENERAL DESCRIPTION OF THE EXPERIMENTAL METHOD.....	10
	II-1. Introduction.....	10
	II-2. Generation of the Photoacoustic Signal.....	11
	II-3. The Near Infrared Laser System.....	12
	II-4. Photoacoustic Sample Cell.....	13
	II-6. Data Acquisition.....	14
	References.....	16
	A Listing of Computer program.....	18
CHAPTER III	EXPERIMENTAL IMPROVEMENT ON PHOTOACOUSTIC SPECTROSCOPY.....	28
	III-1. Introduction.....	28

	III-2. The Promotion of the New Cell Design.....	32
	III-3. Experimental.....	36
	III-4. Results and Discussions.....	39
	III-5. Conclusions.....	45
	Appendix III-A.....	46
	Appendix III-B.....	47
	References.....	49
CHAPTER IV	PHOTOACOUSTIC DETECTION OF N ₂ O AND CO ₂ IN THE NEAR INFRARED.....	58
	IV-1. Introduction.....	58
	IV-2. Experimental.....	59
	IV-3. Results and Discussions.....	61
	IV-4. Conclusions.....	65
	References.....	67
CHAPTER V	OVERTONE TRANSITIONS OF OCS IN THE NEAR INFRARED.....	73
	V-1 Introduction.....	73
	V-2 Experimental.....	74
	V-3. Analysis.....	76
	V-4 Results and Discussions.....	79
	V-5 Conclusions.....	82
	References.....	83
	Listing of Computer Programs.....	85
CHAPTER VI	OVERTONE SPECTROSCOPY OF ¹² CO ₂ AND	

	$^{13}\text{CO}_2$ IN THE NEAR INFRARED.....	103
	VI-1. Introduction.....	103
	VI-2. Experimental.....	106
	VI-3. Results and Discussions.....	109
	VI-4. Conclusions.....	122
	Appendix VI-A.....	124
	References.....	127
	Listing of Computer Programs.....	129
CHAPTER VII	CONCLUSIONS.....	171
	VII-1. On the Experimental Aspects.....	171
	VII-2. On the Heavy-Atom Overtone Studies.....	173
	References.....	175
APPENDIX.....		176
COMPREHENSIVE LIST OF REFERENCES.....		180

LIST OF TABLES

Table		Page
IV-1	Absorption transition intensities of N ₂ O and CO ₂ in the near infrared.....	68
V-1	Molecular parameters for energy calculations and rotational simulations of OCS.....	94
V-2	Assignments and positions of the transitions with polyad quantum number N=22.....	95
V-3	Assignments and positions of the transitions with polyad quantum number N=24.....	96
V-4	Assignments and positions of the transitions with polyad quantum number N=26.....	97
VI-1	Absorption cross sections and relative intensities of the Venus bands for ¹² CO ₂	145
VI-2	Molecular parameters for energy calculations and rotational simulations of ¹² CO ₂	146
VI-3	Coefficients for the rotational simulations of different polyads for ¹² CO ₂	147
VI-4	Rotational constants of ¹² CO ₂ in cm ⁻¹ for some of the highly excited states	148
VI-5	Measured and calculated band origins for the 4v ₂ +5v ₃ triad of ¹² CO ₂	149
VI-6	Spacings and relative intensities for the 5v ₃ +(2v ₁ , v ₁ +2v ₂ , 4v ₂) triad of ¹² CO ₂	150

VI-7	Measured and calculated origins of the $4\nu_1+3\nu_3$ pentad for $^{12}\text{CO}_2$	151
VI-8	Spacings and relative intensities for the $4\nu_1+3\nu_3$ pentad of $^{12}\text{CO}_2$	152
VI-9	The relative intensities and the relative positions to the central component of different triads for $^{12}\text{CO}_2$	153
VI-10	Molecular parameters for energy calculations and rotational simulations of $^{12}\text{CO}_2$	154
VI-11	Band origins and absorption cross sections for the Venus bands of $^{13}\text{CO}_2$	155
VI-12	Absorption cross sections and relative intensities of the Venus bands for both $^{12}\text{CO}_2$ and $^{13}\text{CO}_2$	156
VI-13	Hot band positions associated with the Venus bands for $^{13}\text{CO}_2$	157
VI-14	Measured and calculated band origins for the $4\nu_2+5\nu_3$ triad of $^{13}\text{CO}_2$	158
VI-15	Energy splitting and relative intensity of the $2\nu_1+5\nu_3$ triad for $^{12}\text{CO}_2$ and $^{13}\text{CO}_2$	159
VI-16	Measured and Calculated values of band origins and relative intensities for the $4\nu_1+3\nu_3$ pentad in $^{13}\text{CO}_2$	160
VI-17	Spacing and relative intensities of the $4\nu_1+3\nu_3$ pentad for $^{13}\text{CO}_2$	161

LIST OF FIGURES

Figure		Page
II-1.	A schematic diagram showing the mechanism of the photoacoustic signal generation.....	23
II-2.	Optical layout of the Titanium:Sapphire laser.....	24
II-3.	The single-tubing photoacoustic sample cell.....	25
II-4.	The concentric double-tubing photoacoustic sample cell.....	26
II-5.	A schematic diagram of the photoacoustic spectrometer..	27
III-1.	The acoustic standing wave established in simple pipes...	52
III-2.	The $5\nu_3$ transition of $^{12}\text{CO}_2$ and water overtone bands in the near infrared.....	53
III-3.	The $^{13}\text{CO}_2$ spectrum in the near infrared from 11000-12500 cm^{-1}	54
III-4.	The water free spectrum of $^{13}\text{CO}_2$ in the near infrared.....	55
III-5.	An enlargement of the $4\nu_1+3\nu_3$ pentad of $^{13}\text{CO}_2$	56
III-6.	Water-free spectrum of $^{13}\text{CO}_2$ with dirty cell windows.....	57
IV-1.	N_2O overtone spectrum in the near infrared.....	69
IV-2.	N_2O and water overtone transitions in the near infrared.....	70
IV-3.	CO_2 overtone spectrum in the near infrared.....	71
IV-4.	CO_2 and water overtone transitions in the near infrared...	72
V-1.	OCS spectrum with polyad quantum number $N=22$	98
V-2.	OCS spectrum with polyad quantum number $N=24$	99

V-3.	OCS spectrum with polyad quantum number $N=26$	100
V-4	An enlargement of the $6\nu_3$ band of OCS.....	101
V-5.	Rotational simulation for the $6\nu_3$ band of OCS.....	102
VI-1.	The $5\nu_3$ overtone band of $^{12}\text{CO}_2$	153
VI-2.	The $\nu_1+5\nu_3$ diad of $^{12}\text{CO}_2$	154
VI-3.	The spectrum of the $5\nu_3$ hot band of $^{12}\text{CO}_2$	155
VI-4.	The $5\nu_3$ of $^{12}\text{CO}_2$ and water overtone bands in the near infrared.....	156
VI-5.	The $\nu_1+5\nu_3$ diad of $^{12}\text{CO}_2$ and phenol overtone spectrum.....	157
VI-6.	The $2\nu_1+5\nu_3$ triad of $^{12}\text{CO}_2$	158
VI-7.	The $2\nu_1+5\nu_3$ triad of $^{12}\text{CO}_2$ and water overtone bands.....	159
VI-8.	The $4\nu_1+3\nu_3$ pentad of $^{12}\text{CO}_2$	160
VI-9.	Rotational simulation for the central component of the $2\nu_1+5\nu_3$ triad of $^{12}\text{CO}_2$	161
VI-10.	Rotational simulation for the central component of $4\nu_1+3\nu_3$ pentad of $^{12}\text{CO}_2$	162
VI-11.	Relative intensities of different triads for $^{12}\text{CO}_2$	163
VI-12.	The $5\nu_3$ overtone band of $^{13}\text{CO}_2$	164
VI-13.	The $\nu_1+5\nu_3$ diad of $^{13}\text{CO}_2$	165
VI-14.	Fermi interaction in CO_2	166
VI-15.	The $5\nu_3$ hot band transition of $^{13}\text{CO}_2$	167
VI-16.	The $2\nu_1+5\nu_3$ triad of $^{13}\text{CO}_2$	168
VI-17.	The $2\nu_1+5\nu_3$ triad and the water overtone bands.....	169
VI-18.	The $4\nu_1+3\nu_3$ pentad of $^{13}\text{CO}_2$	170

ABSTRACT

PHOTOACOUSTIC SPECTROSCOPY AND HEAVY-ATOM OVERTONE TRANSITIONS IN THE NEAR INFRARED

by

Xiaoke Yang
University of New Hampshire, December, 1994

This thesis presents vibrational overtone studies on N_2O , $^{12}\text{CO}_2$, OCS , and $^{13}\text{CO}_2$ in the energy range from 10000 cm^{-1} to 14000 cm^{-1} by means of photoacoustic spectroscopy. Many new overtone and combination transitions have been discovered and some of the band intensities have been measured for the carbon dioxide molecule. The observed values of the transition positions and relative intensities are in good agreement with the theoretical calculations that were also performed. In addition, improvements on the experimental apparatus have been made during the investigations on these heavy-atom systems.

The text of this thesis is composed of seven chapters. The first one is an introduction which briefly describes the importance, the challenge of heavy-atom overtone spectroscopy and its relation to other research areas. The second chapter includes the general procedures of the experiments and descriptions of the main components of the apparatus. Chapter III depicts the improvements of the overall performance of the apparatus by introducing a new photoacoustic cell design.

The next three chapters contain the major portion of the thesis. Chapter IV presents the early studies on CO₂ and N₂O in the spectral range from 12500 to 14000 cm⁻¹. One Fermi diad for CO₂ near 12700 cm⁻¹ and three bands for N₂O were observed. The absorption cross sections for these transitions were estimated. Chapter V contains the study of OCS in the spectral range from 10000 to 14000 cm⁻¹. Fourteen overtone transitions have been discovered and assignments have been carried out for this molecule. Chapter VI describes the investigation of ¹²CO₂ and ¹³CO₂ in the same spectral as that for OCS. A total of twenty one overtone and combination transitions have been recorded and sixteen were observed for the first time. Analysis was performed by energy level calculations based on molecular parameters from literature. In addition, transition cross sections for the Venus bands are estimated.

Finally, the last chapter is the conclusion of this thesis. It presents the concluding remarks on what has been learned during the course of this thesis work and possible future research projects.

CHAPTER I

INTRODUCTION

The behavior of highly vibrational excited molecules and their spectroscopic properties have been interesting subjects to chemists, physicists and astrophysics for decades due to their importance in intramolecular dynamics, molecular spectroscopy, and planetary atmospheres. One of the most important experimental information sources regarding the proper understanding and description of highly excited molecular states is absorption spectroscopy of high vibrational overtone transitions [1].

The lofty ideal of reaction dynamics which has been fascinating chemists for years is to take total control of both the reaction rate and selectivity. The first is a function of the energetic threshold of a chemical reaction and the second is a matter of selectively controlling a reaction direction to give a particular product or products. In this point of view, the information on molecules that are far from equilibrium is much more interesting than that at equilibrium, since chemical reaction occurs between molecules that are usually out of equilibrium. To achieve this goal, the behavior of highly excited molecules has to be studied. Clear evidence has shown that obtaining control of reaction selectivity is more difficult than gaining control on reaction rate [2].

The most prominent reason for this difficulty can be properly explained by the phenomenon called intramolecular vibrational-energy redistribution. In the high excitation energy range, a vibrational state is more appropriately described by the local mode model [3,4] and this means that it is

favorable to optically excite a particular bond in a molecule and leave the other bonds undisturbed. However, the vibrational state density is much higher in the high vibrational energy region than that in the low energy region, so that each vibrational state is coupled with many other states. Due to this intramolecular coupling, very fast intramolecular vibrational energy redistribution processes occur, especially for large molecules. Consequently the lifetime of the selectively excited state is too short to allow a particular chemical reaction to occur.

However Heaven never seals off all the exits. It has been demonstrated that reactants in their vibrationally excited states do undergo a much faster reaction than they do in their ground states [5]. Reaction selectivity has been successful with some particular systems [6-10], such as small molecules, or under restricted conditions [11]. The prominent reason is that small molecules have fewer vibrational degrees of freedom or low density of vibrational states so that the lifetime of the selectively excited state is long enough to permit a chemical reaction before intramolecular vibrational relaxation happens.

There are very important projects in this area, both theoretically and experimentally. Much of the area remains to be explored and many questions related to reaction dynamics need to be answered [1]. One such is the question of what is the behavior of a molecule in the excited energy range where the conventional normal mode description starts to fail and, can a reaction spot on a molecule be created by a single photon process? If yes, how long does this spot exist compared to the reaction time? Essentially the elucidation and proper understanding of intramolecular dynamics relies mainly on spectroscopic information of highly excited molecules. A clear description of

highly excited vibrational molecular states cannot be obtained until sufficient spectroscopic data on high overtone vibrations has been accumulated.

Vibrational overtone spectroscopy has also been an important member in the family of molecular spectroscopy. Due to the fact that the overtone transitions are much weaker than those of the fundamental transitions, more sensitive detection methods have to be developed in order to study overtone spectroscopy. Some of the information, such as the absorption cross section, can be obtained only from single photon absorption overtone spectroscopy because it probes directly the process from the ground state to the final states. In the course of studying high vibrational overtones for some model systems, spectroscopic databases, concepts, and theories have been enriched. In addition, by studying very weak overtone transitions, more sensitive spectroscopic techniques have been developed or improved [12-14].

High energy overtone spectroscopy also plays an important role in astrophysics. Experimental information in the laboratory for molecules is useful for identifying new species on other planets [15-17]. Absorption cross sections of certain transitions are required for determining the amount of absorbers on other planets. The bandwidth can be used to determine the conditions such as temperature and pressure, in the atmosphere on other planet.

Vibrational overtone spectroscopy in the near infrared and visible regions has been dominated for a long time by the light-atom stretching-vibrations. The most prominent reasons for this are: First, the fundamental frequency of a light-atom (vibrational motion that involve hydrogen atoms) vibration is much higher than that of a heavy-atom (vibrational motion that does not involve any hydrogen atom) vibration, hence the vibrational quantum number changes for high overtone transitions are smaller than

those of the heavy-atom overtones for the same spectral region.

Consequently, the transition intensity of heavy-atom overtones are much weaker than those of the light-atom overtones. Second, for some heavy-atom systems, such as the molecules studied in this thesis work, the potential wells are much deeper than those of the light-atom systems due to stronger bonds and higher dissociation energies, and this usually leads to less anharmonicity for these heavy-atom systems than the light-atom systems for the same excitation energy. This also leads to weaker intensities for the heavy-atom overtone transitions. Typically, the transition cross sections of heavy-atom overtones are several orders of magnitude smaller than those of the light-atom overtones for a given energy range.

Another challenge for performing heavy-atom overtone spectroscopy comes from the interferences caused by light-atom overtone transitions. Due to the great disparity in absorption cross sections between heavy-atom and light-atom overtone transitions, heavy-atom overtone transitions could be interfered with by light-atom overtone transitions from impurities in the sample. This problem becomes more and more serious as the excitation energy becomes higher and higher. Because of these fundamental difficulties, there have been few studies on heavy-atom overtone spectroscopy in the near infrared. Therefore, the development for heavy-atom overtone spectroscopy in both experimental and theoretical aspects is far behind that of the light-atom overtone spectroscopy. In order to study heavy-atom overtone spectroscopy for high excitation energy levels through a single photon process, extremely sensitive detection methods have to be employed, and interferences from light-atom species, such as water, have to be minimized.

In this thesis work, heavy-atom vibrational overtone transitions in the energy range from 10000 to 14000 cm^{-1} have been studied experimentally by

using the intracavity photoacoustic technique. Molecular systems which have been investigated encompass N_2O , $^{12}\text{CO}_2$, and $^{13}\text{CO}_2$ in the gas phase. Many of the overtone and combination transitions of these species have been observed for the first time during this work. Some of the transition cross sections were estimated by comparing the integrated band intensities to those of the nearby water and phenol overtone bands.

Three of the overtone and combination bands of N_2O in the spectral range of 12500 to 14000 cm^{-1} were investigated in the early study of this thesis work. Although these transitions had been studied by Herzberg and Herzberg by using the long absorbing path apparatus in 1953 [18], they were observed here by using the photoacoustic technique with a much smaller sample size. In addition, the transition cross sections were estimated. Several transitions for N_2O in our spectral range which have not been studied due to the early limitations of our photoacoustic apparatus.

Three groups of overtone and combination bands of OCS in this spectral region were observed for the first time by the same means. The spectra are analyzed by employing the molecular parameters and Hamiltonians from the work of Fayt and co-workers [19]. Those parameters were derived for the energy levels below 5000 cm^{-1} . According to our experimental accuracy, modifications were made on the Hamiltonians during the calculations. It is demonstrated that the molecular parameters of OCS for the low vibrational states can be extended to higher vibrational states. The average deviation is within the experimental accuracy. A total of fourteen transitions were identified, and strong perturbations were observed in the highly excited states for this molecule.

The overtone and combination bands of carbon dioxide in this energy region show well-defined structure, as expected for linear molecules. A total

of seventeen bands were observed for both of the $^{12}\text{CO}_2$ and $^{13}\text{CO}_2$ species not including hot bands. Among those recorded, thirteen were observed for the first time. Associated with the stronger overtone and combination transitions, some of the hot bands were also identified. Transition energies and assignments for the new bands were determined. In addition, transition cross sections for some of these bands were estimated. By examining the experimental conditions and the absorption cross sections, a prediction was made that the overtone and combination transitions of carbon dioxide in the visible region could be observed by means of photoacoustic spectroscopy.

Along with the experimental measurements performed on the $^{12}\text{CO}_2$ and $^{13}\text{CO}_2$ species, theoretical calculations on the eigenvalues of those highly excited states were also carried out. These calculations are based on the molecular parameters from the work of Courtoy [20] and Chedin [21]. From the results of the calculations, relative intensities within a Fermi polyad and rotation constants for those highly excited states were determined. Corresponding values from the measurements and calculations have been compared.

During the course of the heavy-atom overtone studies, the search for a better photoacoustic cell design has never ceased. In order to improve the overall performance of the photoacoustic apparatus, a dozen different cells have been designed, constructed and tested. Most recently, a concentric double-tubing cell design [22] was used for the heavy-atom overtone studies. It has been demonstrated that these cells have sensitivities on the order of 10^{-10} cm^{-1} , and they offer many advantages for heavy-atom overtone studies. A more detailed discussion of the improvements on the apparatus will be presented in the experimental chapters.

In order to give the viewer a clearer picture of this thesis work, some of the general information (notation and selection rules) about the carbon dioxide molecule is given in the Appendix at the end of this thesis. The study of this molecule constitutes a major portion of this thesis.

REFERENCES

- [1]. M. L. Sage, Bond Modes, in *Photoselective Chemistry, Adv. Chem. phys.*, **46** John Wiley and Sons: New York, 1981 p293
- [2]. T. A. Holme and J. S. Hutchinson, *J. Chem. Phys.*, **84** (1986) 5455
- [3]. J. M. Hollas, *Modern Spectroscopy*, John Wiley and Sons, New York, (1990)
- [4]. B. Henry, *Vibrational Spectra and Structure*, J. R. Durig, Ed., Vol. 10, Elsevier, New York, (1981)
- [5]. R. Schinke, V. Engel, P. Andresen, G. G. Balint-Kurti and D. Hauster, *Phys. Rev. Lett.*, **55** (1977) 111
- [6]. R. V. Ambartzumian and V. S. Letokhov, *Multiple Photon Infrared Laser Photochemistry*, in *Chemical and Biochemical Applications of Lasers*, Vol. 3, C. B. Moore, Ed., Academic Press: New York, 1977
- [7]. P. F. Zittel and D. E. Masturzo, *J. Chem. Phys.*, **85** (1986) 4362
- [8]. D. J. Baniford, S. V. Filseth, M. F. Foltz, J. W. Hepburn, and C. B. Moore, *J. Chem. Phys.*, **82** (1985) 3032
- [9]. H. L. Dai, R. W. Field, and J. L. Kinsey, *J. Chem. Phys.*, **82** (1985) 1606
- [10]. K. V. Reddy and M. J. Berry, *Chem. Phys. Lett.*, **66** (1979) 223
- [11]. T. A. Holme, and J. S. Hutchinson, *Chem. Phys. Lett.*, **124** (1986) 181
- [12]. B. R. Henry and M. G. Sowa, *Prog. Analyt. Spectrosc.*, **12** (1989) 349
- [13]. J. Davidsson, J. H. Gutow, and R. N. Zare, *J. Phys. Chem.*, **94** (1990) 4069
- [14]. J. H. Gutow, J. Davidsson, and R. N. Zare, *Chem. Phys. Lett.*, **185** (1991) 120
- [15]. T. Dunham, in *The Atmospheres of the Earth and Planets*, G. P. Kuiper, Ed., University of Chicago Press, 2nd ed., (1952) Chap. XI

- [16]. L. D. Gray, R. A. Schorn, and E. Barker, *Appl. Opt.*, **8** (1969) 2087
- [17]. L. D. G. Young, *ICARUS*, **17** (1972) 632
- [18]. G. Herzberg and L. Herzberg, *J. Chem. Phys.*, **18** (1950) 1551
- [19]. A. Fayt, R. Vandenhoute, and J. G. Lahaye, *J. Mol. Spectrosc.* **119** (1986) 233
- [20]. C. P. Courtoy, *Can. J. Phys.*, **35** (1957) 608
- [21]. A. Chedin, *J. Mol. Spectrosc.*, **76** (1979) 430
- [22]. X. Yang and C. Noda, *J. Phys. Chem.*, Submitted for publication

CHAPTER II

GENERAL DESCRIPTION OF THE EXPERIMENTAL METHOD

II-1 Introduction

Heavy-atom overtone transitions in the near infrared are extremely weak. A typical integrated band absorption cross section is on the order of 10^{-26} cm² per molecule. The absorptivity may be as small as 10^{-9} cm⁻¹ to 10^{-10} cm⁻¹. In order to detect such small signals, extremely sensitive methods have to be employed. Together with other sensitive detection methods, the photoacoustic technique has been widely used for high energy overtone spectroscopy.

Photoacoustic spectroscopy is inherently more sensitive than the conventional absorption spectroscopy because it is background free. Instead of measuring the ratio of the transmitted to the incident light intensities, photoacoustic detection measures the net absorbed radiation energy. From this point of view it even has an additional advantage for high energy overtone spectroscopy over the conventional technique, due to the fact that the higher the energy the photon has, the stronger the signal becomes. Besides, the photoacoustic method does not require large sample sizes and this will be very important for studying isotopic species. Along with the development of laser techniques, the sensitivity of photoacoustic spectroscopy has been increased by several orders of magnitude. It has been demonstrated that the sensitivity of this technique can be on the order of 10^{-10} cm⁻¹ [1-4].

II-2. Generation of the Photoacoustic Signal

Photoacoustic spectroscopy utilizes the photoacoustic effect. A simple description of the effect is that when a gas absorbs a modulated electromagnetic radiation, the energy absorbed will create a pressure fluctuation when the sample is confined in a constant volume. This pressure fluctuation is a sound wave and can be detected by a microphone. A schematic diagram that depicts the mechanism of the photoacoustic detection is given in Figure II-1. There is an extensive literature on the studies of gas phase energy relaxation and photoacoustic signal generation for different spectrophones and operation modes [5-14]. Basically, the photoacoustic signal is proportional to the pressure fluctuation caused by the excitation and deexcitation of the absorber under modulated radiation. In addition, the amplitude of the ultimate signal is also affected by the geometry of the photoacoustic sample cell and the operation mode. Theoretical and experimental studies and reviews on the photoacoustic cell design and operation conditions can be found in a variety of references [15-23].

Typically, the operation of cw photoacoustic spectrometer falls into two categories: resonant and non-resonant modes. If the excitation radiation is modulated at a frequency away from any inherent resonant frequencies of the cell, it is called the non-resonant mode. When the radiation source is modulated at an inherent resonant frequency of the cell, it is called the resonant mode. The resonant mode offers certain advantages [24], such as high sensitivity and immunity to ambient noises. This is the mode used in this thesis study. The final version of the spectrometer (see next chapter) under this operation mode has a sensitivity on the order of 10^{-10} cm⁻¹.

II-3. The Near Infrared Laser System

The near infrared excitation source is a broad band cw titanium:sapphire ring laser (Coherent 899-01) which is pumped by a multiline Ar⁺ laser (Coherent Innova 70-5) with a pumping power of 5-7 W. A schematic diagram of the laser system is shown in Figure II-3. The original optics of the titanium:sapphire laser provides a spectral range of 12500-14300 cm⁻¹. With two additional sets of optics, the spectral range is extended to 10000-14300 cm⁻¹.

High radiation power is favorable for high energy overtone transitions because the transition cross section is so small. In order to increase the laser power inside the ring cavity for intracavity detections, the stock output coupler M4 (95% reflectivity) is replaced with a high reflector (CVI, 99% reflectivity) for the short wavelength optics. For the middle and long wavelength optics, the output coupler M4 is replaced by a high reflector (Coherent, the same mirror as M2 is used). With these high reflectors installed, peak power of 30 mW, 20 mW, and 15 mW could be reached with 5 W pumping power for the short, middle and long wavelength optics, respectively, before the sample cell is placed in the cavity. The bandwidth of the laser is of the order 0.2 cm⁻¹ with the standard output coupler for the short wavelength optics and it is expected to be broader when the high reflector is used.

The tuning of the laser is carried out by tilting an intracavity birefringent filter with a stepper motor (Oriel, model 18510). The stepper motor is controlled by a computer (Apple IIe) drive system. In the early study of this work the calibration of the laser wavelength against the step number

was performed by using a spectrophotometer (Beckman, model DB-GT) with an uncertainty of one nm. Water overtone lines served as wavelength standard for the study of $^{12}\text{CO}_2$ and $^{13}\text{CO}_2$ with an uncertainty of one cm^{-1} . A three degree polynomial least-squares fitting program is used to convert step number to wavelength or wavenumber. Unfortunately, the scanning of the laser wavelength is not perfectly continuous due to the inherent design of the birefringent filter [25]. This results in significant jitter in the center frequency of the laser during the scan. Furthermore, the laser bandwidth does not stay constant as the laser is scanned. Consequently, irregularity has been observed in the rotational structure of the spectra. If the linewidths of the transitions are narrower than the laser linewidth, the varying laser linewidth will affect the integration and introduces a rather large uncertainty in the intensity calibration.

II-4. Photoacoustic Sample Cell

The photoacoustic cells used for the early studies in this thesis work are shown in Figure II-4. Typically the cell is composed of several pieces of glass pipe with a inner diameter about 4 mm and jointed by compression connectors. The central piece of the pipe is a T-shaped glass joiner and the microphone (Knowles, EK-3024) is mounted in one of the arms. All the other appendages, such as glass valve and drying agent finger are attached to the end of the pipe. Optical windows are epoxyed to the main portion of the cell at the Brewster angle. Due to the window absorption and low quality of the acoustic resonance, the sensitivities of those cells are on the order of 10^{-8} cm^{-1} .

In order to improve the sensitivity and overall performance of the photoacoustic sample cell, a new cell design has been introduced. The improvement focuses on two purposes: one is to reduce the background signal caused by window absorption and the other is to eliminate the interfering signals created by impurities in the sample. The new photoacoustic cell is shown in Figure II-5. A detailed description of the improvement is given in the next chapter. The ultimate sensitivity of the new cell is on the order of 10^{-10} cm⁻¹ with our experimental conditions.

The microphone is powered by a 9V DC battery and its signal is fed to a lock-in amplifier (Stanford Research). A stereo phone jack is used to connect the microphone and the power box. All the lines between them are shielded with aluminum foil.

II-5. Data Acquisition

The experimental set-up of the photoacoustic spectrometer is depicted schematically in Figure II-6. The data collection process is controlled by a micro-computer system (Apple II and Macintosh plus). The photoacoustic spectrum is taken as the signal from the microphone vs. the step number of the stepper motor which drives the birefringent filter.

Typically there are three signals to collect for a photoacoustic spectrum: the signal from the microphone; the signal from the photodiode which monitors the laser power; and the step motor position which defines the laser wavelength. The photodiode signal is sometimes replaced by another photoacoustic signal which serves as a wavelength calibration standard, such as water overtone transitions. The photoacoustic signal and the photodiode

signal are fed to the lock-in amplifiers (Stanford Research System, SR510 and Princeton Applied Research, Model 5101) without any pre-amplification. Then signals from the lock-in are digitalized at the primary computer (Apple II). The position of the birefringent filter is created in the primary computer by carrying out a controlling program which drives the step motor, and then all these signals are sent to the secondary computer (Macintosh Plus) where they are stored. The system can handle five signals independently at the same time. A listing of the data collection and controlling program written in BASIC is given at the end of this chapter.

REFERENCES

- [1]. T. F. Deaton, D. A. Depatie, and T. W. Walker *Appl. Phys. Lett.* , **26** (1975) 300
- [2]. J. Davidsson, J. H. Gutow and R. N. Zare, *J. Phys. Chem.* , **94** (1990) 4069
- [3]. X. Yang and C. Noda, *J. Phys. Chem.*, submitted for publication
- [4]. C. K. N. Patel and R. J. Kerl, *Appl. Phys. Lett.*, **30** (1977) 578
- [5]. T. L. Cottrell, J. C. McCoubrey, *Molecular Energy Transfer in Gases*, Butterworths, London, 1961
- [6]. L. B. Kreuzer, *J. Appl. Phys.*, **42** (1971) 2934
- [7]. R. Tripodi and W. G. Vicenti, *J. Chem. Phys.*, **55** (1971) 2207
- [8]. M. Huetz-Aubert and R. Tripodi, *J. Chem. Phys.*, **55** (1971) 5724
- [9]. M. R. Da Silva, *Can. J. Phys.*, **64** (1986) 1098
- [10]. L. B. Kreuzer, in *Optoacoustic Spectroscopy and Detection*, Yoh-Han Pao, Academic, New York, 1977
- [11]. P. Hess, *Topics in Curr. Chem.*, **111** (1983) 1
- [12]. A. C. Tam, in *Ultrasensitive Laser Spectroscopy*, D. S. Kliger, Academic, New York, 1983
- [13]. T. F. Hunter and P. C. Turtle, in *Advances in Infrared and Raman Spectroscopy*, R. J. H. Clark, Vol. 7, Heyden, London, 1980
- [14]. A. Rosencwaig, *Photoacoustics and Photoacoustic Spectroscopy*, in *Chemical Analysis*, P. J. Elcing, and J. D. Winefordner, Eds., John Wiley and Sons: New York Vol. 57 (1980)
- [15]. P. L. Meyer and M. W. Sigrist, *Rev. Sci. Instrum.*, **61** (1990) 1779
- [16]. A. Miklos and A. Lorincz, *Appl. Phys.*, B **48** (1989) 213
- [17]. M. W. Sigrist, *J. Appl. Phys.*, **60** 7 (1986) R83

- [18]. K. Veeken, N. Dam and J Reuss, *Infrared Phys.*, **25**, (1985) 683
- [19]. G. A West, J. J. Barrett, D. R. Siebert and K. V. Reddy, *Rev. Sci. Instrum.*, **54** (1983) 797
- [20]. E. Kritchman, S. Shtrikman and M. Slatkine, *J. Opt. Soc. Am.*, **68** (1978) 1257
- [21]. R. D. Kamm, *J. Appl. Phys.*, **47** (1976) 3550
- [22]. E. Max and L. G Rosengren, *Opt. Commun.*, **11**, (1974) 422
- [23]. L. G. Rosengren, *Infrared Phys.*, **13** (1973) 109
- [24]. M. W. Sigrist, Environmental and Chemical Trace Gas Analysis by Photoacoustic Methods, in Principles and Perspectives of Photothermal and Photoacoustic Phenomena, A. Mandelis, Elsevier: New York (1992)
- [25]. D. R. Preuss and J. L. Gole, *Appl. Opt.*, **19** (1980) 702

LIST OF COMPUTER PROGRAM FOR CONTROL OF THE SPECTROMETER

```

100 REM STEPPER MOTOR DRIVER
110 REM 01/06/91 CN
112 REM 07/01/91 XY - MODIFIED
120 HOME
130 GOSUB 1000: REM INITIALIZATION
202 HOME : PRINT "CURRENT POSIT ION= "; - PS" ";PM
220 PRINT "<, > :: CONTINUOUS ( SLOW)"
230 PRINT "[I :: CHECK CONNEC TION"
240 PRINT "G :: GO TO A WANT ED POSITION"
242 PRINT "C :: CHANGE PARAM ETERS"
243 PRINT "M :: CHANGE GAINS "
244 PRINT "Z :: ZERO BF FILT ER"
258 PRINT "Q :: QUIT": PRINT
260 PRINT "> ";
262 X = PEEK (KB); IF X < 128 THEN GOTO 262
264 A$ = CHR$ (X - 128); POKE K C,0; PRINT A$
290 IF A$ = "," THEN GOSUB 514 2: GOSUB 3500: GOTO 200
300 IF A$ = "." THEN GOSUB 514 2: GOSUB 3700: GOTO 200
310 IF A$ = "G" THEN GOSUB 800 0: GOTO 200
320 IF A$ = "I" THEN GOSUB 521 2: GOTO 200
322 IF A$ = "Q" THEN GOSUB 430 0
324 IF A$ = "C" THEN GOSUB 550 0: GOTO 200
325 IF A$ = "M" THEN GOSUB 554 3: GOTO 200
326 IF A$ = "Z" THEN GOSUB 560 0: GOTO 200
338 PRINT B$;"TRY AGAIN"
340 GOTO 200
999 END
1000 REM INITIALIZATION ROUTINE
1005 W1 = 0:W3 = 1:W5 = 2:W7 = 3
1007 W2 = 4:W4 = 1:W6 = 1:W8 = 6
1010 PS = - 1
1020 PM = 1
1030 DS = 25
1040 DF = 0
1050 A0 = 49240
1060 B0 = A0 + 4
1070 C0 = A0 + 6
1080 D0 = A0 + 2
1090 A1 = A0 + 1:B1 = B0 + 1:C1 = C0 + 1:D1 = D0 + 1
1100 REM
1110 B$ = CHR$ (7):D$ = CHR$ ( 4)
1120 PF = - 16287
1130 PR = - 16286
1140 KB = - 16384:KC = - 16368
1150 GOSUB 1500
1199 RETURN
1500 REM ALL CLEAR
1510 POKE A0,0: POKE B0,0: POKE C0,0: POKE D0,0: RETURN
1600 REM DELAY FOR ONE STEP

```

```

1610 FOR I = 1 TO 10:X = SIN ( 1.0): NEXT
1620 RETURN
2000 REM COUNT UP (CONTINUOUS)
2012 POKE C0,0: RETURN
2023 POKE D1,0: RETURN
2034 POKE A0,0: RETURN
2045 POKE B1,0: RETURN
2056 POKE D0,0: RETURN
2067 POKE C1,0: RETURN
2078 POKE B0,0: RETURN
2081 POKE A1,0: RETURN
2100 REM COUNT DOWN (CONTINUOUS)
2118 POKE A0,0: RETURN
2121 POKE C1,0: RETURN
2132 POKE D0,0: RETURN
2143 POKE A1,0: RETURN
2154 POKE B0,0: RETURN
2165 POKE D1,0: RETURN
2176 POKE C0,0: RETURN
2187 POKE B1,0: RETURN
3500 REM
3510 PS = PS - 1
3520 PM = PM - 1: IF PM = 0 THEN PM = 8
3530 IF PM = 1 THEN GOSUB 2121 : GOTO 3599
3535 IF PM = 2 THEN GOSUB 2132 : GOTO 3599
3540 IF PM = 3 THEN GOSUB 2143 : GOTO 3599
3545 IF PM = 4 THEN GOSUB 2154 : GOTO 3599
3550 IF PM = 5 THEN GOSUB 2
3555 IF PM = 6 THEN GOSUB 2176 : GOTO 3599
3560 IF PM = 7 THEN GOSUB 2187 : GOTO 3599
3565 IF PM = 8 THEN GOSUB 2118
3599 REM
3600 IF PEEK (KB) = 160 THEN GOSUB 1500: POKE KC,0: RETURN
3602 IF PEEK (KB) > 127 THEN POKE KC,0
3605 IF PEEK (PR) > 127 THEN GOSUB 1500: GOSUB 5100: RETURN
3610 FOR I = 1 TO DS:X = SIN ( 1.0): NEXT
3615 GOSUB 5300
3620 GOTO 3510
3700 REM
3710 PS = PS + 1
3720 PM = PM + 1: IF PM = 9 THEN PM = 1
3730 IF PM = 1 THEN GOSUB 2012 : GOTO 3799
3735 IF PM = 2 THEN GOSUB 2023 : GOTO 3799
3740 IF PM = 3 THEN GOSUB 2034 : GOTO 3799
3745 IF PM = 4 THEN GOSUB 2045 : GOTO 3799
3750 IF PM = 5 THEN GOSUB 2056 : GOTO 3799
3755 IF PM = 6 THEN GOSUB 2067 : GOTO 3799
3760 IF PM = 7 THEN GOSUB 2078 : GOTO 3799
3765 IF PM = 8 THEN GOSUB 2081 : GOTO 3799
3799 REM
3800 IF PEEK (KB) = 160 THEN GOSUB 1500: POKE KC,0: RETURN
3802 IF PEEK (KB) > 127 THEN POKE KC,0
3806 IF PEEK (PF) > 127 THEN GOSUB 1500: GOSUB 5000: RETURN
3810 FOR I = 1 TO DS:X = SIN ( 1.): NEXT

```

```

3815 GOSUB 5300
3820 GOTO 3710
4300 REM "END" COMMAND
4310 END
5000 REM PB0 ERROR
5010 PRINT B$;B$;B$
5020 PRINT "FORWARD LIMIT REACH ED"
5030 PRINT CHR$ (4);"IN#0"
5035 RETURN
5040 RETURN
5100 REM PB2 ERROR
5110 PRINT B$;B$;B$
5120 PRINT "REVERSE LIMIT REACH ED"
5130 INPUT "HIT RETURN TO CONTI NUE";Z$
5140 RETURN
5142 REM MESSAGE
5144 PRINT "HIT SPACE BAR TO ST OP"
5145 INPUT "FILE NAME: ";FL$
5146 PRINT CHR$ (4);"PR#2": PRINT CHR$ (4);"IN#2"
5148 PRINT "<"
5150 PRINT FL$
5152 PRINT W2
5154 PRINT W4
5156 PRINT W6
5158 PRINT W8
5160 PRINT DS
5162 FOR I = 6 TO 32
5164 PRINT "0"
5166 NEXT
5200 REM MESSAGE
5205 HOME
5211 RETURN
5212 REM
5214 PRINT CHR$ (4);"PR#2"
5216 PRINT CHR$ (4);"IN#2"
5218 PRINT "#"
5220 INPUT A$
5222 G$ = CHR$ (7)
5224 IF A$ = "!" THEN PRINT G$,G$,G$
5226 PRINT CHR$ (4);"PR#0": PRINT CHR$ (4);"IN#0"
5228 RETURN
5300 REM PRINT CURRENT POSITIO N
5310 VTAB 12
5318 GOSUB 6000
5320 RETURN
5500 HOME
5510 PRINT "DELAY (SLOW) = ";DS
5520 INPUT "NEW VALUE ";DS
5541 RETURN
5543 HOME
5544 GOSUB 9000
5545 PRINT "GAIN FOR CH0= ";W2
5546 INPUT "NEW GAIN FOR CH0 "; W2: IF W2 > 7 THEN PRINT "T RY AGAIN! ": GOTO
5546

```

```

5547 PRINT "GAIN FOR CH1=" ;W4
5548 INPUT "NEW GAIN FOR CH1 "; W4: IF W4 > 7 THEN PRINT "T RY AGAIN! ": GOTO
5548
5549 PRINT "GAIN FOR CH2=" ;W6
5550 INPUT "NEW GAIN FOR CH2 "; W6: IF W6 > 7 THEN PRINT "T RY AGAIN! ": GOTO
5550
5551 PRINT "GAIN FOR CH3=" ;W8
5552 INPUT "NEW GAIN FOR CH3 "; W8: IF W8 > 7 THEN PRINT "T RY AGAIN! ": GOTO
5552
5599 RETURN
5600 REM "Z"
5610 HOME : GOSUB 1500
5620 PRINT "MOVE BF FILTER BEYO ND FORWARD LIMIT"
5630 PRINT "WHEN READY, HIT RET URN"
5640 PRINT "TO CANCEL THIS, HIT ANY KEY AND RETURN"
5650 PRINT
5660 INPUT A$: IF LEN (A$) > 0 THEN RETURN
5670 REM
5680 PS = 1
5690 IF PS = 1 THEN GOSUB 2012
5692 IF PS = 2 THEN GOSUB 2023
5694 IF PS = 3 THEN GOSUB 2034
5696 IF PS = 4 THEN GOSUB 2045
5698 IF PS = 5 THEN GOSUB 2056
5700 IF PS = 6 THEN GOSUB 2067
5702 IF PS = 7 THEN GOSUB 2078
5704 IF PS = 8 THEN GOSUB 2081
5706 IF PEEK (PF) < 128 THEN P M = PS:PS = 0: GOSUB 1500: RETURN
5710 PS = PS - 1: IF PS < 1 THEN PS = 8
5720 GOTO 5690
6000 REM
6010 WA = W1 + 16 * W2:WB = W3 + 16 * W4:WC = W5 + 16 * W6:WD= W7 + 16 * W8
6015 AI13 = - 16256 + 5 * 16
6020 POKE AI13,WA: POKE AI13,WA : POKE AI13,WA: POKE AI13,WA
6022 X = SIN (1.0)
6025 RA = PEEK (AI13 + 1) * 256+ PEEK (AI13)
6035 POKE AI13,WB: POKE AI13,WB : POKE AI13,WB: POKE AI13,WB
6037 X = SIN (1.0)
6040 RB = PEEK (AI13 + 1) * 256+ PEEK (AI13)
6044 POKE AI13,WC: POKE AI13,WC : POKE AI13,WC: POKE AI13,WC
6045 X = SIN (1.0)
6046 RC = PEEK (AI13 + 1) * 256+ PEEK (AI13)
6050 POKE AI13,WD: POKE AI13,WD : POKE AI13,WD: POKE AI13,WD
6051 X = SIN (1.0)
6052 RD = PEEK (AI13 + 1) * 256+ PEEK (AI13)
6054 PRINT - PS;" ";RA;" ";RB; " ";RC;" ";RD
6056 IF PEEK (KB) = 160 THEN GOSUB 6500
6060 RETURN
6500 REM
6505 PRINT 0;" "; - 1;" ";0;" ";0;" ";0
6510 PRINT D$;"PR#0"
6512 PRINT D$;"IN#0"
6515 RETURN
8000 REM FIND STEP POSITION

```

```

8002 PRINT "CURRENT POSITION= " ; - PS
8005 INPUT "NEW POSITION FOR ST EPPER TO GO TO=" ;NP
8007 NP = - NP
8010 IF PS = NP THEN RETURN
8015 IF PS > NP THEN GOTO 8500
8020 IF PS < NP THEN GOTO 8600
8500 PS = PS - 1
8505 PM = PM - 1: IF PM = 0 THEN PM = 8
8510 IF PM = 1 THEN GOSUB 2121 : GOTO 8550
8515 IF PM = 2 THEN GOSUB 2132 : GOTO 8550
8520 IF PM = 3 THEN GOSUB 2143 : GOTO 8550
8525 IF PM = 4 THEN GOSUB 2154 : GOTO 8550
8530 IF PM = 5 THEN GOSUB 2165 : GOTO 8550
8535 IF PM = 6 THEN GOSUB 2176 : GOTO 8550
8540 IF PM = 7 THEN GOSUB 2187 : GOTO 8550
8545 IF PM = 8 THEN GOSUB 2118 : GOTO 8550
8547 IF PEEK (KB) = 160 THEN GOSUB 1500: POKE KC,0: RETURN
8549 IF PEEK (KB) > 127 THEN POKE KC,0
8550 IF PEEK (KB) = 160 THEN GOSUB 1500: POKE KC,0: RETURN
8552 IF PEEK (KB) > 127 THEN POKE KC,0
8554 IF PS = NP THEN GOSUB 150 0: RETURN
8559 GOTO 8500
8600 PS = PS + 1
8605 PM = PM + 1: IF PM = 9 THEN PM = 1
8610 IF PM = 1 THEN GOSUB 2012 : GOTO 8660
8615 IF PM = 2 THEN GOSUB 2023 : GOTO 8660
8620 IF PM = 3 THEN GOSUB 2034 : GOTO 8660
8625 IF PM = 4 THEN GOSUB 2045 : GOTO 8660
8630 IF PM = 5 THEN GOSUB 2056 : GOTO 8660
8635 IF PM = 6 THEN GOSUB 2067 : GOTO 8660
8640 IF PM = 7 THEN GOSUB 2078 : GOTO 8660
8645 IF PM = 8 THEN GOSUB 2081 : GOTO 8660
8660 IF PEEK (KB) = 160 THEN GOSUB 1500: POKE KC,0: RETURN
8665 IF PEEK (KB) > 127 THEN POKE KC,0
8667 IF PS = NP THEN GOSUB 150 0: RETURN
8670 GOTO 8600
9000 PRINT "MANUAL LIST FOR GAIN CHANGE"
9010 PRINT "GAIN#   VOLTAGE RANGE"
9020 PRINT " 0       0 TO 10V"
9030 PRINT " 1       0 TO 2V"
9040 PRINT " 2       0 TO 1V"
9050 PRINT " 3       0 TO 0.2V"
9060 PRINT " 4      -10 TO +10V"
9070 PRINT " 5      -2 TO +2V"
9080 PRINT " 6      -1 TO +1V"
9090 PRINT " 7     -0.2 TO +.2V"
9100 PRINT
9110 RETURN

```

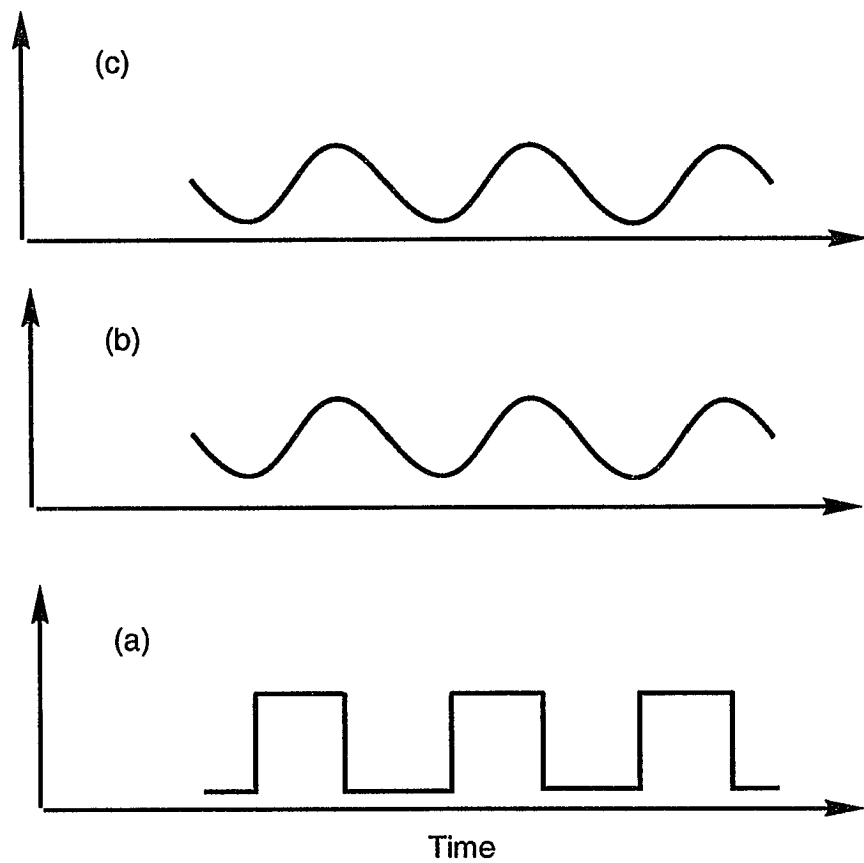



Figure II-1. A schematic diagram showing the mechanism of the photoacoustic signal generation. (a) The modulated laser intensity; (b) The temperature fluctuation; (c) The pressure fluctuation

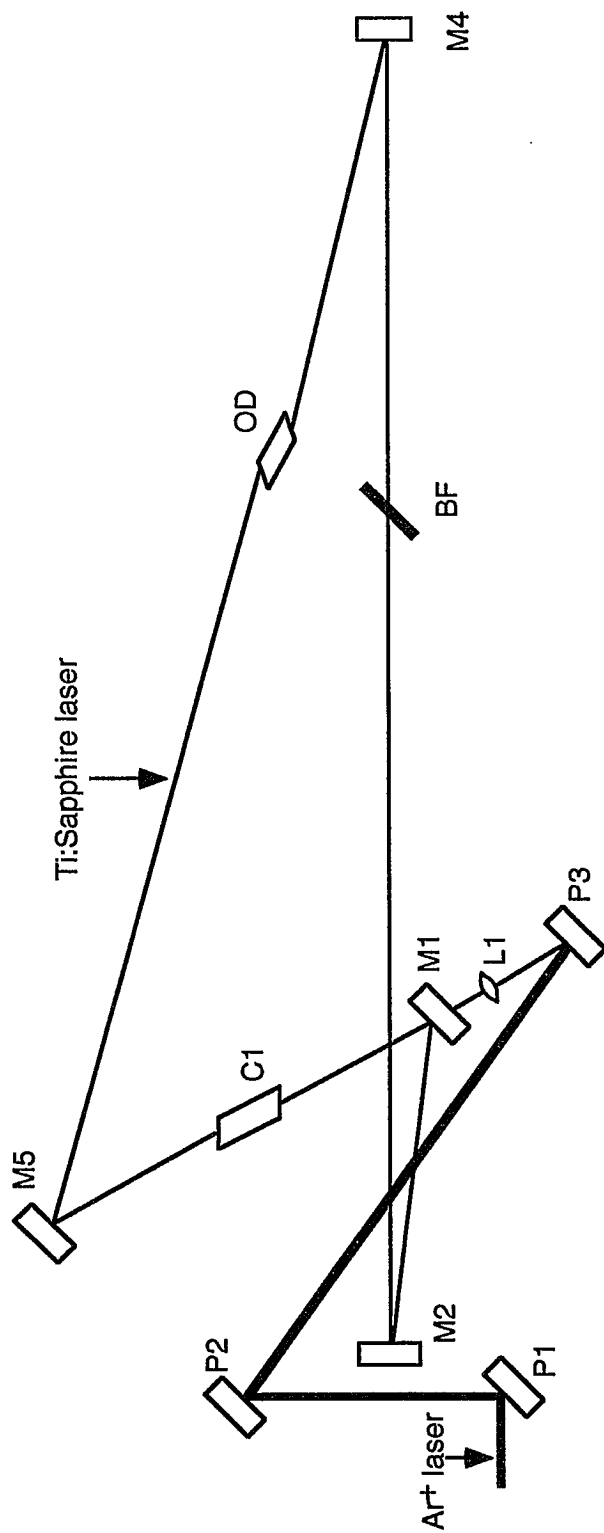


Figure II-3. Optical layout of a Titanium:Sapphire laser (Coherent 899-01). P1 and P2 are the periscope optics; P3 is the pump mirror; M1 and M2 are the folding mirrors; M4 is the output coupler; M5 is the upper folding mirror; L1 is the focusing lens; BF is the birefringent filter; OD is the optical diode

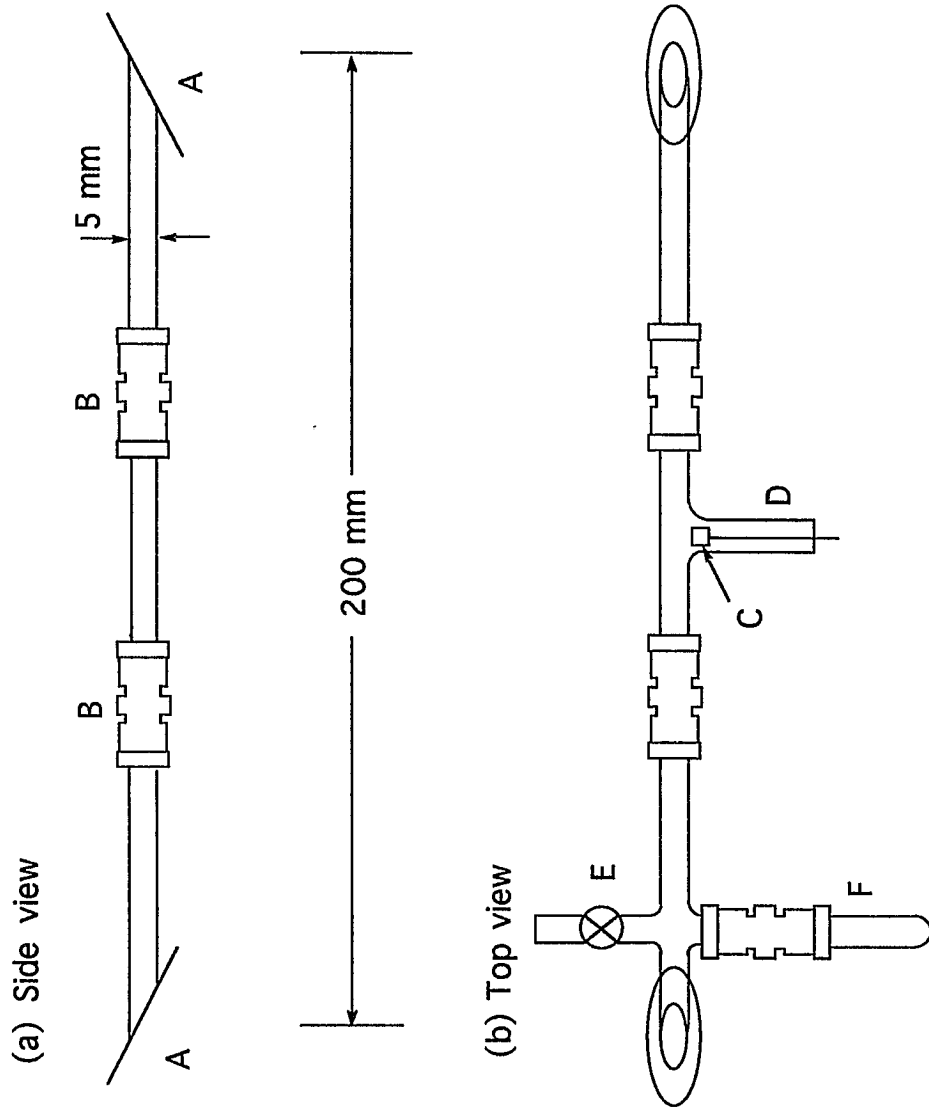


Figure II-4. The single-tubing photoacoustic cell used for our earlier studies on heavy-atom systems. (a) Side view: A. Optical windows; B. Fitting connectors (1/4 in.). (b) Top view: C. Microphphone; D. Signal outlet; E. Gas valve; F. Drying agent finger.

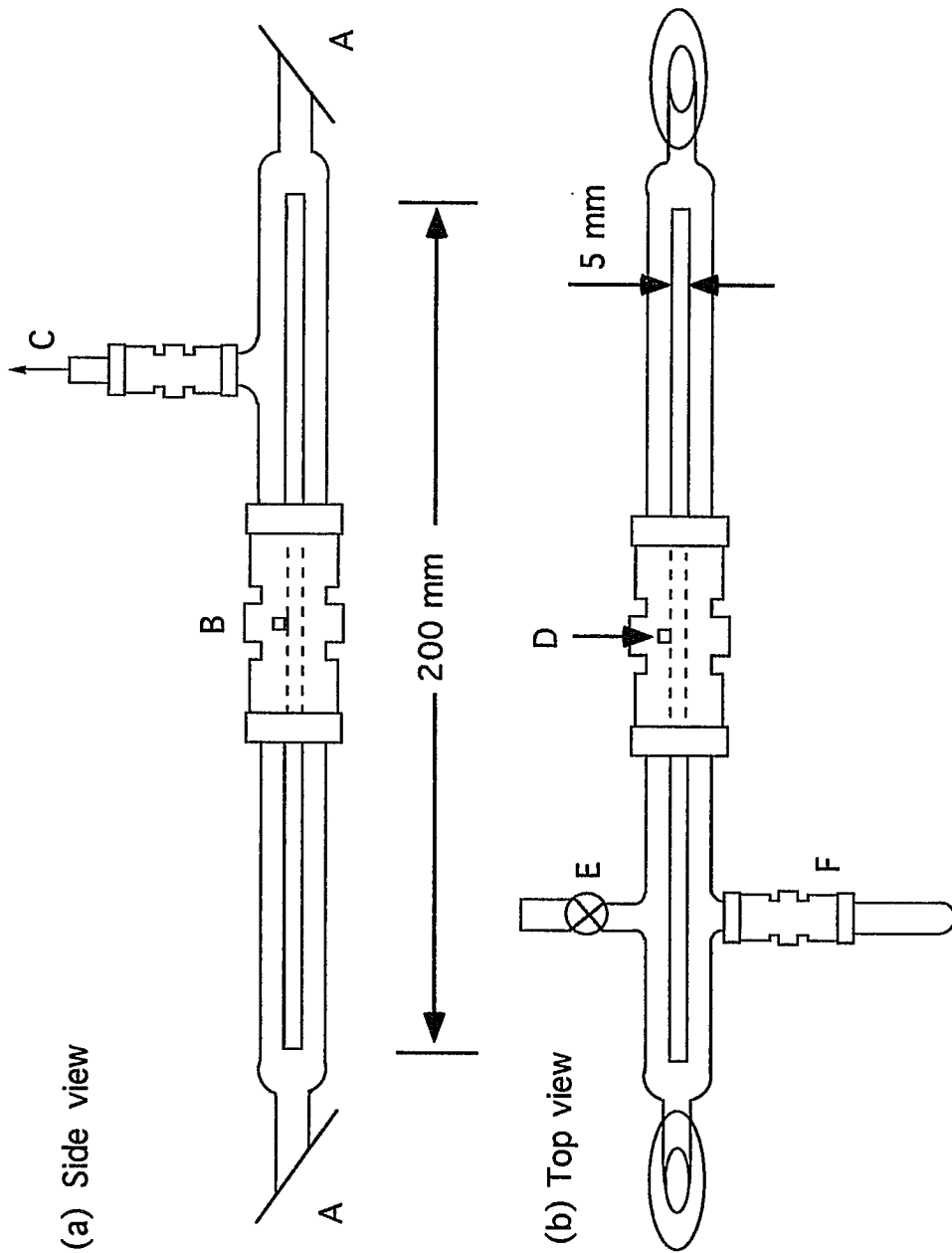


Figure II-5. The concentric double-tubing photoacoustic cell. (a) Side view: A. Optical windows; B. Fitting connector (3/4 in.); C. Fitting connector (1/4 in.); (b) Top view: D. Microphone; E. Gas valve; F. Drying agent finger with 3/8 in fitting connector.

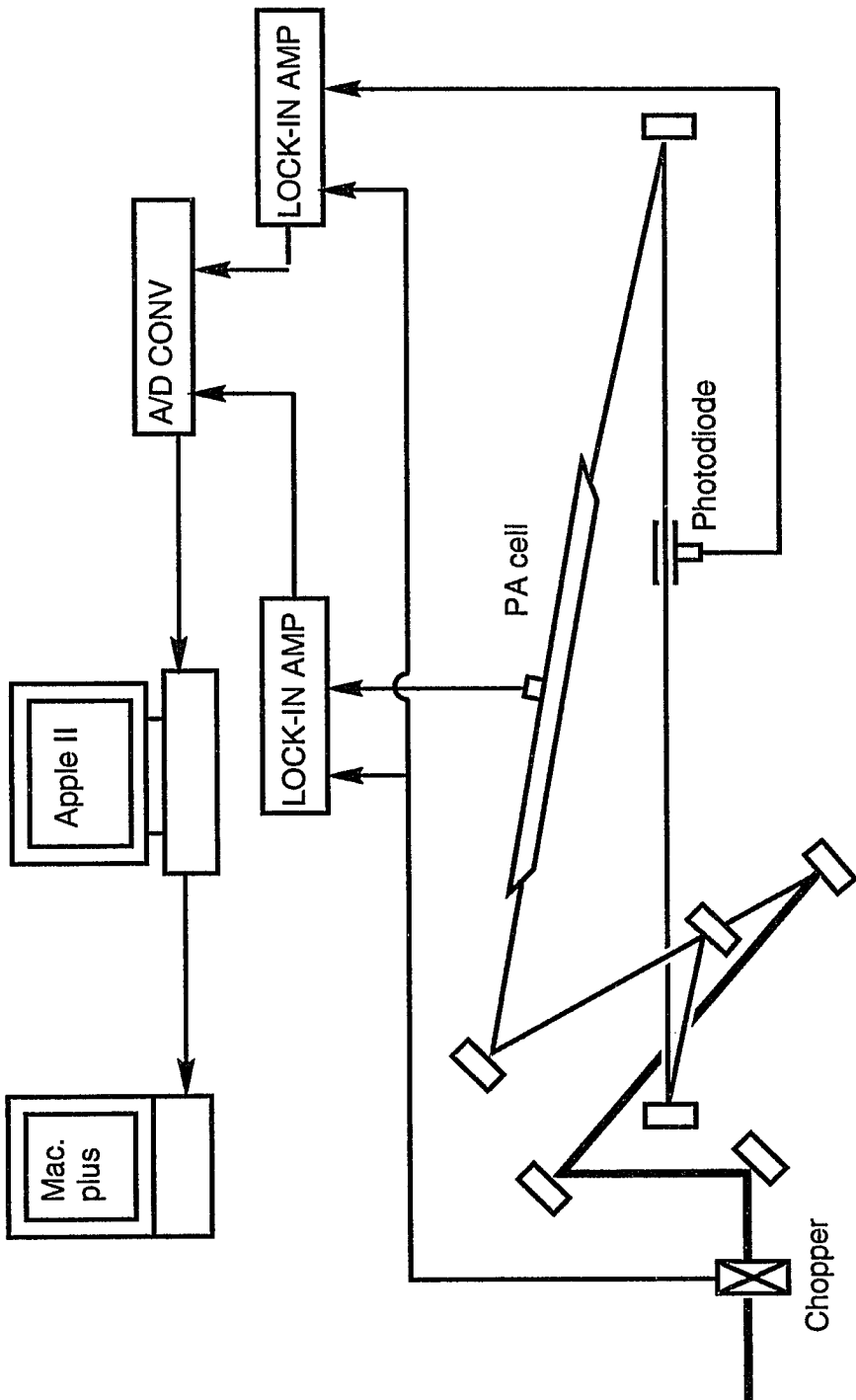


Figure II-6. A schematic diagram of the photoacoustic spectrometer

CHAPTER III

EXPERIMENTAL IMPROVEMENT ON PHOTOACOUSTIC SPECTROSCOPY

III-1 Introduction

Photoacoustic spectroscopy is based on the fact that radiation energy can be converted into acoustic energy, which can be detected by a pressure transducer or microphone. It is well known that absorption of electromagnetic radiation by any substance will increase its temperature if radiative relaxation is not a dominant process. Under certain conditions for example, if the radiation source is modulated, the temperature of the absorbing substance will change periodically. When this absorbing substance is placed in an acoustic conducting medium, or the absorber itself is an acoustic conductor (for example, the absorber is a gas sample), the oscillation of temperature of the system will create periodic pressure change if the volume of the system is fixed. This pressure oscillation is a sound wave which carries the frequency of the modulation of the incident radiation.

The photoacoustic phenomenon was first discovered by Bell [1] in solids in 1880. In the following year, he and his associate, Tainter, investigated the same effect in liquids and gases [2] and they found that the signal produced in the gas sample was somehow stronger than that produced in liquids. During the same period, there were also other investigations on the same effect for gas samples [3,4]. However, applications of the effect were not immediately apparent and further investigations simply stopped. This

was probably due to the fact that other technologies were not advanced enough to utilize this effect. For example, there was no acoustic detector available more sophisticated than the human ear, and neither was there any practical desire to exploit this effect.

The photoacoustic effect was almost forgotten for nearly 50 years until the invention of microphone. In 1938, Viengerov [5] made a fresh start by using the phenomenon to investigate the absorption of infrared radiation in gases and measured concentrations of gaseous samples. By using the photoacoustic method, Viengerov was able to measure CO₂ concentration in N₂ down to several parts per thousand. Measurements at lower concentrations were not possible due to the limited sensitivity of his microphone and the background signals from the solid optical cell windows and walls. Note that from the very beginning, photoacoustic measurements on gaseous samples suffered from the background signals generated by the absorption of the incident radiation especially on the cell windows. Even though the sensitivities of microphones today have been much improved, the background signal from the cell windows is still the most serious problem which are encountered in gaseous photoacoustic spectroscopy.

After Viengerov's investigation, there were several other studies on similar applications of the photoacoustic effect. Probably the most important work was the two-cell spectrophone design described by Luft [6]. His spectrophone was composed of two cells of equal dimensions. One of the cells contained the gas sample mixture and the other contained the same gas mixture without the component to be analyzed. Other conditions for the two cells were identical. The microphone signal was proportional to the pressure difference of the two cells. In this way, the background signals from the cell windows and walls were minimized. A commercial gas analyzer based on

Luft's design became available in 1946. Compared to Viengerov's original apparatus, these instruments could measure the concentrations of CO₂ in N₂ down to several parts per million. It should be noted that all the radiation sources for the investigations mentioned above were conventional sources.

It was not until 1967, however, that conventional light sources for photoacoustic studies were replaced for the first time by laser beams. Kerr and Atwood [7] employed a pulsed ruby laser and a cw CO₂ laser to investigate the absorptivity for the water vapor line at 6943.8 Å and the absorptivity of CO₂-N₂ mixtures around 9.6 μ. Absorptivities of $3 \times 10^{-6} \text{ cm}^{-1}$ and $1.2 \times 10^{-7} \text{ cm}^{-1}$ were obtained for water and CO₂, respectively. They also believed that their photoacoustic system was capable of measuring absorptivities on the order of 10^{-8} cm^{-1} .

In 1975, Deaton, Depatie, and Walker [8], in the measurement of absorption coefficients of nitrous oxides and methane, constructed a differential photoacoustic cell and they claimed that this device could be used to measure absorption coefficients as small as 10^{-10} cm^{-1} with an incident laser power of 100 mW. Some fifteen years later, Davidsson, Gutow, and Zare [9] demonstrated that a photoacoustic apparatus with an acoustically baffled sample cell was capable of detecting a minimum absorptivity of $4 \times 10^{-10} \text{ cm}^{-1}$.

As we look back at the history of photoacoustic spectroscopy, the sensitivity of this technique has been greatly improved since it was first introduced into the field of molecular spectroscopy. Ultimately, all detection techniques are limited by the capability of distinguishing the signal of interest from the background. Like any other detection method, the sensitivity, signal-to-background ratio and signal-to-noise ratio of photoacoustic detection depend on many factors. If the characteristic of the sample is put aside, the ultimate detection capability of this method is determined mainly by the

following factors:

- (1) The power of the incident radiation. Generally speaking, the intensity of the signal will increase linearly with the power of the incident radiation for a given transition as long as the transition is not saturated. However, the increase of the radiation power may also increase the intensity of the background signal.
- (2) The shape of the photoacoustic sample cell. Since the optical signal generated by the absorption of the radiation is carried by an acoustic wave, the geometric shape of the cell will greatly affect the performance of this method.
- (3) The detection capability of the detector. Usually, the detector is a commercial microphone and its sensitivity is frequency dependent. When a modulation frequency has been chosen, the sensitivity of the microphone will be a constant.
- (4) The operation modes. For example, optically and acoustically resonant and non-resonant operations have been performed in photoacoustic spectroscopy. Optically resonant operation (intracavity detection) permits high radiation power. Although the acoustically resonant operation does not increase the signal-to-background ratio, it does give the advantage of increasing the signal-to-noise ratio, which is very important for detecting very weak signals.
- (5) Interference signals generated by unwanted species in the spectral region. Interference signals could become very serious especially when the sample under study is a weaker absorber than the interfering species. For example, water absorption in the near infrared are serious problems when other samples are under investigation in the same spectral region. Typically, the water overtone transitions in the near infrared are several orders stronger than the overtone transitions of other species, such as CO₂ and N₂O [10], so

that the minimization of the water signal is critical.

(6) The characteristics of the buffer gas. For example, heat capacity, density and thermodynamic properties of the buffer gas will affect the overall performance of the photoacoustic system. It has been demonstrated that a buffer gas with small heat capacity and high density [9, 11] will benefit a photoacoustic apparatus which uses a mechanical chopper to modulate the radiation intensity, because the modulation frequency is usually limited below 1000 Hz.

Of course, there are some other factors which also affect the overall performance of the photoacoustic detection technique. However, they are relatively less important compared with the ones mentioned above. Factors (1) and (3) are generally constrained once a laser system and microphone have been chosen. The research interest in our laboratory has recently been focused on heavy-atom overtone transitions in the gas phase and since the transitions under study are so weak, typically pure samples are used. So factor (6) will not be of too much of concern in this paper. Due to the indisputable advantages of resonant operations, both optically and acoustically resonant operations have been employed throughout our studies. This paper will focus mainly on the improvement of factors (2) and (5) by introducing a new photoacoustic cell design. Some of the applications of this new photoacoustic cell on heavy-atom overtone spectroscopy studies and its ultimate sensitivity will also be addressed.

II-2 The Promotion of the New Cell Design

Following the development of laser techniques and sensitive

microphones, photoacoustic spectroscopy has been widely used to study high energy vibrational overtone transitions. In the near infrared, however, these investigations have been concentrated on the so-called light-atom overtones. Heavy-atom overtone studies in the near infrared (8000 – 14000 cm^{-1}) have proved challenging due to the extreme weakness of the transitions and interferences from light-atom species (see Chapter I for explanations).

To the best of our knowledge, there are only three systems, CO [12], CO₂ [13], and N₂O [14], which have been studied in this energy range aside from hydrides and deuterated species. In a series of early investigations on these high energy overtone transitions, photographic absorption technique with long absorbing paths was used [15]. Take CO₂ as an example [13]: A White cell with a total absorbing path of 11000 m·atm had to be employed in order to observe the $5\nu_3+(\nu_1, 2\nu_2)$ doublet transition around 12700 cm^{-1} and an equivalent path of 55000 m·atm was required to detect the strongest component of the $5\nu_3+(2\nu_1, \nu_1+2\nu_2, 4\nu_2)$ triplet transition centered around 13966 cm^{-1} . (Due to the Fermi resonance between the symmetric stretch (ν_1) and the even-numbered bending (ν_2) states, some overtone and combination bands involving ν_1 or even-numbered ν_2 vibrations show multiplet structure.) Needless to say, these transitions are quite weak. It is not difficult to imagine the sample sizes required for those long path experiments. Again, in the case of CO₂, the largest sample used was 5000 liters of CO₂ gas under atmospheric pressure. Consequently, there have not been many studies on heavy-atom overtone transitions in the near infrared and it would be prohibitively expensive to study isotopic species.

In our previous investigations on the overtone transitions of CO₂, N₂O [10] and OCS [16], it was demonstrated that these weak transitions could be detected directly by using the intracavity photoacoustic method. The sample

sizes for these studies were about 5 milliliters at one atm compared with 5000 liters used in the long absorbing path experiments. However, it was found at the same time that (factor 5 in the previous section) the water transitions (light-atom overtones) in the same spectral region were very strong and they mask about two thirds of our spectral range. What made it more serious was that most drying agents could not minimize the water signals sufficiently to permit the weak overtone transitions of interest to be observed. In addition, the water interferences made it impossible to measure the intensities of the transitions of interest accurately.

Another problem (factor 2 in the previous section) was the background signal due to the absorption of the incident radiation by the optical windows. This background signal could be strong enough to mask very weak signals. The sample cells used for these previous studies are shown in the previous chapter (see Figure II-4).

In an attempt to overcome these problems, we tried several different drying agents and cell designs. We found that P_2O_5 is one of the most efficient drying agents [17] although it is very hard to handle. This compound is very glutinous and the powder sticks on the vacuum line and the sample cell. If the powder covers the cell windows, it makes it impossible to perform the intracavity detection.

Due to the weakness of the heavy-atom overtone transitions, they could be easily masked by the background signals. In addition, the background signal greatly affects the accuracy of the intensity calibration because it is so hard to define the integration baseline. Therefore it is absolutely necessary to find better cell designs which will give much better performances for our research interests. The new cell design ideally should have the following features and advantages without sacrificing detection

sensitivity:

- a. It should be a single path cell so that intracavity operations could be easily performed.
- b. It should have different spaces besides the optical path so that the drying agent could be placed as far as possible from the main portion of the sample cell and windows.
- c. It should contribute to the minimization of the background signals.
- d. The main portion of the cell should have as few appendages as possible so that the cell behaves like a simple pipe and the quality of the longitudinal resonance will not be decreased [9]. (See appendix B)
- e. It should be easily constructed and convenient to use. For example, damaged microphones must be able to be replaced without difficulty and dirty windows should be easily cleaned, etc.

There exist several typical cell designs: the two-path design; the two-cell design [18]; the cell with acoustic baffles [9, 18, 19] and even a cell without windows [20], used both for the conventional and laser radiation sources. Basically, most of those designs focus on two purposes: increasing sensitivity and decreasing background signal and noises. The differential types have the advantage of minimizing the background signals. Unfortunately, they cannot easily be used for cw laser intracavity detection since the installation of the sample cell interrupts the laser alignment or decreases the intracavity laser power considerably. The windowless design is not appropriate for our purposes, because a closed system has to be employed.

Although acoustic baffles minimize the window signals, it is believed that they reduce the quality of the resonance [21] and, therefore, decrease the sensitivity. Based on these considerations and limitations of our experimental conditions, we decided that a design with the combined features

of the windowless and the baffled cell designs would be a better candidate for our purposes. We were particularly interested in the design suggested by Davidsson, Gutow, and Zare and the sensitivity they have achieved [9]. The design used by Lehmann, Scherer and Klemperer [22] also gave us much inspiration. We tried to keep the features of these elegant designs and to make improvements over them. The improvements focused on: how to keep the main portion of the cell as simple as possible so that it behaves like a simple pipe and therefore increase the quality of the acoustic resonance; how to minimize the total volume of the optical path so that the sensitivity will not be decreased; and how to store the drying agent without contaminating the cell windows. After about a dozen different designs, we finally decided on a concentric double-tubing cell design [23] which has the proposed features. A picture of this new sample cell can be found in the previous chapter (see Figure II-5).

III-3 Experimental

A broad band cw titanium:sapphire laser (Coherent 899-01) pumped by a 5 W multiline Ar⁺ laser (Coherent Innova 70-5) is used as the near infrared light source. With three different sets of optics, the system provides a spectral range of 10000 – 14000 cm⁻¹. In order to increase the intracavity radiation power, high reflectors (CVI and Coherent, reflectance ~99.9%) have been used in the place of the output coupler and this leads to a tenfold decrease in the output power. Typically, peak output powers of 30 mW, 20 mW, and 15 mW could be reached before the installation of the sample cell for the short wavelength, middle wavelength, and long wavelength optics through the

high reflectors, respectively. The intracavity peak laser power is expected to be one thousand times larger than the output power. The bandwidth of the laser is of the order of 0.2 cm^{-1} when the standard output couplers are used and it is expected to be broader when operated with the high reflectors. The frequency scan of the laser is performed by tilting an intracavity birefringent filter with a stepper motor (Oriel, model 18510). A typical scan rate is about $10 \text{ cm}^{-1}/\text{min}$.

When the transition intensities are studied, the variation of the intracavity laser power as it is scanned must be recorded. The relative intracavity laser power is monitored by a photodiode (EG&G Ortec, UV-100) placed near a laser beam to intercept scattered laser light. The signal from the photodiode is then fed to a lock-in amplifier (Princeton Applied Research, Model 5101).

The photoacoustic sample cell is placed inside the titanium:sapphire ring laser cavity. It is found that the output laser power will decrease by about 20% upon the installation of the sample cell. The intensity of the Ar^+ laser is modulated with a mechanical chopper (Stanford Research System, SR540) tuned to the longitudinal acoustic resonance frequency of the sample cell. The microphone (Knowles, EK-3024) is powered by a 9 V battery and its signal is fed to another lock-in amplifier (Stanford Research Systems, SR510). Great care was taken to shield the connections between the microphone and the power box. For the scan rate given above, a typical time constant of 3 seconds was used. The fine tuning of the chopping frequency and the phase of the lock-in was done by setting the laser frequency on an intense transition and maximize the acoustic signal before each scan. The two signals are recorded on a microcomputer system.

In total, six sample cells with different sizes have been constructed

based on the concentric double-tubing design. Basically, the cell is composed of two tubes with different diameters. The smaller tube is housed concentrically in the larger one. The inner tube is open ended and this will lead to an acoustic node or maximum pressure change in the middle of the tube (Figure III-1) where the microphone is mounted. All the other appendages, such as fingers for drying agent, gas valve, microphone signal outlet and the optical windows, are attached to the outer tube. Pyrex glass tubings with different diameters were used for the construction of the cells. The smaller cells typically have inner tubes of i.d. of 4 mm and length of 200 mm, and outer tube of i.d. of 15 mm and length of 280 mm including the windows. The outer tube has two pieces jointed by a 3/4 in. compression fitting (Cajon Ultra-torr). Smaller fittings (3/8 in. and 1/4 in.) are used for the drying agent finger and the microphone outlet connections, respectively. Optical windows (micro cover glass, VWR Scientific Inc. No. 1^{1/2}) are glued to the outer tube at the Brewster angle with epoxy. The larger cells have the same inner tube diameter but a different length of 240 mm, and outer tubes with i.d. of 22 mm and length of 330 mm including the windows.

The sample cells were evacuated on a vacuum line pumped by an oil diffusion pump with a typical background pressure of several millitorrs. A mechanical pressure gauge (Omega) was used to monitor the sample pressure with an accuracy of 5%. One atm total pressure was used without any buffer gas. The drying agent (P₂O₅) was stored in the cell finger before the cell was evacuated. After the sample was prepared, P₂O₅ could be introduced into the outer tube by simply rotating the cell with an appropriate angle. The cells were first used for the vibrational overtone studies of ¹³CO₂ (Cambridge Isotopic Laboratories Inc., 99% ¹³C) and ¹²CO₂ (Matheson Gas Products, >99.8% bone dry) samples in the near infrared.

III-4 Results and discussions

In order to improve the overall performance of the photoacoustic detection to fulfill our research interests, we focused on two of the important factors that affect the overall performance of the apparatus. The first is that of the signals in the spectral region caused by unwanted species, and the second is the background signal generated by the window absorption of the incident radiation. We will discuss the improvements which have been made in reducing the effects of these factors. As a demonstration of the performance of the new cell, overtone spectra of $^{12}\text{CO}_2$ and $^{13}\text{CO}_2$ in the near infrared will be presented. The ultimate sensitivity and the overall performance of this new photoacoustic cell will also be discussed.

(A) Interference of the Water Transitions

As mentioned before, water overtone transitions in our spectral range are much stronger than those of the heavy-atom overtone transitions. The reason for this is that the vibrational quantum number changes for water transitions are smaller. Besides, water transitions cover a very wide region in our total spectral range. Take the $^{12}\text{CO}_2$ spectrum as an example (Figure III-2), strong water transitions cover about 2/3 of the spectrum. Fortunately, the $^{12}\text{CO}_2$ $5\nu_3$ band is not seriously affected. From the integrated band cross sections, the ratio of the total absorbing cross sections of CO_2 to that of water is estimated to be 3.5×10^{-4} . Notice in Figure III-2 that the sensitivity of the lock-in amplifier was changed by a factor of 10 around 11600 cm^{-1} and the vapor pressure of water was 4% of that of CO_2 .

In order to minimize water interference to a level comparable with the CO₂ band, the partial pressure of water had to be lowered to the millitorr level. This means that the molecular density of water should be smaller than 3×10^{13} molecules/cm³. Probably the only drying agent which can reach this efficiency is P₂O₅ which has the ability to reduce the water density to about 8×10^{11} molecules/cm³.¹⁷ At first, we tried to place P₂O₅ in the finger to avoid window contamination. It was found that it took too long to reduce the water density to a satisfactory level because the effective reaction area in the finger was too small and the drying agent was too far away from the main portion of the sample cell as well. Figure III-3 is a spectrum of ¹³CO₂ which was taken after the sample was prepared for about two months and the water transition intensity was still quite appreciable.

By using the new cell, we can place the P₂O₅ in the space between the two tubes without the likelihood of contaminating the windows. It only takes two or three days to reduce the water intensity to a satisfactory level (Figure III-4). The spectrum not only gave a cleaner baseline for the 5v₃ and 5v₃+(v₁, 2v₂) transitions of ¹³CO₂, it also allowed the observation of the 5v₃ band of ¹²CO₂, which was an impurity in the ¹³CO₂ sample with a concentration of less than 1% (estimated by mass spectroscopy). In addition, the extremely weak bands, two of the stronger components of the 4v₁+3v₃ pentad of ¹³CO₂, surprisingly appeared in the same spectrum (marked with asterisks in Figure III-4; an enlargement is shown in Figure III-5). More detailed information about these weak bands should be published in the near future. We estimate that these 4v₁+3v₃ transitions are at least 100 times weaker than that of the 5v₃ transition in the same spectrum. Water transitions are still observable although the band intensity has been reduced by six orders of magnitude.

(B) Background Signals

Background signal due to window absorption of the radiation has been a major problem for high sensitivity gas phase photoacoustic spectroscopy [24]. This limitation becomes more critical for detection of extremely weak transitions. There were many attempts made to overcome this limitation. One common approach is to keep the windows as clean as possible. Figure III-6 depicts a water free spectrum of the same $^{13}\text{CO}_2$ sample as in Figure III-4 but with dirty windows. It is obvious that the background signal in this spectrum was strong enough to mask the $4\nu_1+3\nu_3$ transitions of $^{13}\text{CO}_2$ (compare with Figure III-4). The baseline also reflected the relative intracavity laser power. Another approach is to search for appropriate geometric cell design to minimize the window absorption. For example, our new cell design is a combination of taking the attractive features of the baffled cells and the "windowless" cells.

It is well known that for an open-ended pipe, the standing acoustic wave has a displacement node at the middle of the pipe and antinodes at the ends (Figure III-1a). On the other hand, a close-ended pipe has its displacement antinode at the middle and nodes at the ends (Figure III-1b). The maximum pressure change or condensation is at the displacement node in a pipe and so should be the maximum sound intensity (see appendix B).

To take the advantage of this phenomenon, the microphone is mounted at the middle of the inner tube where the maximum sound intensity from the signal is located. In order to confirm this effect, cells with different microphone mounting positions were constructed. It was found that by mounting the microphone at the middle of the tube, the sensitivity was increased by a factor of five compared with the sensitivity with the

microphone mounted near the end. On the other hand, the background signal generated by window absorption is approximately in resonance with the outer tube which is close-ended, so that the minimum intensity of the background should be located at the middle. There is mass transfer between the volumes of the inner and the outer tubes due to the difference in the power absorbed per unit volume when absorption occurs. This effect will reduce the intensity of the background signal from the windows propagating into the inner tube where the microphone is mounted.

Background signal due to window absorption is further reduced by the baffling effect. Since the cross sectional area ratio of the inner and outer tubing is very small, and the window signal is dispersed to a much larger area of the outer tube, the window signal is further reduced. In addition, the microphone is mounted in the inner tubing which is fixed concentrically in the outer tubing by small springs so that the microphone is more isolated than the conventional single-tubing cells. This helps to minimize the ambient noises (see the baseline in Figure III-4).

As mentioned in the experimental section, micro cover glass is used as optical windows on these new cells due to the cost, while fused silica has been used in other studies [9]. However, we occasionally observe that the birefringence of the windows, either intrinsic or stress-induced, interferes with the birefringent filter, resulting in discontinuous scan in laser wavelength and fluctuation in laser power. If extremely high sensitivity is required, we suggest that these less expensive windows be replaced by fused quartz or fused silica windows.

(C) Overall Performance and Sensitivity

Operation of the new cell is convenient. The 4 mm i.d. of the inner

tube of the cell permits easy laser alignment for intracavity operation. The cell can be taken apart for cleaning, microphone changing, etc. A second component, such as a drying agent, or an intensity calibration standard, can be introduced to the cell without much difficulty. The component can be held in the finger or in the space between the tubes. Due to the simplicity of the inner tube, the longitudinal resonant frequency of the cell can be easily predicted by the following equation [9, 25]:

$$v = \frac{c}{2L} n \quad n = 1, 2, 3, \dots$$

where v is the resonant frequency of the acoustic wave, c is the speed of sound of the gas sample, and L is the length of the inner tube. A simple comparison shows that the resonant frequency of the new cell matches the calculated value very well using the above equation. For example, the speed of sound [26] is 267 m/s for $^{12}\text{CO}_2$ and 264 m/s for $^{13}\text{CO}_2$ (assuming that $^{13}\text{CO}_2$ has the same heat capacity as $^{12}\text{CO}_2$) at 20 °C, $\ell = 20$ cm, for the first harmonic resonance $n=1$, and this gives the resonant frequencies 667 Hz for $^{12}\text{CO}_2$ and 660 Hz for $^{13}\text{CO}_2$, respectively. The actual resonant frequency used at the same temperature was 665 Hz for $^{12}\text{CO}_2$ and 653 Hz for $^{13}\text{CO}_2$. It is also found that a frequency fluctuation within 5 Hz did not affect the signal intensity significantly. A typical mechanical chopper can handle this requirement without any difficulty.

The ultimate sensitivity of the new photoacoustic cell can be estimated conservatively by using the $5\nu_3$ transition of $^{12}\text{CO}_2$ in the $^{13}\text{CO}_2$ sample. If we take the concentration of $^{12}\text{CO}_2$ as 1% (measured by mass spectroscopy), the corresponding molecular density will be 2.5×10^{17} molecules/cm³. The integrated band cross section of the $5\nu_3$ band for $^{12}\text{CO}_2$ is 2.4×10^{-25} cm²

according to Rank and co-workers [27]. One of the rotational transitions near the hot band has an intensity about 1% of the total band intensity. This will yield an absorptivity about $6.0 \times 10^{-10} \text{ cm}^{-1}$ with a S/N ratio of 10:1. If the S/N ratio is decreased to 2:1, an absorptivity of $1.2 \times 10^{-10} \text{ cm}^{-1}$ could be reached. A detailed calculation is shown in appendix A.

The most sensitive photoacoustic apparatus which have been reported so far are the differential type used by Deaton, Depatie and Walker [8] and the baffled cell design suggested by Davidsson, Gutow and Zare [9]. The former reported a photoacoustic minimum absorptivity of 10^{-10} cm^{-1} . They used a CO₂ laser with a power of 100 mW. Their equivalent background signal was $3.3 \times 10^{-9} \text{ cm}^{-1}/\text{W}$. According to this value and the laser power, their background signal was $3.3 \times 10^{-10} \text{ cm}^{-1}$. If the minimum absorptivity is the same as the background, the S/N ratio was 1:1. Our power is about 100 times higher than theirs but their typical integration time was 100 times longer than ours. In addition, our S/N ratio is still higher. When all these factors are taken into account, our sensitivity is comparable with theirs. This comparison is based on the assumption that their background signal intensity would not increase proportionally with laser power. Just as Davidsson, Gutow and Zare [9] have pointed out: "It is unclear whether their technique would perform this well, since the window noise must match in two cells".

A minimum absorptivity of $4 \times 10^{-10} \text{ cm}^{-1}$ was reported by Davidsson, Gutow and Zare [9] using their baffled photoacoustic sample cell. Compared with their apparatus and operating conditions, their laser power is stronger by about a factor of two, but our integration time is longer by about the same factor. The other conditions are comparable, except that they used two microphones in the cell and we only used one; however, our sensitivity is higher by an factor of three if the S/N ratio is considered. Another factor one

should be aware of is that in the calculation of our sensitivity from the $^{12}\text{CO}_2$ spectrum, the total integrated cross section of the rotational transition was used. Otherwise, the cross section of the transition would be even smaller and so would be the minimum absorptivity.

III-5 Conclusions

A new photoacoustic cell design has been introduced. Its performance and sensitivity have been tested by recording the heavy-atom overtone of $^{13}\text{CO}_2$ and $^{12}\text{CO}_2$ in the near infrared. A conservative value of $1.2 \times 10^{-10} \text{ cm}^{-1}$ has been reported for the minimum absorptivity under our experimental conditions. The construction of the design is relatively simple and inexpensive. The cell may be used for many systems and it is very easy to operate and maintain. In addition to all these features, it is extremely sensitive. Although the design may not be appropriate for every purpose, such as a flowing system, we believe that it does offer many advantages over the conventional single path design, especially for intracavity operation studies on very weak transitions.

APPENDIX III-A

CALCULATION OF THE MINIMUM ABSORPTIVITY

The minimum absorptivity, α , of an apparatus given in units of cm^{-1} is determined by the relation [28]

$$\alpha = N m \sigma(\nu) \quad (\text{A1})$$

where N is the total molecular density in molecules cm^{-3} , m is the minimum mole fraction of the absorbing species to give a certain signal to noise ratio and $\sigma(\nu)$ is the absorption cross section for a given wavenumber interval in $\text{cm}^2 \text{ molecule}^{-1}$.

Take the experimental conditions in this study as an example, we can calculate the sensitivity of the apparatus by using equation (A1). For the spectrum obtained on the $^{13}\text{CO}_2$ sample, the mole fraction of $^{12}\text{CO}_2$ is about 1%, total molecular density is 2.5×10^{19} molecules cm^{-3} . The total absorption cross section of the $5\nu_3$ band according to Rank et al [27] is $2.4 \times 10^{-25} \text{ cm}^{-1} \text{ cm}^2 \text{ molecule}^{-1}$. If one of the rotational transitions near the hot band is considered, it has about 1% of the total band cross section. i.e. $2.4 \times 10^{-27} \text{ cm}^{-1} \text{ cm}^2 \text{ molecule}^{-1}$ and a signal to noise ratio about 10:1. The detectability will be

$$\alpha = 2.5 \times 10^{19} \times 10^{-2} \times 2.4 \times 10^{-27} = 6.0 \times 10^{-10} \text{ cm}^{-1}$$

If the S/N ratio is further decreased to 2:1, then the detectability will be

$$\alpha = 1.2 \times 10^{-10} \text{ cm}^{-1}$$

Note that this calculation pertains to the integrated cross section for a rotational line; otherwise, the α value will be still smaller.

APPENDIX III-B

STATIONARY ACOUSTIC INTENSITY DISTRIBUTION IN PIPES

In order to formulate a simple theoretical model for an acoustic wave in a pipe, it is necessary to make the following assumptions [29].

First, the diameter of the pipe should be sufficiently large to justify neglecting energy loss due to the viscous effect, and sufficiently small compared with the length of the pipe (denoted by L) and the wavelength of the acoustic wave; second, the walls of the pipe should be rigid; and third, pressure change should be adiabatic with very small amplitude. When the cylindrical gas column in the pipe is set into resonant vibration, the wave equation has the form:

$$\Phi = \left[A \cos\left(\frac{2\pi\nu x}{c}\right) + B \sin\left(\frac{2\pi\nu x}{c}\right) \right] \cos(2\pi\nu t) \quad (\text{B1})$$

where Φ represents the acoustic wave function, ν is the frequency of the acoustic wave and c the speed of sound. If the pipe is open-ended, there are displacement antinodes at the ends, $d\Phi/dx = 0$ at $x = 0$ and $x = L$. This gives $B=0$; then the wave equation becomes

$$\Phi = \left[A \cos\left(\frac{2\pi\nu x}{c}\right) \right] \cos(2\pi\nu t) \quad (\text{B2})$$

The pressure change [30] δp is proportional to the condensation $-d\Phi/dx$, i.e.

$$\delta p = \kappa \left(-\frac{d\Phi}{dx} \right) \quad (B3)$$

where κ is the elasticity of the medium. Combining equations (B2) and (B3), we have

$$\delta p = \kappa \left(-\frac{d\Phi}{dx} \right) = -\kappa \frac{2\pi v A}{c} \sin\left(\frac{2\pi v x}{c}\right) \cos(2\pi v t) \quad (B4)$$

If the gas column is subject to the fundamental frequency [29] which is $v=c/(2L)$, then we reach the following expression for the pressure change:

$$\delta p = -\kappa \frac{\pi A}{L} \sin\left(\frac{\pi x}{L}\right) \cos\left(\frac{\pi c t}{L}\right) \quad (B5)$$

From equation (B5), it is clear that the pressure change distribution in a pipe is a sine wave in x . Note that the maximum pressure change, $(\delta p)_{\max}$, is located at $x = L/2$, and the minima are at $x = 0$ and $x = L$ for the fundamental frequency. Consequently the maximum sound intensity is also located at the middle of the pipe ($x = L/2$), since sound intensity is proportional to $[(\delta p)_{\max}]^2$.

According to this simple theory without the end corrections, there should be no pressure change at the ends for an open pipe. We found that mounting the microphone near the end of the pipe still delivers appreciable signals. However, the intensity of the signal does increase (at least by a factor of five) when the microphone is mounted toward the middle.

REFERENCES

- [1]. A. G. Bell, *Am. J. Sci.* , **20** (1881) 305
- [2]. A. G. Bell, *Philos. Mag.* , **11** (1881) 510
- [3]. J. Tyndall, *Proc. R. Soc. Lond.* , **31** (1881) 307
- [4]. W. C. Roentgen, *Philos. Mag.* , **11** (1881) 308
- [5]. M. L. Viengerov, *Dokl. Akad. Nauk. SSSR* , **19** (1938) 678
- [6]. K. F. Luft, *Z. Tech. Phys.* , **24** (1943) 97
- [7]. E. L. Kerr, and J. G. Atwood, *Appl. Opt.* , **7** (1968) 915
- [8]. T. F. Deaton, D. A. Depatie and T. W. Walker, *Appl. Phys. Lett.* , **26** (1975) 300
- [9]. J. Davidsson, J. H. Gutow and R. N. Zare, *J. Phys. Chem.* , **94** (1990) 4069
- [10]. X. Yang, C. Petrillo and C. Noda, *Chem. Phys. Lett.* , **214** (1993) 536
- [11]. L. J. Thomas III, M. J. Kelly and N. M. Amer, *Appl. Phys. Lett.* , **32** (1978) 736
- [12]. G. Herzberg and K. N. Rao, *J. Chem. Phys.* , **17** (1949) 1099
- [13]. G. Herzberg and L. Herzberg, *J. Opt. Soc. Am.* , **43** (1953) 1037
- [14]. G. Herzberg and L. Herzberg, *J. Chem. Phys.* , **18** (1950) 1551
- [15]. A series of papers were published by Herzberg and other authors, which are listed below for reference purposes.

CHF₃: H. J. Bernstein and G. Herzberg, *J. Chem. Phys.* , **16** (1948) 30

CO: G. Herzberg and K. N. Rao, *J. Chem. Phys.* , **17** (1949) 1099

Cyclopropane (C₃H₃): S. P. Sinha, *J. Chem. Phys.* , **18** (1950) 217

Methyl Fluoroform (CH₃CF₃): R. D. Cowan, G. Herzberg and S. P. Sinha, *J. Chem. Phys.* , **18**, (1950) 1538

Isocyanic Acid (HNCO): C. Reid, *J. Chem. Phys.* , **18** (1950) 1544

- N₂O: g. Herzberg and L. Herzberg, *J. Chem. Phys.*, **18** (1950) 1551
- Dideuteroacetylene (C₂D₂): B. D. Saksena, *J. Chem. Phys.*, **20** (1952) 95
- Trideuteromethylacetylene (CD₃CCH) and Diacetylene (C₄H₂): A. V. Jones, *J. Chem. Phys.*, **20** (1952) 860
- HCN and DCN: A. E. Douglas and D. Sharma, *J. Chem. Phys.*, **21** (1953) 448
- Tri-Deuteromethane (CHD₃): L. F. H. Bovey, *J. Chem. Phys.*, **21** (1953) 830
- CO₂: G. Herzberg and L. Herzberg, *J. Opt. Soc. Am.*, **43** (1953) 1037
- [16]. X. Yang and C. Noda, in preparation
- [17]. D. R. Lide, *CRC Handbook of Chemistry and Physics*, 73rd Ed. 1992-1993, p. 15-21
- [18]. L. G. Rosengren, *Appl. Opt.*, **14** (1975) 1960
- [19]. V. P. Zharov and V. S. Letokhov, *Laser Photoacoustic Spectroscopy*. In *Springer Series in Optical Sciences*; Springer: Berlin, 1986, Vol. 37
- [20]. A. Miklos and A. Lorincz, *Appl. Phys.*, B **48** (1989) 213
- [21]. C. F. Dewey Jr., *Opt. Eng.*, **13** (1974) 483
- [22]. K. K. Lehmann, G. J. Scherer and W. Klemperer, *J. Chem. Phys.*, **77** (1983) 2853
- [23]. A drawing of the cell is available from the author upon request.
- [24]. A. Rosencwaig, *Photoacoustics and Photoacoustic Spectroscopy*. In *Chemical Analysis*; Elving, P. J., Winefordner, J. D., Eds.; John Wiley and Sons: New York, 1980, Vol. 57
- [25]. G. West, J. J. Barrett, D. R. Siebert, and K. V. Reddy, *Rev. Sci. Instrum.*, **54** (1983) 797
- [26]. A. B. Wood, *A Textbook of Sound*, 3rd ed.; G. Bell and Sons: London, 1955; p. 246

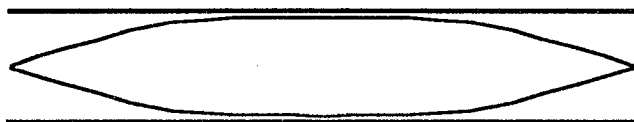
- [27]. D. H. Rank, U. Fink, J. V. Foltz, and T. A. Wiggins, *Astrophys. J.* , **140**
(1964) 366
- [28]. M. Sigrist, Environmental and Chemical Trace Gas Analysis by
Photoacoustic Methods. In Principles and Perspectives of
Photothermal and Photoacoustic Phenomena; Mandelis, A., Ed.;
Elsevier: New York, 1992; Chapter III
- [29]. Ref. 26, pp. 179-180
- [30]. Ref. 26, p. 54

(a) Open pipe

1. Displacement

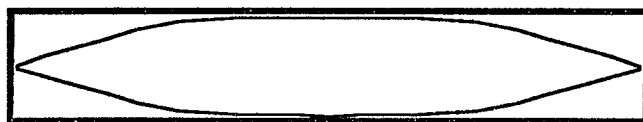


2. Pressure change



(b) Closed pipe

1. Displacement



2. Pressure change



Figure III-1. The acoustic standing wave established in simple pipes: (a) For open-ended pipe: 1. the acoustic displacement node is at the middle and the antinodes at the ends; 2. The pressure change has its maximum at the middle and minimum at the ends. (b) For closed-ended pipe.

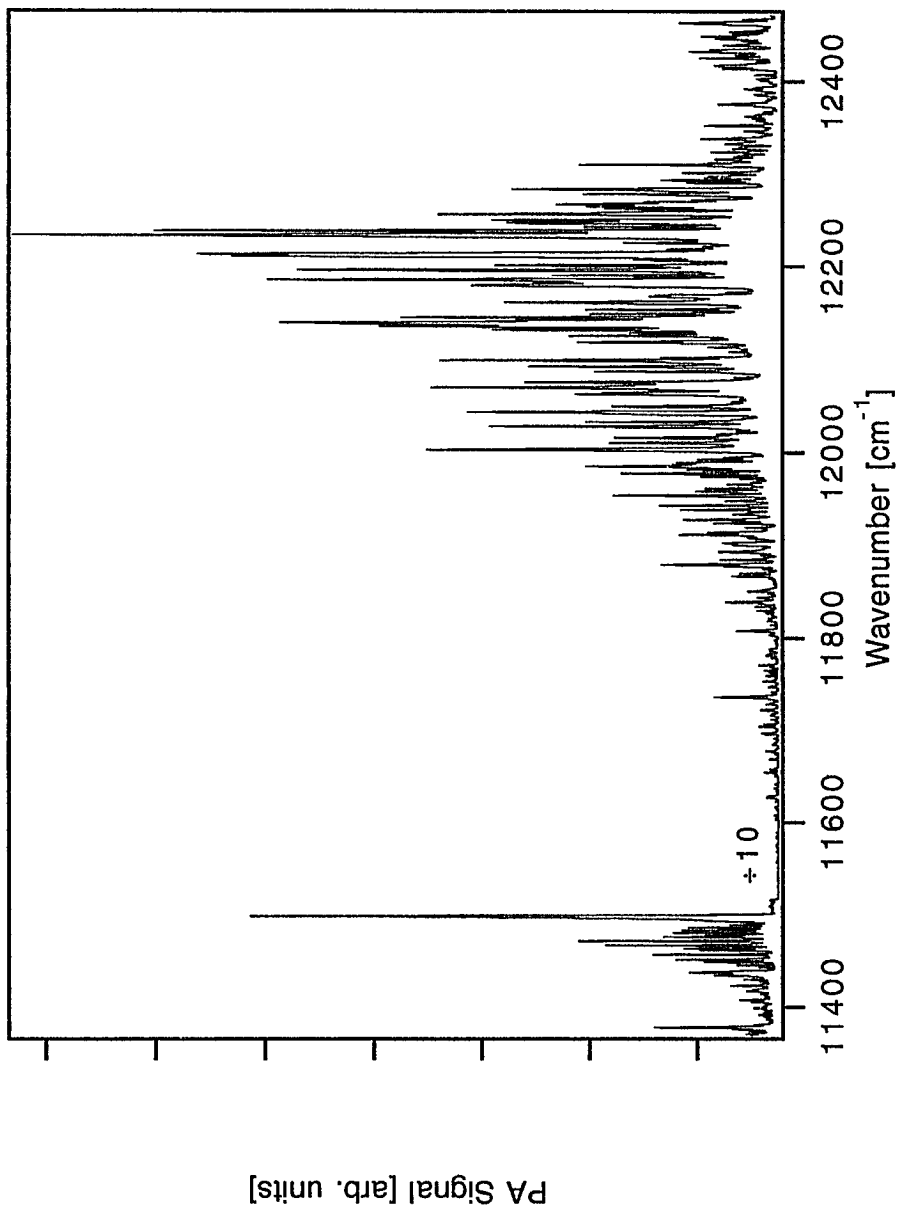


Figure III-2. The $5\nu_3$ transition of $^{12}\text{CO}_2$ near 11500 cm^{-1} and water overtone bands. The pressures are 1.0 atm and 20 Torr for $^{12}\text{CO}_2$ and water, respectively. Notice that the sensitivity scale of the spectrometer was changed by a factor of ten after the $5\nu_3$ band was recorded.

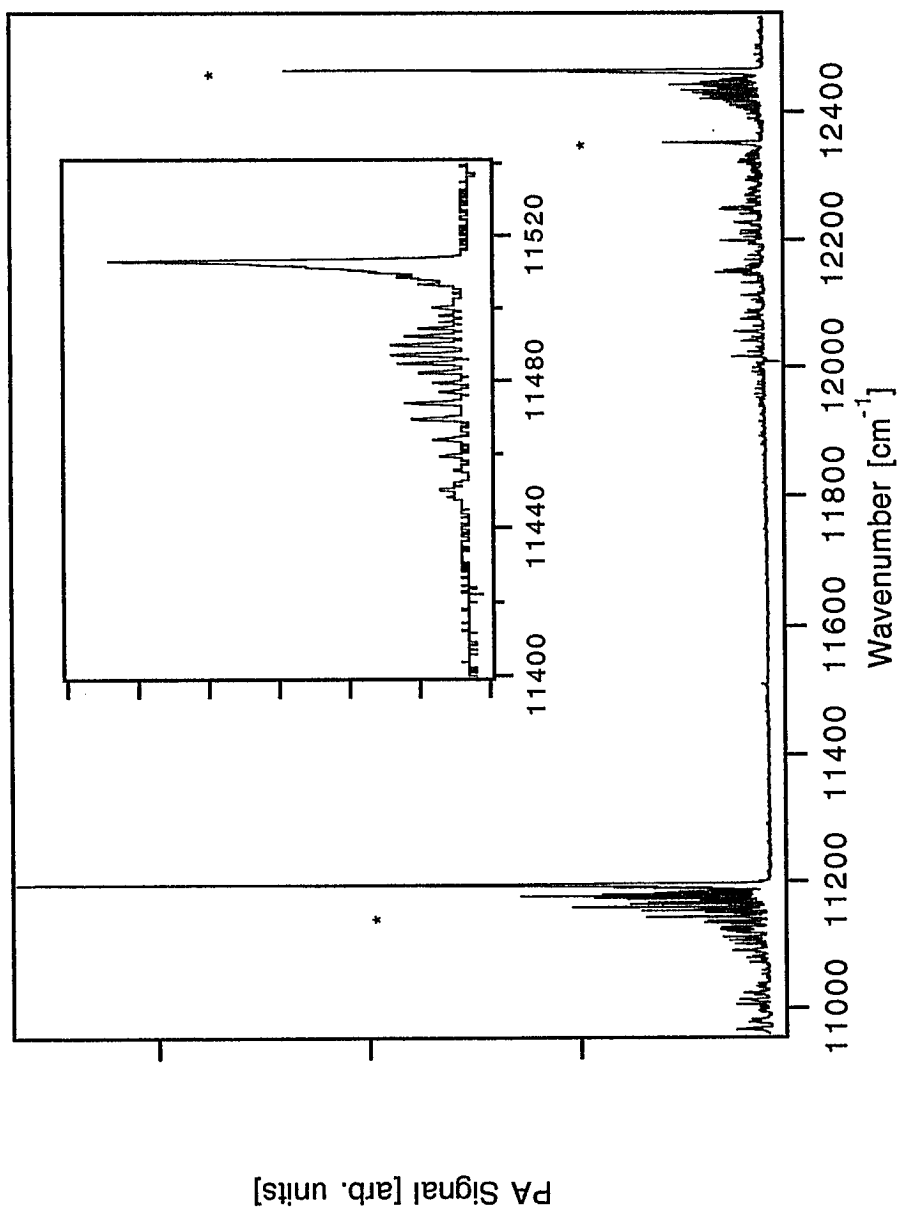


Figure III-3. The $^{13}\text{CO}_2$ spectrum in the near infrared. The strong transition are the $5\nu_3$ and the $\nu_1 + 5\nu_3$ diad (marked with asterisks). The $5\nu_3$ band of $^{12}\text{CO}_2$ near 11500 cm^{-1} can also be identified in this spectrum. The water band intensity is still quite appreciable.

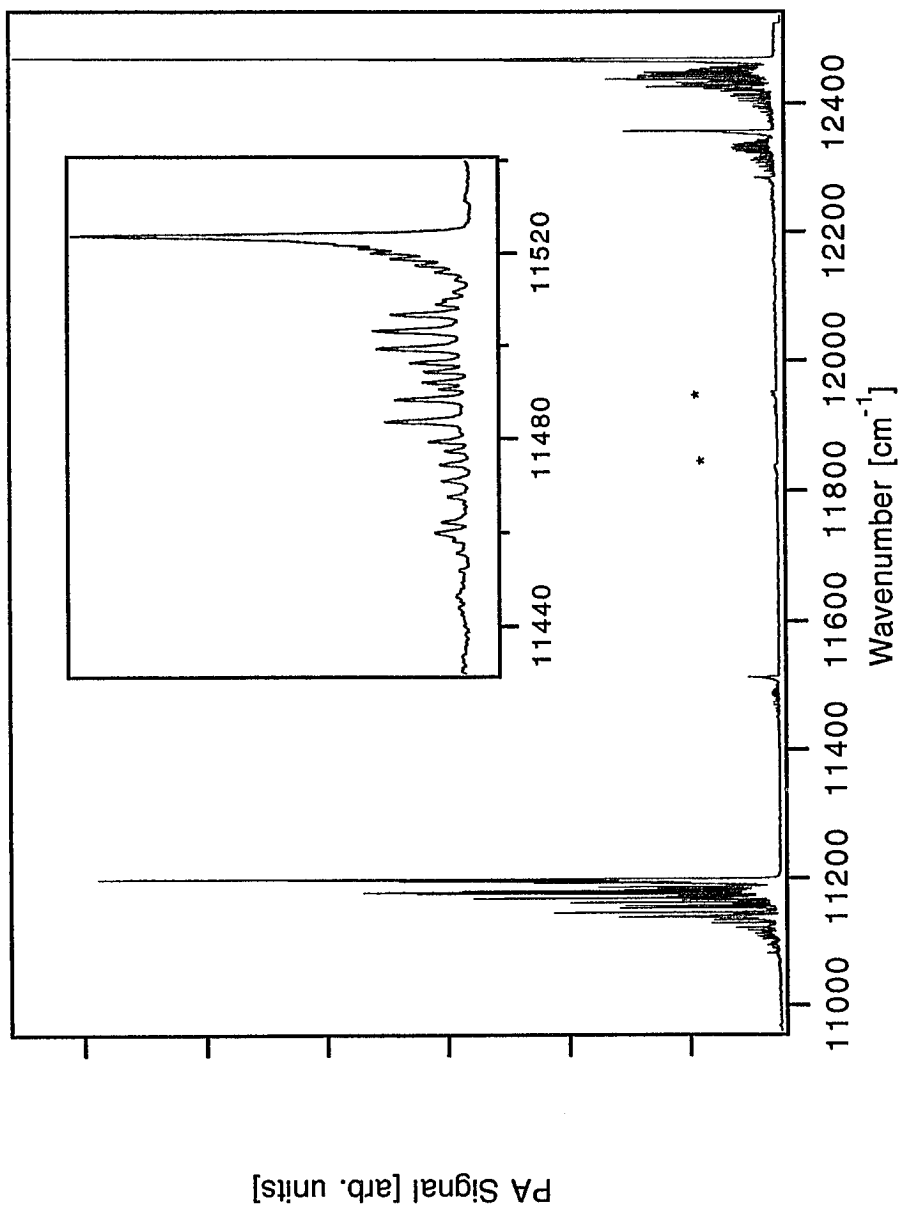


Figure III-4. The water free spectrum of $^{13}\text{CO}_2$. It shows three groups of bands for $^{13}\text{CO}_2$: From left to right, the $5\nu_3$, two components of the pentad (marked with asterisks), and the diad. The $5\nu_3$ band of $^{12}\text{CO}_2$ also shows on the right of the $5\nu_3$ band of $^{13}\text{CO}_2$ (an enlargement of this band is shown in the inset).

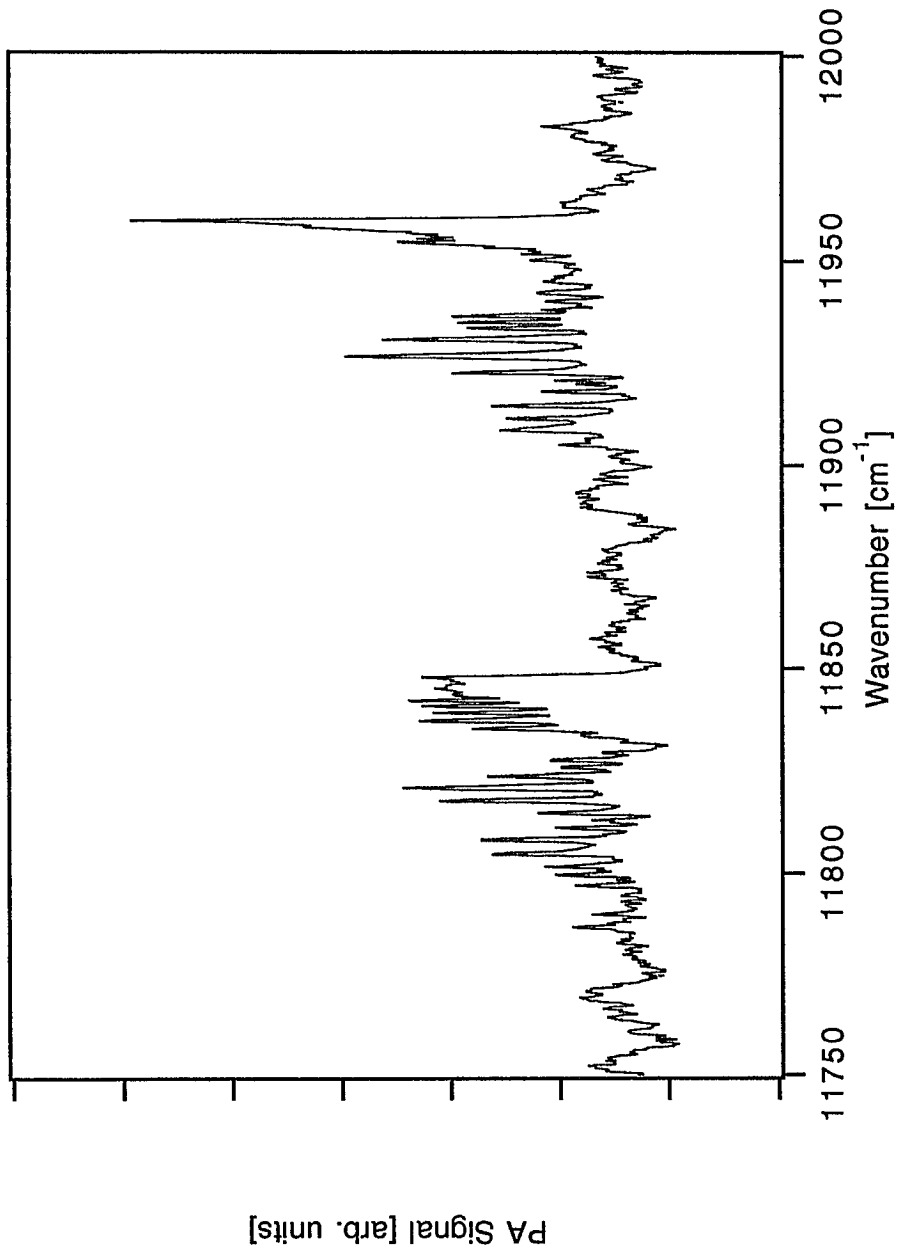


Figure III-5. An enlargement of the $4\nu_1+3\nu_3$ pentad for $^{13}\text{CO}_2$. Only two of the stronger components were observed.

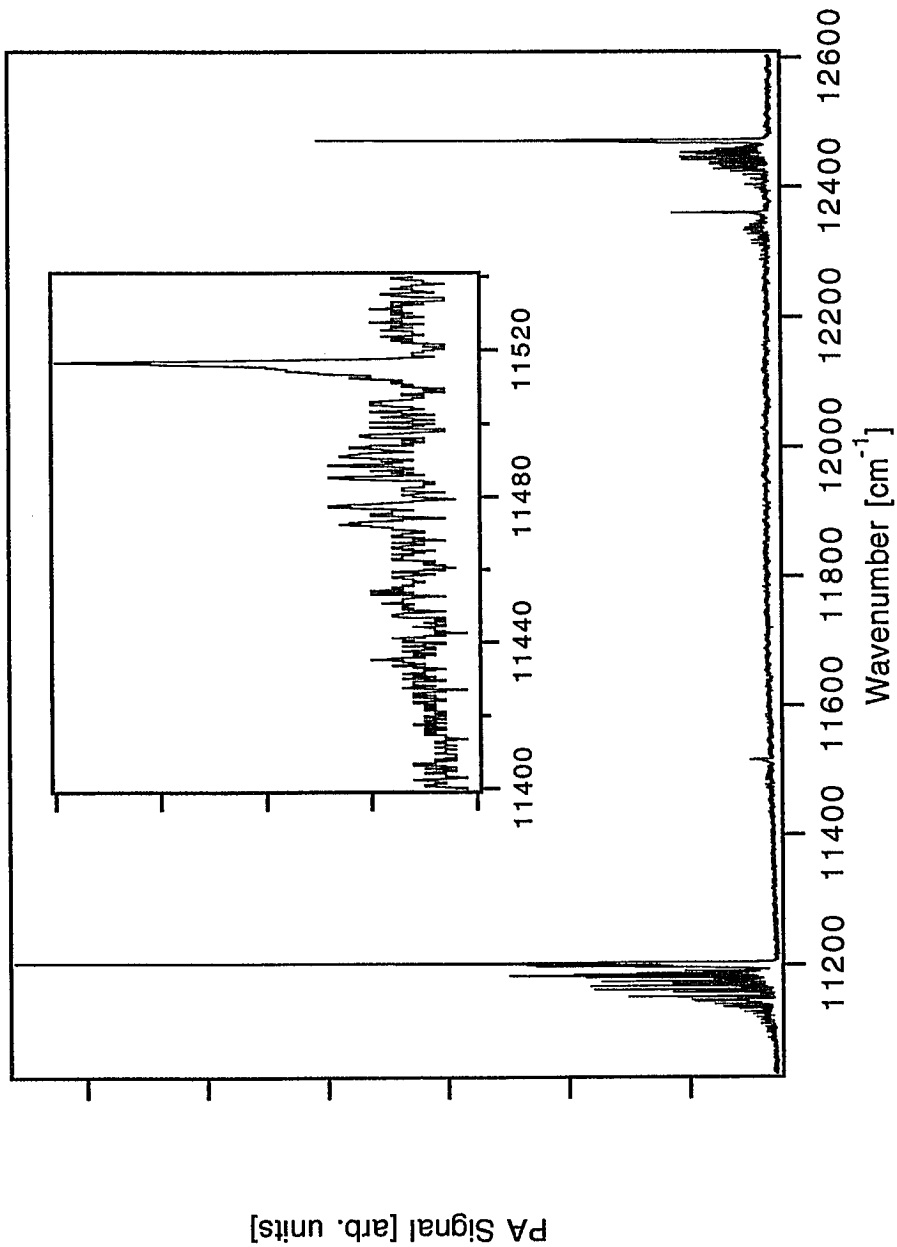


Figure III-6. Water free spectrum of ¹³CO₂ with dirty cell windows. The background signal is so strong that the pentad bands of ¹³CO₂ are masked. Also notice that the baseline reflects the intracavity laser power. The inset shows an enlargement of the 5ν₃ band of ¹²CO₂ as an impurity in the sample.

CHAPTER IV

PHOTOACOUSTIC DETECTION OF N₂O AND CO₂ OVERTONE TRANSITIONS IN THE NEAR INFRARED

IV-1 Introduction

There has been considerable interest in highly vibrationally excited molecules [1]. The interest stems from both fundamental and practical viewpoints. The recent proliferation of laser techniques has allowed us to investigate various aspects of the chemistry of highly vibrationally excited species. To date, however, these efforts have been mainly centered on the H-X stretching vibrations (X = C, N, and O) due to the reasons mentioned in the previous chapters. In this chapter, a study of heavy-atom overtone transitions of N₂O is presented. The near-infrared bands of the N₂O molecules are examined and the integrated absorption intensities are estimated by comparing the photoacoustic signal to those of the nearby H₂O overtone transitions.

N₂O is one of the important components in the atmosphere. The spectroscopic information about this molecule is of chemical, environmental and spectroscopic importance. The overtone transitions of N₂O was investigated using a photographic absorption technique by Herzberg and Herzberg [2] in the 700 – 1200 nm region. A number of bands were identified and rotational and distortion constants were determined. They assigned the bandhead at 12891 cm⁻¹ to the (0, 0⁰, 6) – (0, 0⁰, 0) transition and

the bandhead at 12821 cm^{-1} to the overlapping $(6, 2^0, 2) - (0, 0^0, 0)$ and $(0, 1^1, 6) - (0, 1^1, 0)$ transitions (hereafter, each band will be identified by the bandhead position). A multipass cell was used with a path length of 4 km at an N_2O pressure of one atm.

The near infrared absorption bands of CO_2 were first observed in the Venus atmosphere [3] and were later analyzed by Adel and Dennison [4], who assigned two vibrational bands at 12682 and 12784 cm^{-1} to a Fermi resonance diad, $(0, 2^0, 5)$ and $(1, 0^0, 5)$. Detailed rotational analysis was also carried out by these authors [5]. However, their attempt to detect these bands in the laboratory did not succeed even though samples as optically dense as forty meters of CO_2 gas at three atmospheres pressure were utilized. The laboratory observation of these bands was accomplished by Herzberg and Herzberg [6], who employed a multipass absorption cell with a path length of 5.5 kilometers with CO_2 under two atm pressure.

In this chapter, the detection of these near infrared bands of N_2O and CO_2 was accomplished by using the photoacoustic technique. The sensitivity of the method is discussed. In addition, rough estimates for the absorption cross sections are reported.

IV-2 Experimental

(A) Laser System

A broad-band titanium:sapphire laser (Coherent Radiation 899-01) was pumped by a multiline 5 Watt output from an Ar^+ laser (Coherent Innova 70-5). The output power of the laser with the standard output coupler was

0.3 – 1 W. For the intracavity operation, the stock output coupler was replaced by a high reflector (CVI, reflectivity > 99 % in the spectral region of 700 – 800 nm), and the output power became ten times smaller when the high reflector was installed. The bandwidth of the laser was of the order of 0.2 cm^{-1} with the standard output coupler, and was expected to be broader when the high reflector was used. The scanning of the laser was achieved by tilting a birefringent filter with a stepper motor (Oriel, Model 18510) controlled by a home made control system. A typical scan rate is about 20 $\text{cm}^{-1}/\text{min}$.

(B) Calibration

The wavelength of the laser was measured by a spectrophotometer (Beckman, Model DB-GT) with an uncertainty of one nm. A second order least-squares fit program was then used to convert the stepper motor position to wavelength. The intracavity laser power was monitored by measuring the scattered light intensity with a photodiode (EG&G Ortec, UV-100), which was placed near a laser beam inside the cavity. The signal from the photodiode is fed to a lock-in amplifier (Princeton Applied Research, Model 5101). This setup enabled us to obtain the relative laser power in the laser cavity when the laser is scanned.

(C) Experimental Conditions

The nitrous oxide (Airco UPS grade) gas was contained in a pyrex photoacoustic sample cell. The length of the cell was 25 cm with an inner diameter of 5 mm. Pyrex windows were glued to the cell at the Brewster angle. The cell was equipped with a commercial transducer (Knowles, EK-3024) powered by a 9 V battery. The pressure of the sample was monitored by a mechanical pressure gauge (Omega), whose accuracy was estimated to be ± 5

% of the reading. Typically, one atm of the sample was used without any buffer gas.

The optoacoustic cell was placed inside of a cw broadband titanium:sapphire laser cavity. It has been pointed out that the sensitivity of the photoacoustic detection can be increased if the frequency of the generated acoustic wave matches the resonant frequency of the sample cell [7]. To achieve this, the Ar⁺ pumping laser was chopped with a mechanical chopper (Stanford Research System, SR540) tuned at the acoustic resonance frequency of the sample cell. Throughout the experiment, the high reflector and a short wavelength optics set were used, which limited the accessible wavelength range to 700 – 800 nm and the laser bandwidth to ~0.5 cm⁻¹. The setup is controlled by a microcomputer system (Apple II and Macintosh Plus).

IV-3 Results and Discussion

(A) N₂O overtone transitions

Two vibrational bands of N₂O are observed at 12820 cm⁻¹ and 12899 cm⁻¹, respectively, as shown in Figure IV-1. The 12899 cm⁻¹ band assigned to (6, 0⁰, 0)–(0, 0⁰, 0) has a well-defined rotational structure, while the 12820 cm⁻¹ band only shows a diffuse bandhead. This observation is consistent with that reported by Herzberg and Herzberg [6], and the diffuseness of the band arises from two bands appearing at nearly the same frequency.

Fortunately these bands are away from the H₂O overtone transitions. Figure IV-2 depicts the spectrum with saturated water vapor present in a cell.

The absorption cross sections of these bands are estimated by the following procedure: (i) The photoacoustic signal is integrated over the band

profile in wavenumbers for the N₂O bands and the H₂O overtone bands in the same spectral region. For the water transitions, neither band could be integrated in its entirety due to the limited scanning range of the laser. For the (1, 0, 3) – (0, 0, 0) water band near 723 nm, the integration was carried out for the P-branch section of the band and the result is doubled to obtain the integrated band intensity. For the (3, 0, 1) – (0, 0, 0) band, similar treatment was carried out for the R branch section. (ii) The laser power in the cavity is estimated from the photodiode signal detecting the scattering light intensity. The wavelength dependence of the photodiode sensitivity and the intensity of Rayleigh scattering are included in the calibration of the laser power. (iii) Using the above information, the knowledge of vapor pressures of N₂O and water (saturated vapor at the ambient temperature), and the sum of the intensities of the water (3, 0, 1) – (0, 0, 0) and (1, 0, 3) – (0, 0, 0) bands from the HITRAN 1991/2 database [8], the absorption intensities of the N₂O bands are obtained. The reported values are given as the sum of intensity, S, i.e.,

$$S = \int_{\text{band}} a d\tilde{\nu} = \int_{\text{band}} \frac{A}{bc} d\tilde{\nu} = \int_{\text{band}} \frac{\log_{10}(I_0/I)}{bc} d\tilde{\nu} \quad (1)$$

where a is absorptivity, A absorbance, b path length [cm], and c concentration [molecule cm⁻³].

This procedure of obtaining the overtone absorption cross section has been suggested by Davidsson, Gutow, and Zare [7]. Our approach deviates from theirs in that the water overtone bands are used as the standard. They suggested that water may not be a reliable standard, since the vapor pressure is affected by wall adsorption. We have, however, maintained an

equilibrium so that the vapor is saturated. The possible error introduced is much smaller than the other sources of error, as described below.

Unfortunately, the accuracy of these estimates is rather limited due to the laser system, which is not stabilized, and to the scanning performed by a mechanical means. This results in significant jitter in the center frequency of the laser during the scan. Furthermore, the laser bandwidth does not stay constant as the laser is scanned. As can be seen from the spectra, the rotational structure is not regular. This is caused by the fact that the laser frequency was not smoothly changed during the scan. Since the linewidths of the transitions are narrower than the laser linewidth, the varying laser linewidth affects the integration and introduces a rather large uncertainty.

The sum of intensities for the 12899 cm^{-1} band is $3.7 \times 10^{-25} \text{ cm}^{-1} \text{ molecule}^{-1} \text{ cm}^2$, while that for the 12820 cm^{-1} band is $1.1 \times 10^{-25} \text{ cm}^{-1} \text{ molecule}^{-1} \text{ cm}^2$ (also see Table I). We estimate that the values are accurate within a factor of two for the former and a factor of 3 for the latter. However, the values may be affected by the pressure-induced absorption, and interpretation must be made with care. Also note that the 12820 cm^{-1} band actually consists of two transitions and the value presented here is a sum for these bands.

The sum of the intensities of the fundamental ν_3 band of N_2O is $5.00 \times 10^{-17} \text{ cm}^{-1} \text{ molecule}^{-1} \text{ cm}^2$ [9]. The rule of thumb for overtone intensity gives a factor of one hundred for the first overtone, an additional factor of ten for each successive order of overtone, and a factor of ten for a combination band. Based on this rather crude rule, we expect a decrease in intensity by eight orders of magnitude for these bands, which is consistent with the observation.

(B) CO₂ overtone transitions

Two vibrational bands of CO₂ are observed at positions of 12682 cm⁻¹ and 12784 cm⁻¹, respectively, as shown in Figure III-3. These two bands, previously assigned to the Fermi diad (1, 0⁰, 5)-(0, 0⁰, 0) and (0, 20, 5)-(0, 0⁰, 0) transitions, show well-defined rotational structure. Figure III-4 depicts the spectrum with saturated water vapor present in the sample cell for transition intensity calibration.

A similar approach to that used for N₂O is employed to obtain the absorption cross sections for CO₂ overtone bands. Unfortunately, the CO₂ bands are weaker than that of N₂O and lie closer to the H₂O (3, 0, 1)-(0, 0, 0) band. In fact, the 12683 cm⁻¹ band of CO₂ is overlapped by the H₂O lines and the band profile could not be integrated when water is present. Thus, we estimated the band intensity for the CO₂ 12784 cm⁻¹ band, which can be observed when water is present, first from this measurement (see Figure III-4). Then the intensity of the 12682 cm⁻¹ band was determined by the ratio of these two CO₂ bands obtained from a "water-free" spectrum. The results are listed in Table III-1 [11]. We conservatively estimate that the uncertainties for these intensity measurements are a factor of five for both bands, reflecting the complications discussed above. The intensity of the 12682 cm⁻¹ band is 85% of the 12784 cm⁻¹ band. This differs from Herzberg and Herzberg's visual estimate that the former is only 30% of the latter [6].

With the cross section known, it is straightforward to calculate the absorbances for the bands. As an example, we take the CO₂ 12784 cm⁻¹ band. If we assume a linewidth (FWHM) of 0.1 cm⁻¹ at 300 K, the absorbance of the strongest P-branch line (J=26) will be 0.01 for the absorbing pressure-path of 120 m atms, and 0.97 for 11000 m atms, corresponding to the Adel and Dennison's [4] and Herzberg and Herzberg's [6] conditions, respectively.

The sum of intensities for the fundamental ν_3 band is $9.16 \times 10^{-17} \text{ cm}^{-1} \text{ molecule}^{-1} \text{ cm}^2$ [10]. Again, by applying the previously mentioned rule of thumb, we expect a decrease in intensity by seven orders of magnitude as compared to the fundamental transition. If the intensities of these two overtone bands are added to account for the intensity sharing, the resulting sum of intensities $3.7 \times 10^{-25} \text{ cm}^{-1} \text{ molecule}^{-1} \text{ cm}^2$ is eight orders of magnitude smaller than the fundamental. The observed intensity is less than what is expected from the simple estimation, but can nevertheless be considered reasonable.

IV-4 Conclusion

Higher-order vibrational overtone transitions associated with vibrational motions not involving any H atoms are very weak in intensity due to low anharmonicity and low fundamental vibrational frequencies. Therefore, the experimental measurements on these high vibrational levels have been traditionally obtained from electronic emission spectroscopy. By using the photoacoustic detection technique, however, it is demonstrated that the high energy overtone transitions of N_2O and CO_2 can be observed directly in the near-infrared, and that it is possible to estimate the absorption cross sections.

An additional advantage is that the amount of sample required for the measurements is several orders of magnitude less than that needed for a multipass absorption spectroscopy. Because of this, overtone transitions of isotopic species can be readily studied.

Due to the limited spectral range of our near infrared laser, several bands have not been recorded by the photoacoustic method. The failure for

detecting the band near 14000 cm^{-1} is because of the water interference. It is obvious that water interference in the spectral range is a serious problem for heavy-atom overtone spectroscopy.

REFERENCES

- [1] See, for example, general discussion, *J. Chem. Soc. Farad. Trans. II*, **84** (1988) 1555
- [2] G. Herzberg and L. Herzberg, *J. Chem. Phys.*, **18** (1950) 1551
- [3] W. S. Adams and T. Dunham, Jr, *Publ. Astron. Soc. Pacific.*, **44** (1932) 243
- [4] A. Adel and D. M. Dennison, *Phys. Rev.* **43** (1933) 716. See also A. Adel and D. M. Dennison, *Phys. Rev.*, **44** (1933) 99
- [5] A. Adel and V. M. Slipher, *Phys. Rev.*, **46** (1934) 240
- [6] G. Herzberg and L. Herzberg, *J. Opt. Soc. Am.*, **43** (1953) 1037
- [7] J. Davidsson, J. H. Gutow and R. N. Zare, *J. Phys. Chem.*, **94** (1990) 4069
- [8] L. S. Rothman, R. R. Gamache, G. H. Tipping, C. P. Rinsland, M. A. H. Smith, D. C. Banner, V. M. Devi, J.-M. Flaud, C. Camy-Peyret, A. Perrin, A. Goldman, S. T. Massie, L. R. Brown, R. A. Toth, *J. Quant. Spectrosc. Radiat. Transfer*, **48** (1992) 469, and references therein
- [9] L. S. Rothman, R. R. Gamache, A. Goldman, L. R. Brown, R. A. Toth, H. M. Pickett, R. L. Poynter, J.-M. Flaud, C. Camy-Peyret, A. Barbe, N. Husson, C. P. Rinsland, and m. A. H. Smith, *Appl. Opt.*, **26** (1987) 4058, and references therein
- [10] L. S. Rothman, R. L. Hawkins, R. B. Wattson, R. R. Gamache, *J. Quant. Spectrosc. Radiat. Transfer*, **48** (1992) 537, and reference therein.
- [11] The intensities of these bands have been reexamined later by using the phenol overtone band as a standard (see Chapter VI for detailed discussion).

Table IV-1. The overtone transitions of N₂O and CO₂ in the 700 – 800 nm range. The values for the band origin (v₀) and the band head (v_h), and the assignment are from Ref. 2 and Ref. 6 for N₂O and CO₂, respectively.

v ₀ [cm ⁻¹]	v _h [cm ⁻¹]	Assignment	Sum of Intensity (cm ⁻¹ molecule ⁻¹ cm ²)
N ₂ O			
————	12820.81	$\left\{ \begin{array}{l} (6,2^0,2) - (0,0^0,0) \\ (0,1^1,6) - (0,1^1,0) \end{array} \right.$	1.1 x 10 ⁻²⁵
12891.1	12899.25	(0, 0 ⁰ , 6) – (0, 0 ⁰ , 0)	3.7 x 10 ⁻²⁵
14016.7	14016.7	(1, 0 ⁰ , 6) – (0, 0 ⁰ , 0)	*
CO ₂			
12672.28	12682.31	$\left\{ \begin{array}{l} (0,2^0,5) - (0,0^0,0) \\ (1,0^0,5) - (0,0^0,0), \end{array} \right.$	1.7 x 10 ⁻²⁵
12774.73	12784.03		2.0 x 10 ⁻²⁵
————	13966.2	(1, 2 ⁰ , 5) – (0, 0 ⁰ , 0)	*

*: Not observed in this work due to overlapping water absorption bands.

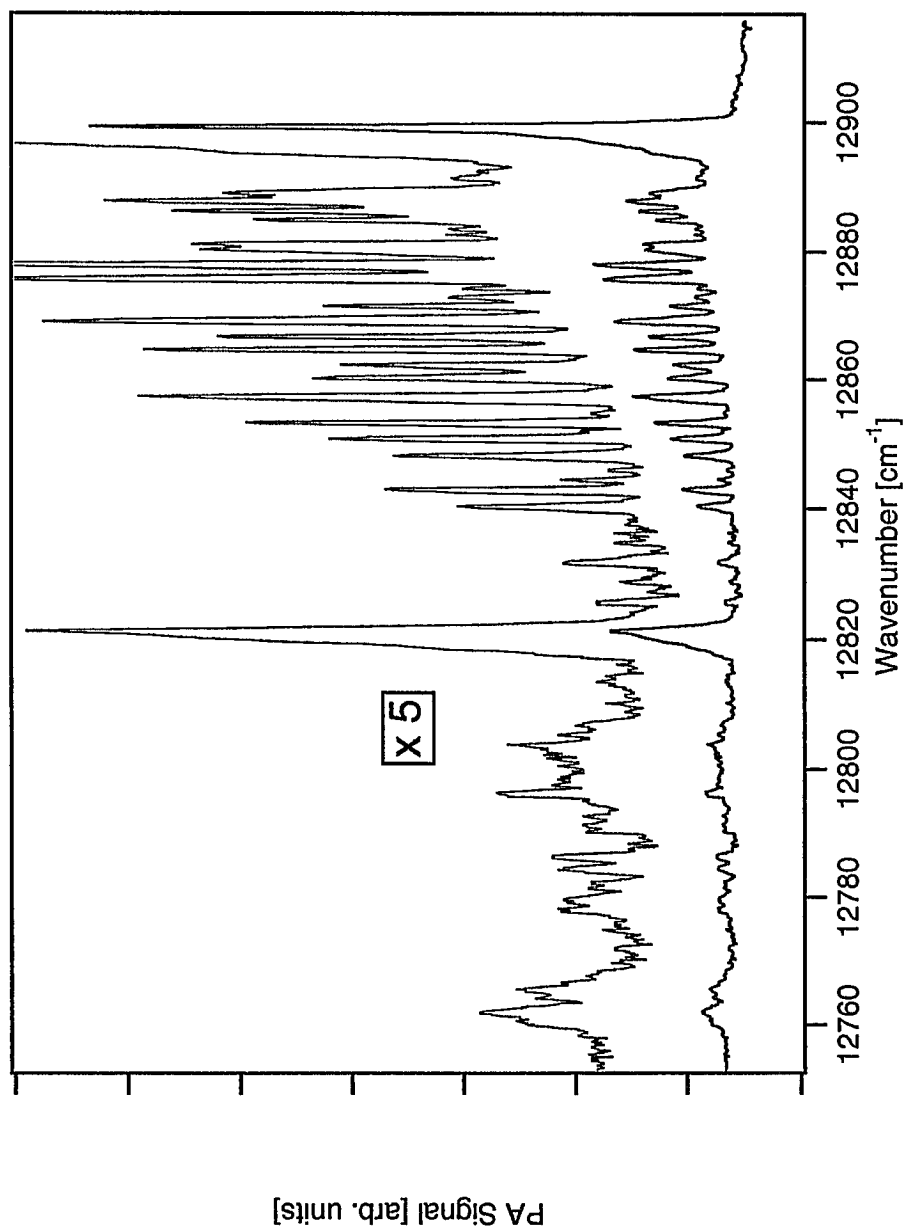


Figure IV-1. The overtone transitions of N₂O near 12800 cm⁻¹. The top trace is the same spectrum plotted with a factor of five magnification.

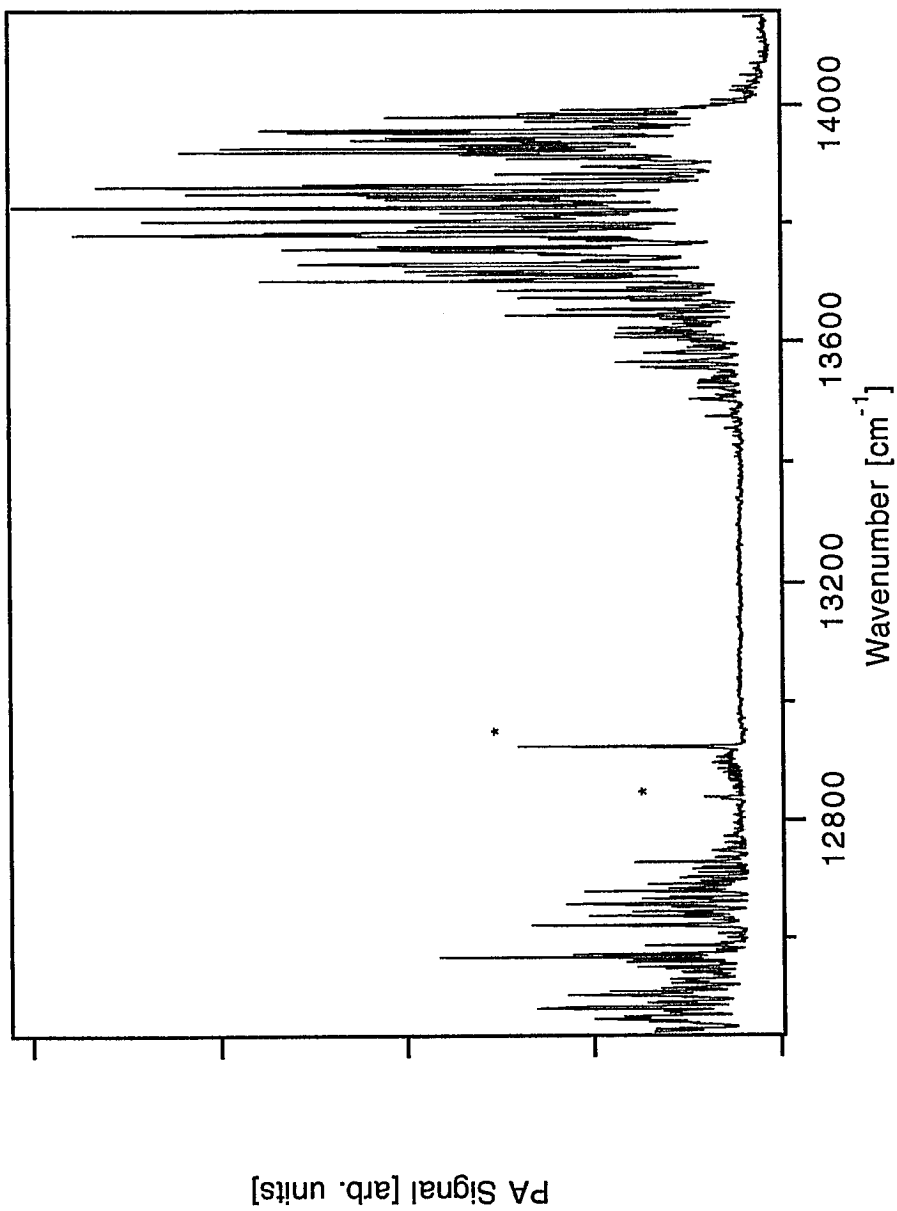


Figure IV-2. The overtone transitions of N₂O (with bandheads indicated by asterisks and water. The vapor pressure of N₂O and water are 1.0 atm and 20 Torr, respectively.

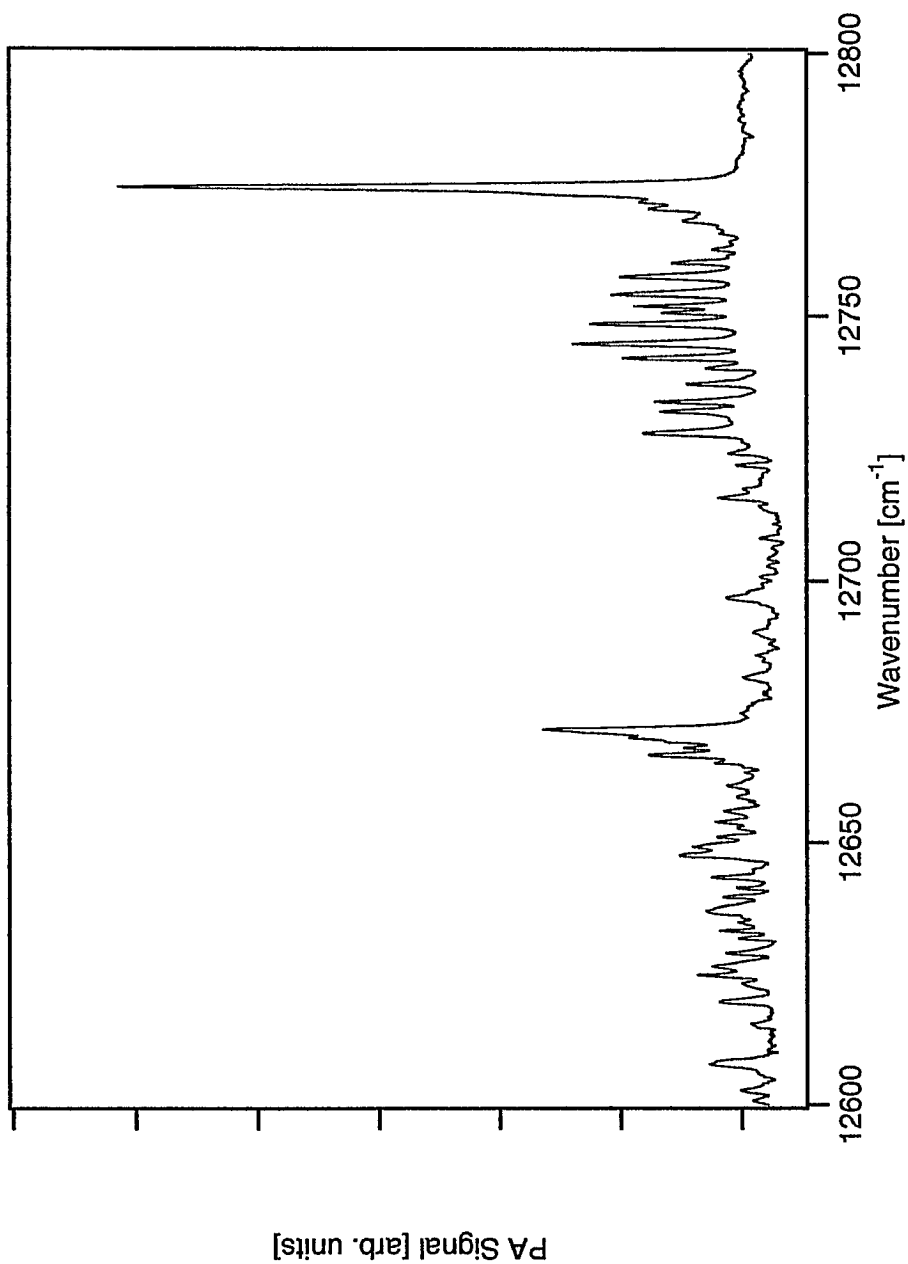


Figure IV-3. The overtone transitions of CO₂ near 12700 cm⁻¹

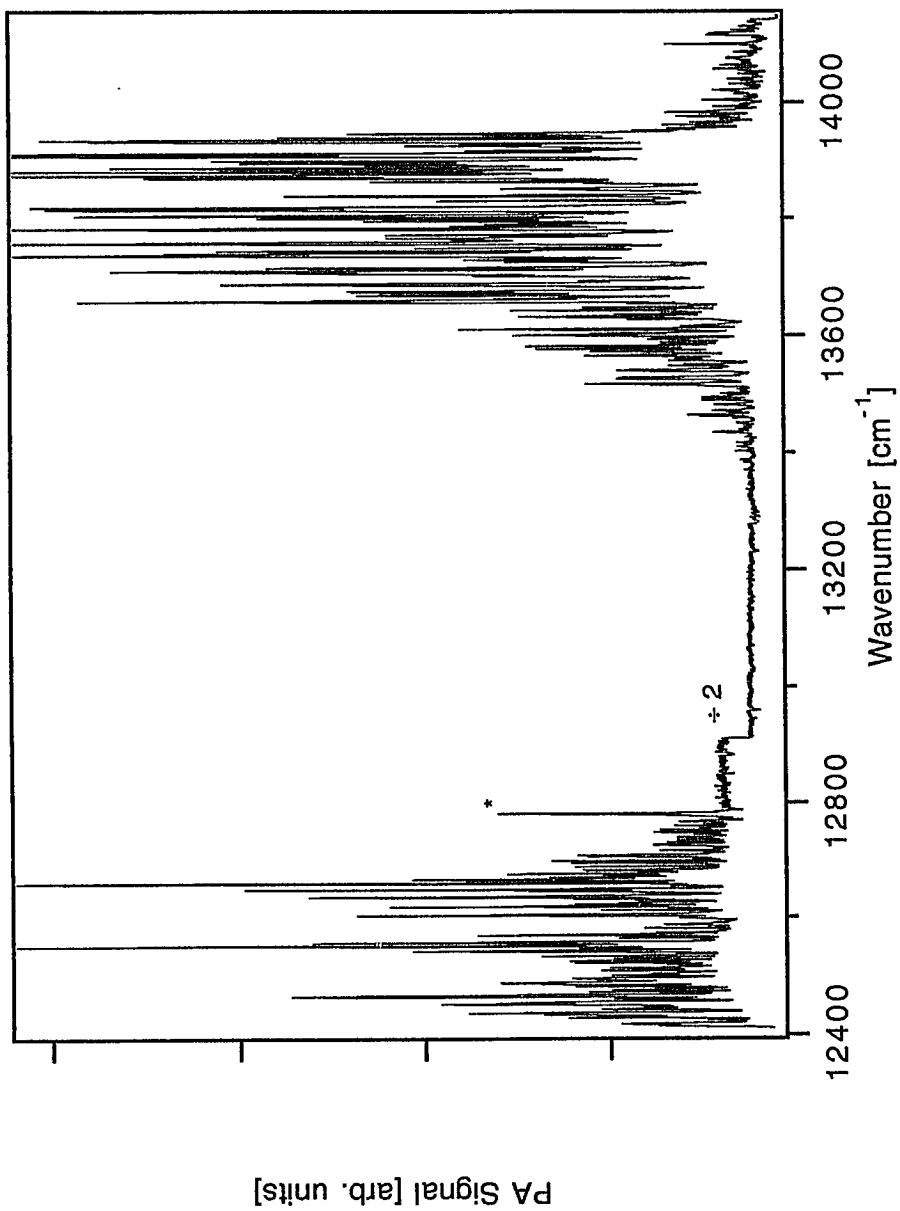


Figure IV-4. The overtone transitions of CO_2 (with band head indicated by an asterisk) and water. The CO_2 overtone band at 12682 cm^{-1} is masked by the water band. The vapor pressure of CO_2 and water are 1.0 atm and 20 Torr, respectively.

CHAPTER V

OCS OVERTONE TRANSITIONS IN THE NEAR INFRARED

V-1 Introduction

OCS has been one of those molecules which are of astrophysical, spectroscopic and chemical interest [1]. The study of infrared transitions of OCS started in 1932 [2], and since then there have been many investigations on both the fundamentals and overtone transitions [3-15]. Before this work, however, the highest observed overtone transition of OCS was $\nu_1+3\nu_3$ band which has a transition energy of 6955.0 cm^{-1} [12]. The overtone transitions of this molecules in the near infrared, due to low fundamental frequencies, involve large change in vibrational quantum number compared with the overtone transitions involving a hydrogen atom. As a consequent result, the transition intensities are extremely weak so that the conventional spectroscopic methods cannot be used to detect these signals.

During the period of late 40's and early 50's, long absorbing path experimental apparatus were developed, and vibrational overtone transitions of heavy-atom molecules like CO [16], CO₂ [17] and N₂O [18], in the near infrared were studied. However, due to the long path length of the sample chamber, huge amount of sample was required. Take the CO₂ case as an example: the largest sample required for the long absorbing path experiment was 10000 liters under atmospheric pressure. Because of the limitation like this, overtone studies on molecules such as OCS in the near infrared were not

explored. With the development of laser techniques and high sensitivity detection methods, the direct detection of such weak overtone transitions become possible.

In our previous investigations for the overtone transitions of CO₂ and N₂O [19], it was demonstrated that these weak transitions could be detected directly by using the intracavity photoacoustic technique with a sample size about 10 milliliters. In this chapter, a study of OCS overtone transitions in the near infrared is presented. A total of fourteen transitions recorded for the first time in the spectral range of 10000-14000 cm⁻¹. The band head positions were measured and band origins were determined. Assignments of the transitions were also carried out by employing the molecular parameters from Ref. [12]. The differences between the measured and the calculated positions are found to be within our experimental accuracy.

V-2 Experimental

(A) Laser System

The laser system is basically the same as described in the previous chapter except that three sets of optics were used to extend the spectral range from 700 - 800 nm to 700 - 960 nm. Briefly, a broad-band titanium:sapphire ring laser (Coherent 899-01) was pumped by a multiline Ar⁺ laser (Coherent 70-5). With 5 W pumping power, the short wavelength optics set delivers a spectral range of 700 - 800 nm and a emerging peak power about 30 mW. With the same pumping power, the middle wavelength optics supplies two spectral ranges, one is 760 - 808 nm with a peak power about 20 mW and the other 805 - 918 nm with a peak power about 15 mW. With 7 Watt pumping power, the

long wavelength optics delivers a spectral range of 900 - 960 nm with a peak power about 75 mW. Throughout the experiments, high reflectors instead of output couplers were used in order to increase the power in the laser cavity. With a standard output coupler and the short wavelength optics, the bandwidth of the laser was of the order of 0.2 cm^{-1} , and it was expected to be broader with high reflectors installed for the whole spectral ranges. The frequency of the laser was scanned by tilting an intracavity birefringent filter with stepper motor (Oriel, model 18510) Typical scan rate is about $50 \text{ cm}^{-1}/\text{min}$.

(B). Calibration

Instead of a spectrophotometer in our previous work (see previous chapter), a wavemeter (Burleigh, WA-20VIS) was used to measure the laser wavelength and this provided a uncertainty of 0.1 cm^{-1} . The same procedure [18] was performed to convert the stepper motor position into wavelength. The relative intracavity laser power is monitored by a photodiode (EG&G Ortec, UV-100) placed near a laser beam to intercept scattered laser light. The signal from the photodiode is fed to a lock-in amplifier (Princeton Applied Research, Model 5101).

(C). Experimental Conditions

The sample cell was evacuated on a vacuum line pumped by an oil diffusion pump with a background pressure of several millitorrs. A mechanical pressure gauge (Omega) was used to monitor the sample pressure with an accuracy of 5%.

The carbonyl sulfide gas (Matheson Gas Products) was then introduced to the photoacoustic cell which was described before [4]. One atm of the sample gas

was used without any buffer gas. In order to minimize water contamination in the spectral range, the sample was passed through a P₂O₅ trap before introduced to the photoacoustic cell.

The sample cell was placed inside the cavity of the titanium:sapphire ring laser. It was found that the output laser power will decrease about 25% after the installation of the sample cell. The Ar⁺ pumping laser was modulated with a mechanical chopper (Stanford Research System, SR540) which was tuned to the acoustic resonance frequency of the sample cell to obtain maximum sensitivity. Typical chopper frequency was about 700 Hz. Single microphone was used in the sample cell. A 9-Volte DC battery was used as the power source of the microphone and its signal was fed to a lock-in amplifier (Stanford Research Systems, SR510). Great care was taken to shield the connections between the microphone and the power box. No pre-amplifier was used. For the scan rate given above, a typical time constant of 3 seconds was used. In order to perform fine tuning of the chopping frequency and the phase of the lock-in, the laser frequency was set on an intense transition and the signal was then maximized. The whole set-up was controlled by a microcomputer system (Apple II and Macintosh Plus).

V-3 Analysis

A global ro-vibrational analysis of carbonyl sulfide has been performed by Fayt and co-workers [12] for transition energies bellow 5000 cm⁻¹. In their analysis, all interaction terms in the Hamiltonian, such as anharmonic l-type, Stark, and polarizability, were taken into account in a one step diagonalization procedure. A total of 66 zero field molecular parameters were

deduced. We used their molecular parameters and Hamiltonian and extended from energy levels below 5000 cm⁻¹ to energy levels between 10000 - 14000 cm⁻¹. Considering our experimental accuracy, simplifications and modification were made on the Hamiltonian. Basically, only the strong interactions terms were taken into account for the calculation. First, the rotational l-type resonance interactions were eliminated. Secondly, only the J=0 states were taken into account for the calculation. Third, the Hamiltonian were divided into sub-matrices, and each of which contains all states with a the same superpolyad quantum number [20], N= 2v₁+ v₂ + 4v₃. Then the matrix corresponding to a superpolyad quantum number was diagonalized and the energy levels referred to the ground state were obtained. According to Fayt and co-workers [12], the Hamiltonians have the following terms:
The vibrational diagonal term:

$$\begin{aligned} & \langle v_1 v_2^l v_3 \parallel v_1 v_2^l v_3 \rangle \\ & = \sum_i \omega_i^0 v_i + \sum_{i \leq j} x_{ij}^0 v_i v_j + x_{ll}^0 l^2 + \sum_{i \leq j \leq k} y_{ijk}^0 v_i v_j v_k + \sum_i y_{iii} v_i l^2 + z_{2222} v_2^4 \end{aligned}$$

The first-order anharmonic resonance between v₁ and 2v₂:

$$\begin{aligned} & \langle v_1 v_2^l v_3 \parallel v_1-1, v_2+2^l, v_3 \rangle \\ & = \frac{1}{2} \left\{ v_1 \left[(v_2 + 2)^2 - l^2 \right] \right\}^{1/2} \left\{ w_{122} + \lambda_1 (v_1 - 1) + \lambda_2^0 v_2 + \lambda_3 v_3 + \lambda_{22} v_2^2 - l^2 \right\} \end{aligned}$$

The first-order anharmonic resonance between 2v₁ and v₃:

$$\langle v_1 v_2^l v_3 \parallel v_1-2, v_2^l v_3+1 \rangle$$

$$= \left\{ \frac{1}{2} v_1(v_1+1)(v_3+1) \right\}^{1/2} \left\{ \frac{1}{2} k_{113} + \lambda_1 \left(v_1 + \frac{1}{2} \right) + \lambda_2 \left(v_2 + \frac{1}{2} \right) + \lambda_3 (v_3+1) - I^2 \right\}$$

The second-order anharmonic resonance between v_1+2v_2 and v_3 :

$$\langle v_1 v_2^1 v_3 \parallel v_1-1, v_2-2^1, v_3+1 \rangle$$

$$= \frac{1}{2} k_{1223} \left\{ v_1(v_2^2 - I^2)(v_3+1) \right\}^{1/2}$$

The third order anharmonic resonance between $4v_2$ and v_3

$$\langle v_1 v_2^1 v_3 \parallel v_1, v_2-4^1, v_3+1 \rangle$$

$$= \frac{1}{8} k_{22223} \left\{ (v_2^2 - I^2) \left[(v_2^2 - 2)^2 - I^2 \right] (v_3+1) \right\}^{1/2}$$

A list of the parameters from Ref. [12] used for the construction of the Hamiltonian can found in Table V-1 at the end of this chapter.

Compared with the analysis for CO₂ [21], more off-diagonal terms have to be included for OCS. This is mainly due to the symmetry properties of the two molecules. CO₂ belongs to the point group D_{∞h} and OCS belongs to the point group C_{∞v}. In the analysis of CO₂, the superpolyads only contain v_1 and v_2 vibrations because v_3 does not joint the interaction due to its different symmetry. However, the symmetry restriction does not exist in OCS, and more interactions have to be considered. Consequently, for a given number of excitation, OCS has many more states than that for CO₂. For example, the

$\nu_1+5\nu_3$ polyad of CO₂ contains only two components, and the same polyad for OCS contains 22 components though most of them were not observed.

In order to determine the hot band positions, energy levels corresponding to $l=1$ were calculated. The hot band transition energies were then determined by subtracting the corresponding lower level transition energy from the upper level energies. Assignments were made according to the comparison with the measured positions to the calculated positions.

V-4 Results and Discussions

According to the superpolyad quantum number, the spectra of OCS in our spectral range can be divided into three groups. Each group has a strong band and some other weak satellite bands. The bandhead positions of these strong bands are 10927.0 cm⁻¹, 12033.9 cm⁻¹ and 12867.3 cm⁻¹ for the $\nu_1+5\nu_3$, $6\nu_3$ and $\nu_1+6\nu_3$ transitions, respectively. This feature of the spectra shows that the main transitions are split due to the perturbations of some other states. For example, the $6\nu_3$ band is accompanied by several weaker transitions. Even though the rotational structures are not resolved, all the main bands show P and R band (as a bandhead) profiles as expected for a Σ - Σ transition from a linear molecule.

Figure V-1 shows the transitions with the superpolyad quantum $N=22$, which contains 42 states. Due to the strong water interference in this region, only three transitions were identified with confidence. They are the $\nu_1+5\nu_3$, its hot band and $\nu_1+4\nu_2+4\nu_3$ transitions. The positions and assignments for those bands are given in Table V-2. Note that the notations for the

transitions of OCS are analogous to those used for CO₂ (see Appendix for explanation).

The transitions with N=24 are shown in Figure V-2. A total of five transitions were identified including one hot band. The strongest transition in this group is the 6v₃ band which shows a well defined rotational structure. Two of the transitions on the lower energy side to the 6v₃ band are strong enough to show P and R rotational structure. The assignments and transition energies of those bands are given in Table V-3.

Figure V-3 is a spectrum in the short wavelength region of our spectral range. This group of transitions belong to the superpolyad quantum N=26. The degeneracy of the Hamiltonian matrix associated with this quantum number is 56. A total of six transitions were identified including one hot band which is associated with the v₁+6v₃ transition. The strongest band in this group is the v₁+6v₃ transition which shows the expected rotational structure. The positions and assignments for those transitions are given in Table V-4.

Since the measured positions for all the bands are bandhead positions and the calculated positions are band origins, a rotational structure simulation was carried out to calculate the bandhead positions relative to the band origins. Then the calculated head positions are subtracted from the corresponding measured positions to give band origins. An enlargement of the 6v₃ transition and its simulation are shown in Figure V-4 and Figure V-5. The computer program for the simulation is listed at the end of this chapter. The molecular parameters for those simulations can also be found in Table V-1.

The intensities of the v₁+5v₃ and 6v₃ transitions are very similar and that of the v₁+6v₃ transition is about 10 times weaker than those of the 6-

quantum ones. These intensity comparison was made just by visual estimation without the laser power normalization.

It is interesting to compare the spectra of OCS to that of CO₂. The most distinguish feature between the spectra of OCS and that of CO₂ is the complexity caused by different interactions within the molecules. Since CO₂ belongs to the point group D_{∞h}, only the ν_1 and ν_2 vibrations may interact each other and this defines the number of bands for a given polyad, such as monad, diad, triad, etc. However, OCS belongs to the point group C_{∞v}, all the three vibrations may interact each other to give more complicated band features. For a given superpolyad, the number of bands observed depends on the intensities of the component transitions. In addition, the even numbered ν_3 transitions are strictly forbidden for CO₂, but they are allowed for OCS.

The position measurements in this study was performed by means of a wavemeter as mentioned in the experimental section and this provided more accurate results than using a spectrophotometer in our previous study. Compared the measured band origins to those calculated values, the average deviation is within our experimental accuracy which is about one cm⁻¹. The differences between the measured and the calculated values for different transitions can be found in the Tables V-2, V-3 and V-4.

Under our resolution, the rotational structure of CO₂ was resolve except the irregularities due to the jitter of the birefringent filler. But the rotational structure of OCS was not resolved at all due to the much smaller rotational constant for OCS. However, the bands for both molecules form bandheads in the R-branches as expected for Σ - Σ transitions of linear molecules.

The water overtone transitions in the spectral range are so strong, even though the P₂O₅ trap was used to reduce the intensities of those water

transitions, they are still there as shown in the spectrum. For the three strong bands this is not a serious problem, however, it is a big threat to the weak transitions, since they could be totally masked by the water transitions. If there were no water interferences, more OCS transitions could have been identified.

V-5 Conclusions

Vibrational overtone transitions of OCS in the 10000 - 14000 cm^{-1} range have been observed for the first time by means of photoacoustic technique. The analysis of the spectra was carried out by using the molecular parameters and Hamiltonian of OCS from the work of Fayt and co-workers [12] and these parameters were derived for the energy levels below 5000 cm^{-1} . It is demonstrated that the molecular parameters of OCS for the low vibrational states can be extended to higher vibrational states. The average deviation is within the experimental accuracy. Due to the symmetry property of this molecule, heavy coupling were observed in the highly excited vibrational states.

REFERENCES

- [1]. M. Winnewiser, General Discussion, *J. Chem. Soc. Farad. Trans. II*, **84**, (1988) 1564
- [2]. C. R. Bailey and A. B. D. Cassie, *Proc. Roy. Soc. London*, **135** (1932) 375
- [3]. C. R. Bailey and A. B. D. Cassie, *Proc. Roy. Soc. London*, **140** (1933) 605
- [4]. P. F. Bartunek and E. F. Barker, *Phys. Rev.*, **48** (1935) 516
- [5]. H. J. Callomon and H. W. Thompson, *Proc. Roy. Soc., A*, **222** (1954) 431
- [6]. A. G. Maki, E. K. Plyer, and E. D. Tidwell, *J. Res Natl. Bur. Std.*, **A 66** (1962) 163
- [7]. A. Fayt, *Ann. Soc. Sci. Bruxelles*, **84** (1970) 69
- [8]. A. Fayt, *Ann. Soc. Sci. Bruxelles*, **86** (1972) 61
- [9]. F. Mayer-Bourbonneux, J. Dupre-Maquaire, and C. Mayer, *J. Mol. Spectrosc.*, **63** (1976) 288
- [10]. J. Walrand, G. Blanquet, and C. P. Courtoy, *J. Mol. Spectrosc.*, **74** (1979) 165
- [11]. A. G. Maki, W. B. Olson, and R. L. Sams, *J. Mol. Spectrosc.*, **81** (1980) 122
- [12]. A. Fayt, R. Vandenhoute, and J. G. Lahaye, *J. Mol. Spectrosc.* **119** (1986) 233
- [13]. J. G. Lahaye, R. Vandenhoute, and A. Fayt, *J. Mol. Spectrosc.* **123** (1987) 48
- [14]. L. S. Masukidi, J. G. Lahaye, and A. Fayt, *J. Mol. Spectrosc.* **148** (1991) 281
- [15]. L. S. Masukidi, J. G. Lahaye, and A. Fayt, *J. Mol. Spectrosc.* **154** (1992) 137
- [16]. G. Herzberg and K. N. Rao, *J. Chem. Phys.*, **17** (1949) 1099
- [17]. G. Herzberg and L. Herzberg, *J. Opt. Soc. Am.*, **43** (1953) 1037
- [18]. G. Herzberg and L. Herzberg, *J. Chem. Phys.*, **18** (1950) 1551

- [19]. X. Yang, C. Petrillo and C. Noda, *Chem. Phys. Lett.* , **214** (1993) 536
- [20]. M. E. Kellman, *J. Chem. Phys.* , **93** (1990) 6630
- [21]. C. P. Courtoy, *Can. J. Phys.*, **35** (1957) 608

LIST OF COMPUTER PROGRAM FOR OCS ENERGY CALCULATIONS

```
REM Calculation of OCS vibrational energy levels
REM This program uses molecular parameters from JMS 119 (1986) 233
REM matrix diagonalization with the same superpolyad quantum number
REM To use just input the superpolyad quantum number and return
REM allocate enough memory if running as a compiled program
IF (SYSTEM(4) = 1) THEN CLEAR ,850000&,1200000&
REM DEFDBL a-z
begintime$=TIME$
DIM w0(3),x(3,3),y(3,3,3), va(3), vb(3)
REM define the matrix to be solved
w0(1)=866.067399#
w0(2)=520.197494#
w0(3)=2071.543051#
x0(1,1)=-2.749686
x0(1,2)=-3.271051
x0(2,2)=.592604
x0(1,3)=-6.492815
x0(2,3)=-7.416281
x0(3,3)=-11.463769#
y0(1,1,1)=.002514
y0(1,1,2)=.022594
y0(1,2,2)=-.04708
y0(2,2,2)=-.00967
y0(1,1,3)=-.079487
y0(1,3,3)=.014733
y0(1,2,3)=.02981
y0(2,2,3)=.07409
y0(2,3,3)=-.032744
y0(3,3,3)=.0124
z2222=.00004459981#
w122=-28.280649#
d1=.696004
d02=.437731
d3=-.509878
d22=.002119
w113=-25.478277#
d1p=-.453263
d2p=.138404
d3p=.788724
k1223=5.964629
k2223=-1.030753

REM subroutine for state selection
REM for OCS the superpolyad is superN=2v1+v2+4v3
REM for a given superN v1 changes from 0 TO superN/2, v2 change from 0 TO q AND v3 from 0
TO q/4
INPUT "superpolyad quantum number"; superN
m=superN
a=m/2
c=m/4
```

```

      *m*c
      qa(size),qb(size),qc(size)

      v1=0 TO a
      v2=0 TO m
      v3=0 TO c
      v1+v2+4*v3
      =superN THEN
      +1
      n)=v1
      n)=v2
      n)=v3
      ND IF
      EXT
      EXT
      NEXT
      PRINT "superN= "; superN
      FOR i=1 TO n
      PRINT qa(i),qb(i),qc(i)
      NEXT
      DIM a(n,n),d(n),v(n,n),b(n),:
      REM INPUT a$
      FOR ia=1 TO n
      FOR ib=1 TO n
      a(ia,ib)=0
      NEXT
      NEXT
      FOR ia=1 TO n
      va(1)=qa(ia)
      va(2)=qb(ia)
      va(3)=qc(ia)
      FOR ib=1 TO n
      vb(1)=qa(ib)
      vb(2)=qb(ib)
      vb(3)=qc(ib)
      REM PRINT vb(1), vb

      REM diagonal term
      IF ia=ib THEN
      sum=0
      FOR i=1 TO 3
      sum=sum+w0(i)*va(i)
      NEXT
      FOR j=1 TO 3
      FOR k=j TO 3
      sum=sum+x0(j,k)*v2
      NEXT
      NEXT

      FOR i=1 TO 3
      FOR j=i TO 3
      FOR k=j TO 3
      sum=sum+y0(i,j,k)
      NEXT

```



```

size=a*m*c
DIM qa(size),qb(size),qc(size)
n=0
FOR v1=0 TO a
FOR v2=0 TO m
FOR v3=0 TO c
s=2*v1+v2+4*v3
IF s=superN THEN
n=n+1
qa(n)=v1
qb(n)=v2
qc(n)=v3
END IF
NEXT
NEXT
NEXT
PRINT "superN= "; superN, "number of states= "; n
FOR i=1 TO n
PRINT qa(i),qb(i),qc(i)
NEXT
DIM a(n,n),d(n),v(n,n),b(n),z(n)
REM INPUT a$
FOR ia=1 TO n
FOR ib=1 TO n
a(ia,ib)=0
NEXT
NEXT
FOR ia=1 TO n
va(1)=qa(ia)
va(2)=qb(ia)
va(3)=qc(ia)
FOR ib=1 TO n
vb(1)=qa(ib)
vb(2)=qb(ib)
vb(3)=qc(ib)
REM PRINT vb(1), vb(2), vb(3)

REM diagonal term
IF ia=ib THEN
sum=0
FOR i=1 TO 3
sum=sum+w0(i)*va(i)
NEXT
FOR j=1 TO 3
FOR k=j TO 3
sum=sum+x0(j,k)*va(j)*va(k)
NEXT
NEXT

FOR i=1 TO 3
FOR j=i TO 3
FOR k=j TO 3
sum=sum+y0(i,j,k)*va(i)*va(j)*va(k)
NEXT

```

```

NEXT
NEXT
a(ia,ib)=sum+z2222*va(2)^4
END IF
REM PRINT a(ia,ib)
REM first-order anharmonic resonance between v1 and 2v2
IF (vb(1)=va(1)-1) AND (vb(2)=va(2)+2) AND (vb(3)=va(3)) THEN
temp=w122+d1*(va(1)-1)+d02*va(2)+d3*va(3)+d22*va(2)*va(2)
a(ia,ib)=.5*SQR(va(1)*(va(2)+2)^2)*(temp)
a(ib,ia)=a(ia,ib)
END IF

REM first-order anharmonic resonance between 2v1 and v3
IF (vb(1)=va(1)-2) AND (vb(2)=va(2)) AND (vb(3)=va(3)+1) THEN
temp=w113+d1p*(va(1)-1)+d2p*va(2)+d3p*va(3)
a(ia,ib)=SQR(1/2*va(1)*(va(1)-1)*(va(3)+1))*(temp)
a(ib,ia)=a(ia,ib)
REM PRINT a(ia,ib),a(ib,ia)
END IF

REM second-order anharmonic resonance between v1+2v2 and v3
IF (vb(1)=va(1)-1) AND (vb(2)=va(2)-2) AND (vb(3)=va(3)+1) THEN
a(ia,ib)=.5*k1223*SQR(va(1)*va(2)*va(2)*(va(3)+1))
a(ib,ia)=a(ia,ib)
REM PRINT a(ia,ib),a(ib,ia)
END IF

REM third-order anharmonic resonance between 4v2 AND v3
IF (vb(1)=va(1)) AND (vb(2)=va(2)-4) AND (vb(3)=va(3)+1) THEN
a(ia,ib)=1/8*k22223*SQR(va(2)*va(2)*(va(2)-2)^2*(va(3)+1))
a(ib,ia)=a(ia,ib)
REM PRINT a(ia,ib)
END IF
NEXT
NEXT

PRINT "JACOBI called"
IF kdb=1 THEN
OPEN "matrix elements" FOR OUTPUT AS 2
FOR i=1 TO n
FOR j=1 TO n
WRITE #2, qa(i), qb(i), qc(i), qa(j), qb(j), qc(j), a(i,j)
NEXT
NEXT
CLOSE 2
END IF
CALL jacobi(a(), n, np, d(), v(), b(), z(), nrot)
REM print solution
PRINT "Eigenvalues"
REM sorted eigenvalues and states
FOR i = 1 TO n
min=d(i)
jmin=i
FOR j=i+1 TO n

```

```

IF d(j)<min THEN
min=d(j)
jmin=j
END IF
NEXT
SWAP d(i), d(jmin)
SWAP qa(i), qa(jmin)
SWAP qb(i), qb(jmin)
SWAP qc(i), qc(jmin)
PRINT qa(i), qb(i), qc(i), d(i)
FOR j=1 TO n
SWAP v(i,j), v(jmin,j)
NEXT
FOR j=1 TO n
SWAP v(j,i), v(j,jmin)
NEXT
NEXT
endtime$=TIME$
INPUT a$
f$=FILES$(0)
IF f$<>""THEN
OPEN f$ FOR OUTPUT AS 1
PRINT #1, "OCS Matrix 042392a", DATE$
PRINT #1, "superN= "; m
PRINT #1, "# of all states= ",n
PRINT #1, "Started at ", begintime$
PRINT #1, "Finished at ", endtime$
PRINT #1, "Emin = ", emin
PRINT #1, "Emax = ", emax
PRINT #1, "Molecular Parameters"
PRINT #1, "w0(1)=", w0(1)
PRINT #1, "w0(2)=",w0(2)
PRINT #1, "w0(3)=", w0(3)
FOR i= 1 TO 3
FOR j= i TO 3
PRINT #1, "i, j, x0(i,j)"; i; j; x0(i, j)
NEXT
NEXT
FOR i= 1 TO 3
FOR j= i TO 3
FOR k= j TO 3
PRINT #1, "i, j, k, y0(i, j, k)"; i; j; k; y0(i, j, k)
NEXT
NEXT
NEXT
PRINT #1, "z2222", z2222
PRINT #1, "w122 = ", w122
PRINT #1, "d1=", d1
PRINT #1, "d02=", d02
PRINT #1, "d3 = ", d3
PRINT #1, "d22=", d22
PRINT #1, "w113=",w113
PRINT #1, "d1p=", d1p
PRINT #1, "d2p=", d2p

```

```

PRINT #1, "d3p=", d3p
PRINT #1, "k1223=", k1223
PRINT #1, "k22223=", k22223
FOR i=1 TO n
PRINT #1, i, qa(i),qb(i),qc(i), d(i)
NEXT
PRINT #1, "E is the eigenvalue, and v is the interaction overlap"
FOR i=1 TO n
PRINT #1, "i= "; i
PRINT #1, qa(i),qb(i),qc(i), "E= ";d(i)
FOR j=1 TO n
IF ABS (v(i,j))>.1 THEN
PRINT #1, qa(j), qb(j), qc(j), "v= ";v(i,j)
END IF
NEXT
NEXT
END IF
CLOSE 1
END
SUB jacobi(a(), n, np, d(), v(), b(), z(), nrot) STATIC
REM eigenvalue solver using JACOBI method
REM translated from Fortran (Numerical Recipes)
FOR ip = 1 TO n
FOR iq = 1 TO n
v(ip, iq) = 0
NEXT
v(ip,ip)=1
b(ip)=a(ip,ip)
d(ip)=b(ip)
z(ip)=0
NEXT
nrot = 0
FOR i = 1 TO 50
sm = 0!
FOR ip = 1 TO n-1
FOR iq = ip+1 TO n
sm=sm+ABS(a(ip,iq))
NEXT
NEXT
IF (sm = 0!) THEN EXIT SUB
IF (i < 4) THEN
tresh = .2 * sm /n^2
ELSE
tresh = 0
END IF
FOR ip = 1 TO n-1
FOR iq = ip+1 TO n
g=100!*ABS(a(ip, iq))
IF ((i > 4) AND (ABS(d(ip))+g = ABS(d(ip))) AND (ABS(d(iq))+g = ABS(d(iq)))) THEN
a(ip,iq)=0
ELSEIF(ABS(a(ip, iq)) > tresh) THEN
h=d(iq)-d(ip)
IF (ABS(h)+g = ABS(h)) THEN
t = a(ip,iq)/h

```

```

ELSE
theta=.5*h/a(ip, iq)
t = 1!/(ABS(theta)+SQR(1+theta^2))
IF (theta < 0) THEN t=-t
END IF
c=1!/SQR(1+t^2)
s=t*c
tau=s/(1+c)
h=t*a(ip,iq)
z(ip)=z(ip)-h
z(iq)=z(iq)+h
d(ip)=d(ip)-h
d(iq)=d(iq)+h
a(ip,iq)=0
FOR j=1 TO ip-1
g=a(j,ip)
h=a(j,iq)
a(j,ip)=g-s*(h+g*tau)
a(j,iq)=h+s*(g-h*tau)
NEXT
FOR j=ip+1 TO iq-1
g=a(ip,j)
h=a(j,iq)
a(ip,j)=g-s*(h+g*tau)
a(j,iq)=h+s*(g-h*tau)
NEXT
FOR j=iq+1 TO n
g=a(ip,j)
h=a(iq,j)
a(ip,j)=g-s*(h+g*tau)
a(iq,j)=h+s*(g-h*tau)
NEXT
FOR j = 1 TO n
g=v(j,ip)
h=v(j,iq)
v(j,ip)=g-s*(h+g*tau)
v(j,iq)=h+s*(g-h*tau)
NEXT
nrot=nrot+1
END IF
NEXT
NEXT
NEXT
FOR ip=1 TO n
b(ip)=b(ip)+z(ip)
d(ip)=b(ip)
z(ip)=0
NEXT
NEXT
END SUB

```

LIST OF COMPUTER PROGRAM FOR ROTATIONAL STRUCTURE SIMULATION OF OCS

```

REM this is the simulation program of the OCS rotational structure
REM the molecular constants are from the work of Fayt and co-workers
INPUT "Enter FWHM ", fwhm
INPUT "Enter 1 to see plot after each peak ", viewflag
interval = 1
jmax =100
nshape = fwhm*12/interval
nshape2 = nshape/2
DIM eu(jmax), el(jmax)
INPUT "Enter v1 ", v1
INPUT "Enter v2 ", v2
INPUT "Enter v3 ", v3
CALL calparm(v1,v2,v3, bv, dv, hv)
CALL calparm(0!, 0!, 0!, b000,d000,h000)
PRINT "B, D, H= ", bv,dv,hv
PRINT "B0, D0, H0= ", b000,d000,h000
jmax=0
FOR j=jmin TO jmax
fj=j*(j+1)
eu(j)=bv*fj-dv*fj*fj+hv*fj*fj*fj
el(j)=b000*fj-d000*fj*fj+h000*fj*fj*fj
NEXT
npeak=2*jmax
DIM position(npeak), intensity(npeak), shape(nshape)
FOR i=1 TO jmax
position(i)=eu(i)-el(i-1)
position(i+jmax)=eu(i-1)-el(i)
intensity(i)=(2*i+1)*EXP(-el(i)/208)
intensity(i+jmax)=intensity(i)
NEXT
minpos=1E+10
maxpos=-1E+10
FOR i=1 TO npeak
IF minpos>position(i) THEN minpos=position(i)
IF maxpos<position(i) THEN maxpos=position(i)
NEXT
numpoints=(maxpos-minpos)/interval+fwhm/interval*20
minpos=minpos-fwhm*10
DIM x(numpoints), y(numpoints)
parm=fwhm^2/4
FOR i=0 TO nshape
z=i*interval - fwhm*6
shape(i) = 1/(z*z+parm)
NEXT
FOR i=0 TO numpoints
x(i)=minpos + i*interval
y(i)=0
NEXT
FOR j=1 TO npeak
peakcenter=(position(j)-minpos)/interval

```

```

peakwidth = fwhm/interval
intj=intensity(j)
IF (peakcenter - nshape2<0) THEN GOTO skippeak
IF (peakcenter + nshape2 > numpoints) THEN GOTO skippeak
FOR i=peakcenter-nshape2 TO peakcenter+nshape2
y(i)=y(i)+intj*shape(i-peakcenter+nshape2)
NEXT
IF (viewflag =1) THEN
CALL plotxy(x(),y(), numpoints)
ELSE
PRINT j
END IF
skippeak:
NEXT
REM band head
peakmax=0
FOR i=1 TO numpoints
IF (peakmax<y(i)) THEN
peakmax=y(i)
index=i
END IF
NEXT
IF (viewflag<>1) THEN CALL plotxy(x(),y(), numpoints)
CALL printfile(x(),y(), numpoints)
INPUT h$
END

```

```

SUB calparm(v1,v2,v3,b,d,h) STATIC
b0=.2028567
alpha1=.00067165179#
alpha2=-.0003547811#
alpha3=.00123848127#
gamma11=-.0000030641#
gamma12=-.0000025716#
gamma13=.0000069667#
gamma22=-.00000396802#
gamma23=.0000105179#
gamma33=-.00000289195#
gammaLL=.00000229086#
e222=-.00000001500094#
d0=.00000004341158#
beta1=.00000000033154#
beta2=.00000000070203#
beta3=-.00000000036001#
beta22=-2.43432D-12
lq=0
b=b0-alpha1*v1-alpha2*v2-alpha3*v3+gamma11*v1^2+gamma12*v1*v2
b=b+gamma13*v1*v3+gamma22*v2^2+gamma23*v2*v3+gamma33*v3^2
b=b+gammaLL*lq^2+e222*v2^3
d=d0+beta1*v1+beta2*v2+beta3*v3+beta22*v2^2
h=-2.579284D-15
END SUB

```

```

REM SUB plotxy(x(), y(), ndata) STATIC

```

```

start=1
scrbotom = 250
scrtop=20
scrleft=20
scrright=450
xmin=1E+10
xmax=-1E+10
ymax=-1E+10
ymin=0
FOR i=start TO ndata
IF (xmin>x(i)) THEN xmin=x(i)
IF (xmax<x(i)) THEN xmax=x(i)
IF (y(i)>ymax) THEN ymax=y(i)
NEXT
IF ymin=ymax THEN ymax=ymin+100
CLS
LINE (scrleft, (scrtop)-(scrright, scrbotom),b
CALL MOVETO(scrleft, scrbotom+12)
PRINT xmin;
CALL MOVETO(scrright-30, scrbotom+12)
PRINT xmax;
xscale=(xmax-xmin)/(scrright-scrleft)
yscale=(ymax-ymin)/(scrtop-scrbotom)
FOR i=start TO ndata
px=(x(i)-xmin)/xscale+scrleft
py=(y(i)-ymin)/yscale+scrbotom
IF i=start THEN LINE (px,py)-(px,py)
LINE -(px,py)
NEXT
END SUB
SUB printfile(x(),y(), ndata) STATIC
SHARED fwhm, v1,v2,v3,b000,d000,h000,bv,dv,hv,index
f$="OCS "+STR$(fwhm)+" v"+STR$(v1)+STR$(v2)+STR$(v3)
OPEN f$ FOR OUTPUT AS 1
OPEN f$+".info" FOR OUTPUT AS 2
PRINT #2, "FWHM= ", fwhm
PRINT #2, "v1,v2, v3= ";v1;v2;v3
PRINT #2, "B000,D000,H000= "; b000;d000;h000
PRINT #2,"Bv,Dv,Hv= ";bv, dv,hv
PRINT #2, "Bandhead at "; x(index)
CLOSE 2
FOR i=1 TO ndata
WRITE#1, x(i),y(i)
NEXT
CLOSE 1
END SUB

```


Table V-1 Molecular parameters from Ref. 12 for the energy calculation and rotational structure simulations of OCS

ω°_1 866067399	ω°_2 520.197494	ω°_3 2071.543051	x°_{11} -2.749686
x°_{12} -3.271051	x°_{22} 0.592604	x°_{13} -6.492815	x°_{23} -7.416281
x°_{33} -11.463769	x°_{11} -0.164826	y°_{111} 0.002514	y°_{112} 0.022594
y°_{122} -0.047080	y°_{222} -0.007670	y°_{113} -0.079487	y°_{133} 0.014733
y°_{123} 0.029810	y°_{223} 0.07409	y°_{233} -0.032744	y°_{333} 0.012400
y_{111} 0.049578	y_{211} 0.009678	y_{311} -0.055773	z_{222} 4.459981e-05
w_{122} -28.280649	λ_1 0.696004	λ°_2 0.437731	λ_3 -0.509878
w_{113} -25.478277	λ'_1 -0.453263	λ'_2 0.138404	λ'_3 0.788724
k_{1223} 5.964629	k_{22223} -1.030753	λ_j 12.684456e-05	λ'_j -3.511379e-05
B_0 0.20285674167	α°_1 67.165179e-05	α°_2 -35.47811e-05	α°_3 123.848127e-05
γ°_{11} -0.30641e-05	γ°_{12} -0.25716e-05	γ°_{22} -0.396802e-05	γ°_{13} 0.696670e-05
γ°_{23} 1.051790e-05	γ°_{33} -0.289195e-05	γ_{11} 0.229086e-05	ϵ_{222} -1.500094e-08
D_0 4.341158e-08	β°_1 0.033154e-08	β°_2 0.070203e-08	β°_3 -0.036001e-08
β_{22} -0.243432e-11	H_0 -2.579284e-15	q_0 -21.219376e-05	q°_1 0.879601e-05
q°_2 -0.100995e-05	q°_3 -0.179794e-05	q_{11} 51.107360e-08	q_{12} 26.224052e-08
q_{22} -6.487141e-08	q°_j 14.264825e-11	q_{j2} -1.672145e-11	q_{jj} -0.374667e-15
ρ 0.514878e-11	λ_{22} 0.002119		

Table V-2 Assignments and positions of the transitions with polyad quantum number N=22

Assignment	Obs. position [cm ⁻¹]	Cal. position [cm ⁻¹]	Obs. - Cal. [cm ⁻¹]
$\nu_1+5\nu_3$	10927.0	10925.7	1.3
$\nu_1+4\nu_2+4\nu_3$	10941.7	10940.7	1.0
$\nu_1+\nu_2+5\nu_3-\nu_2$	10879..2	10877.4	1.8

Table V-3 Assignments and positions of the transitions with polyad quantum number N=24

Assignment	Obs. position [cm ⁻¹]	Cal. position [cm ⁻¹]	Obs. - Cal. [cm ⁻¹]
2v ₁ +5v ₃	11767.4	11767.0	0.4
v ₁ +2v ₂ +5v ₃	11893.4	11891.4	2.0
v ₂ +6v ₃ -v ₂	11984.1	11983.6	0.5
6v ₃	12033.9	12032.9	1.0
4v ₂ +5v ₃	12062.8	12062.5	0.3

Table V-4 Assignments and positions of the transitions with polyad quantum number N=26

Assignment	Obs. position [cm ⁻¹]	Cal. position [cm ⁻¹]	Obs. - Cal. [cm ⁻¹]
$3\nu_1+8\nu_2+3\nu_3$	12594.0	12593.5	0.5
$2\nu_1+2\nu_2+5\nu_3$	12714.9	12712.3	2.6
$\nu_1+6\nu_3$	12867.3	12867.2	0.1
$\nu_1+\nu_2+6\nu_3-\nu_2$	12812.8	12812.2	0.6
$\nu_1+4\nu_2+5\nu_3$	12884.4	12883.9	0.5
$2\nu_2+6\nu_3$	12995.7	12993.6	2.1

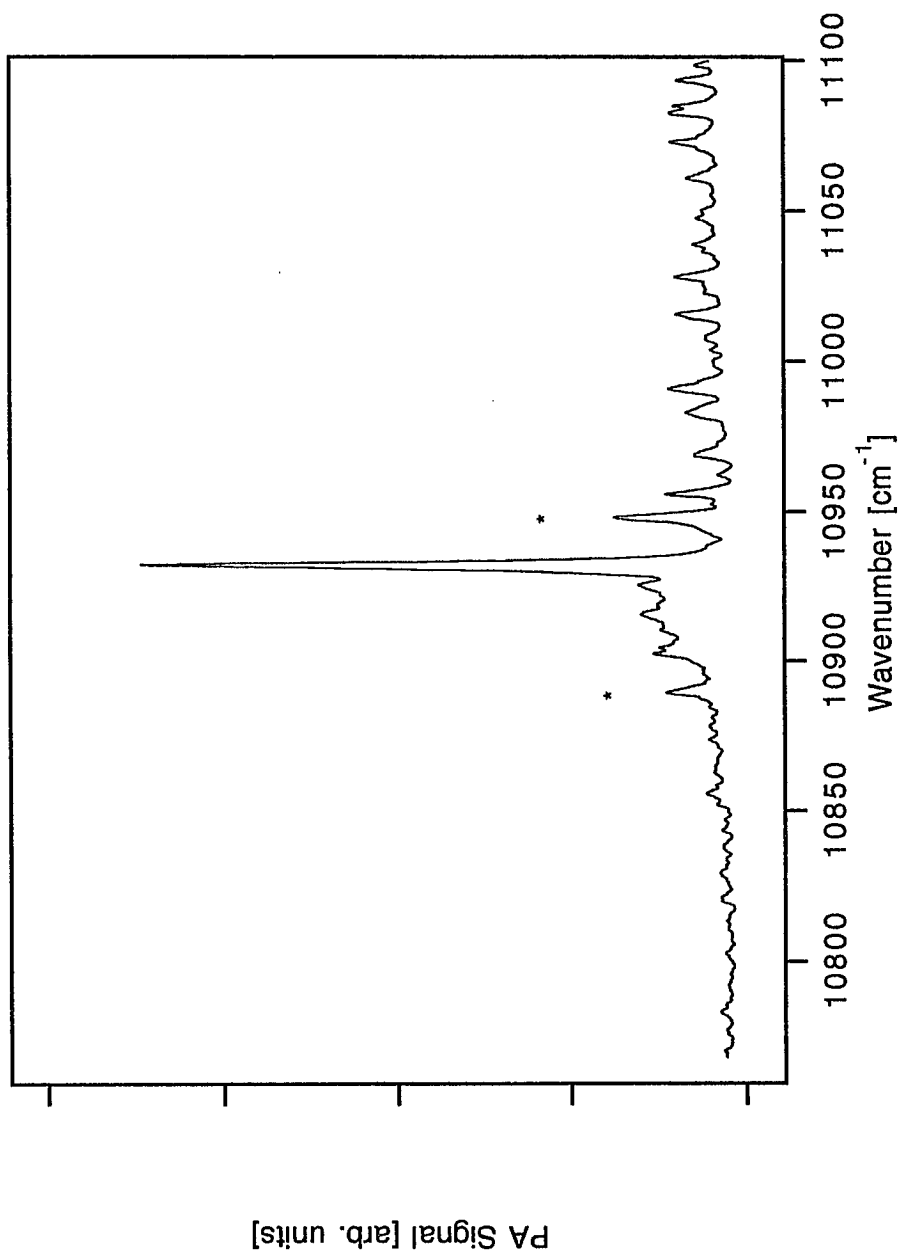


Figure V-1. OCS spectrum with polyad quantum number $N=22$. the strongest is the $\nu_1+5\nu_3$ transition. The weaker bands are indicated with asterisks.

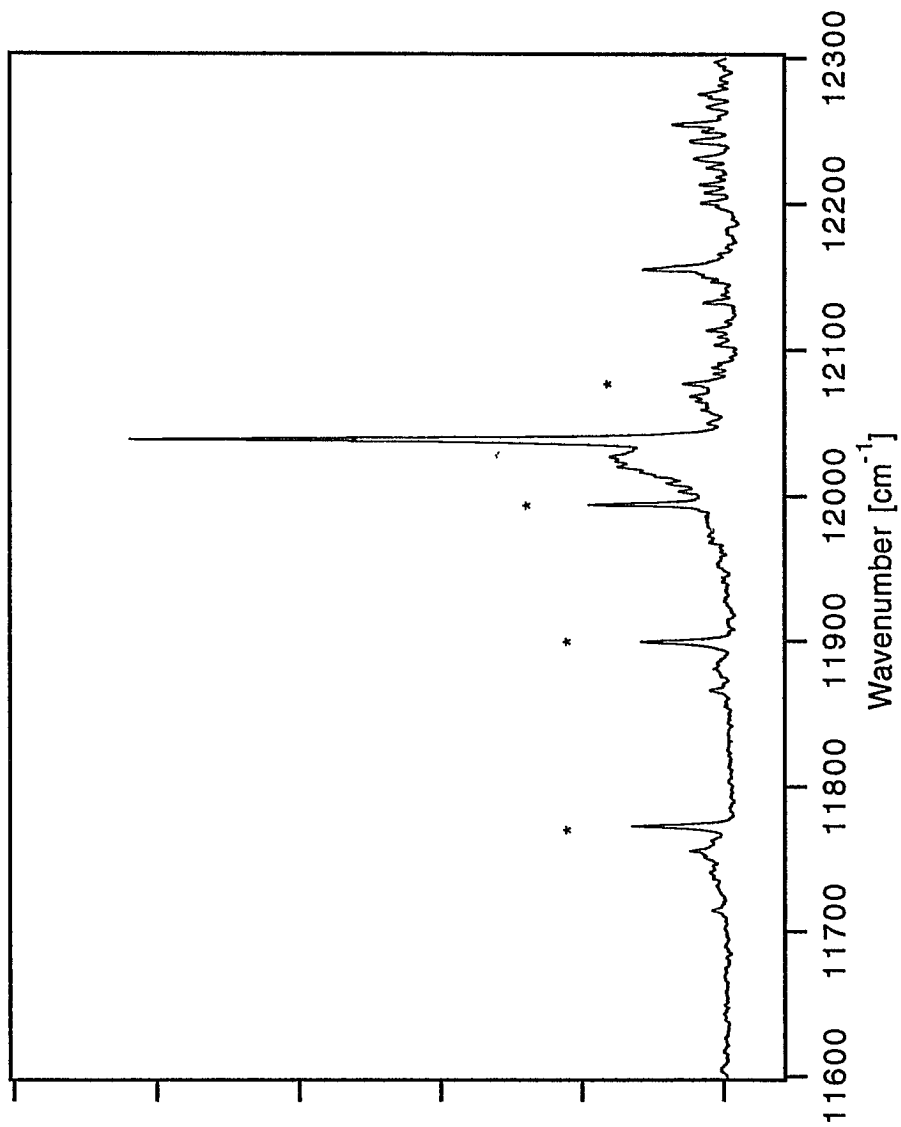


Figure V-2. OCS spectrum with polyad quantum number N=24. The strongest is the 6v₃ transition. All the other weaker bands are indicated with asterisks.

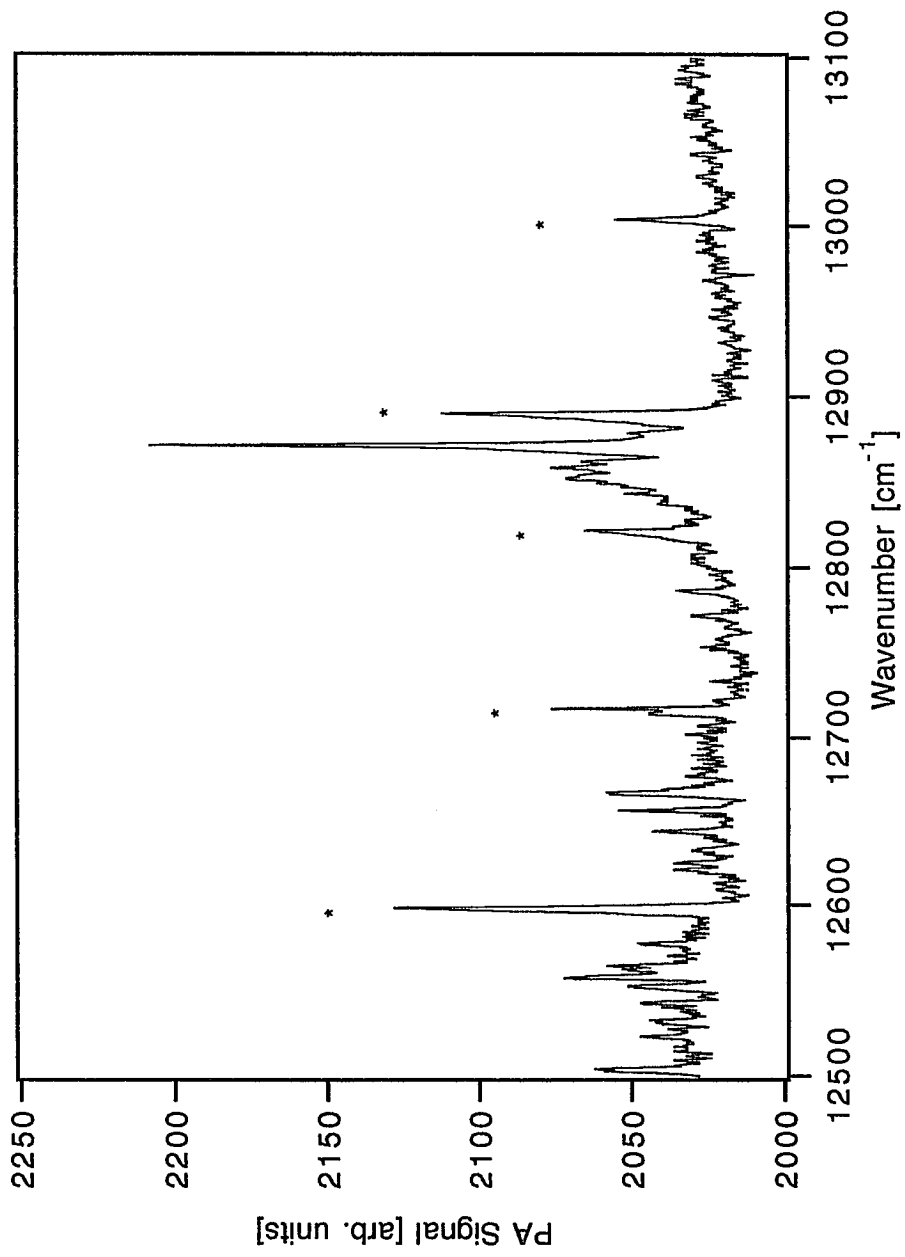


Figure V-3. OCS spectrum with polyad quantum N=26. The strongest is the $\nu_1+\nu_3$ transition. All the other weaker bands are indicated with asterisks.

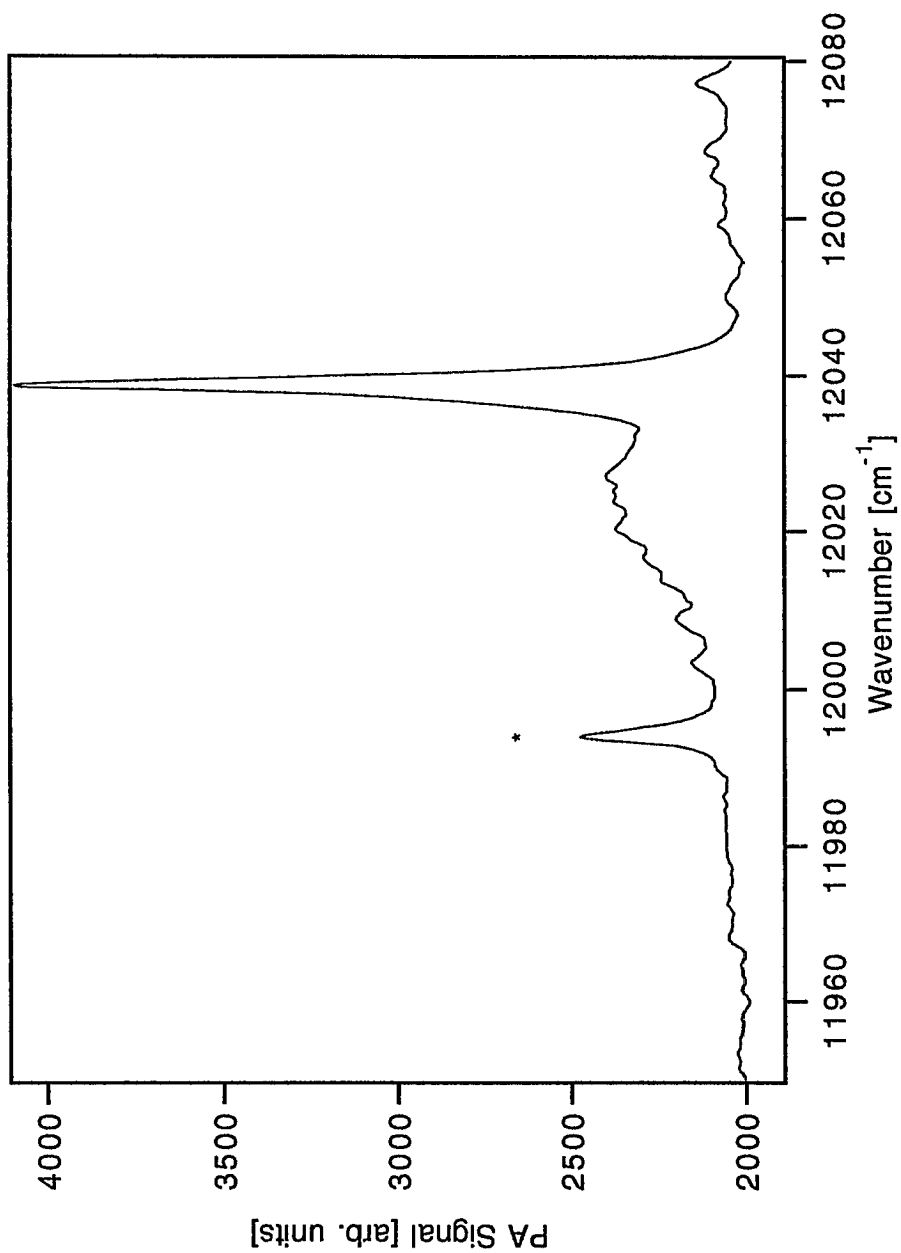


Figure V-4. An enlargement of the ν_3 band of OCS. The hot band is indicated with an asterisk.

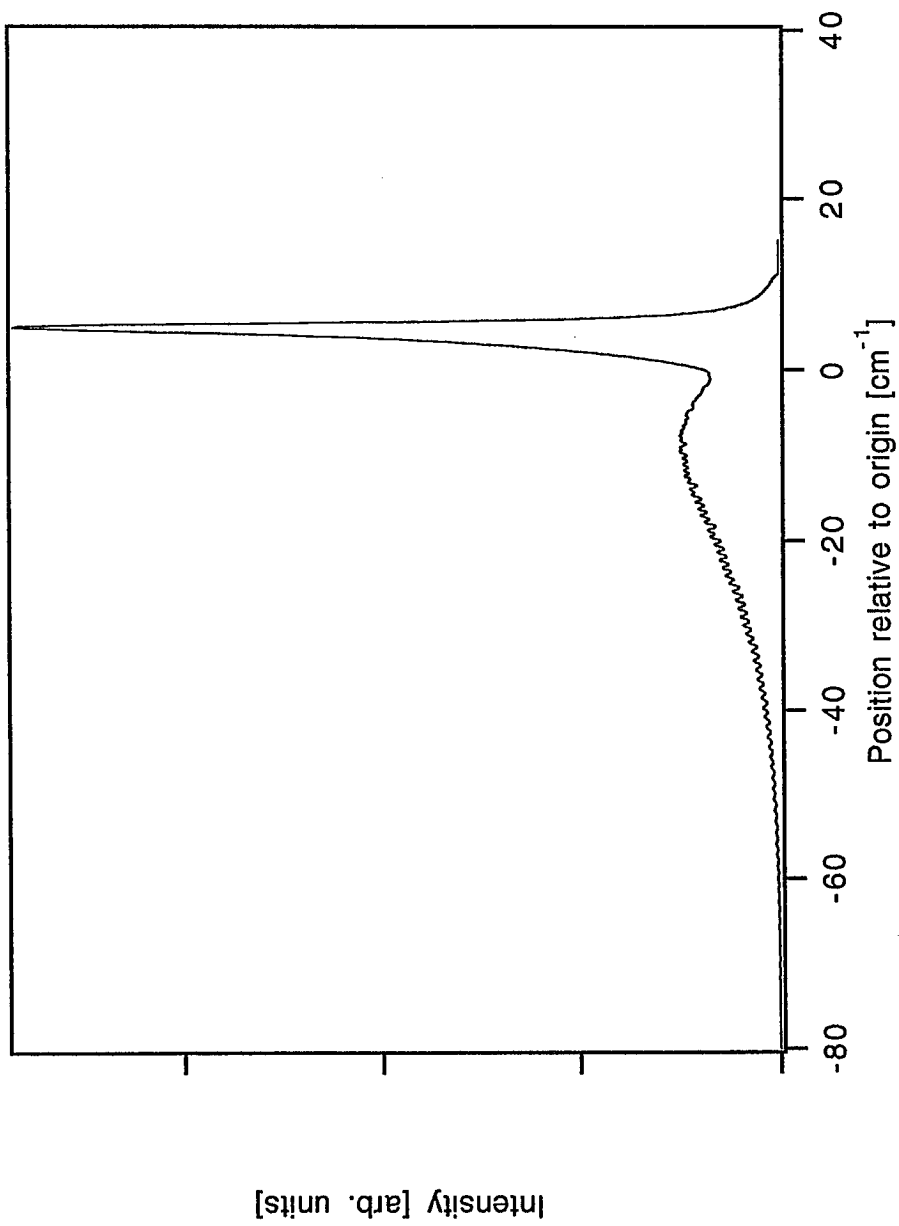


Figure V-5. A simulation of the rotational structure of the 6v₃ band of OCS.

CHAPTER VI

OVERTONE SPECTROSCOPY OF $^{12}\text{CO}_2$ AND $^{13}\text{CO}_2$ IN THE NEAR INFRARED

VI-1 Introduction

Due to its inherent characteristics and importance in spectroscopy and astrophysics, carbon dioxide has been one of the most thoroughly studied molecules spectroscopically. The investigation of overtone and combination bands in the photographic infrared region of this molecule started after the observation of these transitions in the spectrum of Venus in 1932 [1]. The reproduction of the $5\nu_3$ band at 11496 cm^{-1} in the laboratory was performed two years later by Adel and Slipher [2]. In order to detect this transition, a pathlength of $45\times 47\text{ m}\cdot\text{atm}$ had to be used. Under the same conditions, they could not evince any trace of the $\nu_1+5\nu_3$ Fermi diad at positions of 12672 and 12774 cm^{-1} . It was not until about 10 years after the first observation of these Venus bands, Herzberg and Herzberg [3] reproduced these bands completely in laboratory using a pathlength of $11000\text{ m}\cdot\text{atm}$. These latter authors also detected a faint bandhead at the position of 13966 cm^{-1} by using a pathlength of $55000\text{ m}\cdot\text{atm}$. This head should belong to the strongest component of the $2\nu_1+5\nu_3$ triad. The relative intensities of these bands were also estimated by Herzberg and Herzberg. From the experimental conditions employed for these early investigations on these transitions, it is obvious that these transitions are quite weak.

In 1964, Rank and co-workers [4] performed the first intensity measurement on these Venus bands using pathlengths from 2290 to 4576 m-atm. They found that the $5\nu_3$ bandhead had an integrated intensity of $0.319 \text{ cm}^{-1} \text{ km}^{-1} \text{ amagat}^{-1}$ corresponding to a total band absorption cross section of $2.4 \times 10^{-25} \text{ cm}^{-1} \text{ cm}^2 \text{ molecule}^{-1}$. They also measured the head intensity of the stronger component of the $\nu_1+5\nu_3$ diad, which is $0.078 \text{ cm}^{-1} \text{ km}^{-1} \text{ amagat}^{-1}$ corresponding to a band absorption cross section of $5.8 \times 10^{-26} \text{ cm}^{-1} \text{ cm}^2 \text{ molecule}^{-1}$. Five years later, Gray, Schorn, and Barker [5] estimated that the intensity ratio of $\nu_1+5\nu_3$ diad was 1.8-2. In 1971, Young and co-workers [6,7], by measuring the equivalent widths of the $\nu_1+5\nu_3$ diad, determined that the weaker component of the diad had a band intensity of about $0.08 \text{ cm}^{-1} \text{ km}^{-1} \text{ atm}^{-1}$, which is the same as a cross section of $3.0 \times 10^{-26} \text{ cm}^{-1} \text{ cm}^2 \text{ molecule}^{-1}$. Due to the weakness of these transitions, all the measurements mentioned above were performed either under long pathlength conditions or from the spectrum of Venus.

Along with the development of laser techniques and more sensitive detection methods, investigations on these weak transitions with shorter pathlengths and much smaller sample sizes became possible. In our previous studies [8], it was demonstrated that by employing the laser photoacoustic technique, the overtone and combination bands of CO_2 in the photographic infrared region could be studied directly with a sample size about several milliliters under a pressure of one atm. In addition, the absolute intensity of the stronger component of $\nu_1+5\nu_3$ diad was estimated. It is obvious that the advantage of the photoacoustic detection method on sample size over the long pathlength apparatus has very promising applications on isotopic studies.

However due to the limitation of the spectral range of the Ti:Sapphire laser in our previous studies, only the $\nu_1+5\nu_3$ diad of the Venus bands was investigated. The intensity measurement also suffered from the water interference, especially for the weaker component of the diad. In order to extend our spectral range, new optics were used to cover much wider frequency range into the longer wavelength region. In addition, new photoacoustic cell design has been employed to minimize the water interference and increase the sensitivity [9]. It has been demonstrated that the new cell has a sensitivity about 10^{-10} cm^{-1} . In addition, water interference has been minimized to a level of satisfaction.

In this chapter, investigations of the overtone and combination transitions in the spectral range from 10000 - 14000 cm^{-1} for both $^{12}\text{CO}_2$ and $^{13}\text{CO}_2$ will be presented. These transitions include the $5\nu_3$ and $5\nu_3+(\nu_1, 2\nu_2)$ Venus bands, the entire $5\nu_3+(2\nu_1, \nu_1+2\nu_2, 4\nu_2)$ triad and the stronger components of the $3\nu_3+(4\nu_1, 3\nu_1+2\nu_2, 2\nu_1+4\nu_2, \nu_1+6\nu_2, 8\nu_2)$ pentad for both species.

For the Venus bands, four transitions have been observed for $^{12}\text{CO}_2$ including one hot band associated with the $5\nu_3$ transition. For $^{13}\text{CO}_2$, a total of six bands have been observed for the first time. Bandhead positions of these new transitions were determined by using the water lines as wavelength standards. The integrated transition intensities are estimated by comparing the photoacoustic signal of $5\nu_3$ and $5\nu_3+(\nu_1, 2\nu_2)$ bands of $^{12}\text{CO}_2$ to those of the nearby H_2O and phenol bands, respectively. The intensities of the other bands are calibrated against the $5\nu_3$ band. Besides, the relative intensities of the $\nu_1+5\nu_3$ diad for $^{12}\text{CO}_2$ and $^{13}\text{CO}_2$ were compared.

All the transitions other than the Venus bands for these two species have been recorded for the first time except the strongest component of the

$5\nu_3+(2\nu_1, \nu_1+2\nu_2, 4\nu_2)$ triad for $^{12}\text{CO}_2$ observed by Herzberg and Herzberg [3]. The positions of the triad for both $^{12}\text{CO}_2$ and $^{13}\text{CO}_2$ were also determined by using water lines as wavelength standards. Due to their extreme weakness, the head positions of the components of the pentad for $^{12}\text{CO}_2$ are calibrated against those of the $^{13}\text{CO}_2$ $5\nu_3+(\nu_1, 2\nu_2)$ bands in the same spectrum, and those for $^{13}\text{CO}_2$ are calibrated to those of the $5\nu_3$ bands of $^{12}\text{CO}_2$ and $^{13}\text{CO}_2$, and $5\nu_3+(\nu_1+2\nu_2)$ bands of $^{13}\text{CO}_2$ in the same spectrum.

In addition to the observations and measurements mentioned above, theoretical calculations for the energy levels and rotational structure simulations have been performed. The measured positions were then compared with those calculated values. Besides, comparison between similar Fermi polyads on the relative intensities and spacing of the components were discussed.

VI-2 Experimental

A broad band cw Titanium:sapphire laser (Coherent 899-01) pumped by a 5-W multiline Ar^+ laser (Coherent Innova 70-5) was used as the near infrared excitation source. With three different optics sets, the system has a spectral range of 10000-14000 cm^{-1} . In order to increase the intracavity radiation power, high reflectors (CVI ~99.9%) have been used in the place of the output coupler and this leads to a tenfold decrease in the output power. Typically, peak output power of 30 mW, 20 mW, and 15 mW could be reached before the installation of the cell for the short wavelength, middle wavelength, and long wavelength optics through the high reflectors, respectively. The intracavity peak laser power is expected to be one hundred

times larger than the output power. The bandwidth of the laser is of the order of 0.2 cm^{-1} when the standard output couplers are used and it is expected to be broader when operated with the high reflectors. The frequency scan of the laser is performed by tilting an intracavity birefringent filter with a stepper motor (Oriel, model 18510). A typical scan rate is about $10 \text{ cm}^{-1}/\text{min}$. The relative intracavity laser power is monitored by a photodiode (EG&G Ortec, UV-100) placed near a laser beam to intercept scattered laser light. The signal from the photodiode is then fed to a lock-in amplifier (Princeton Applied Research, Model 5101).

The photoacoustic sample cell is placed inside the Titanium:sapphire ring laser cavity. It is found that the output laser power will decrease by about 20% due to the installation of the sample cell. The intensity of the Ar^+ laser is modulated with a mechanical chopper (Stanford Research System, SR540) tuned to the longitudinal acoustic resonance frequency of the sample cell. The microphone (Knowles, EK-3024) is powered by a 9-V DC battery and its signal is fed to another lock-in amplifier (Stanford Research Systems, SR510). Great care was taken to shield the connections between the microphone and the power box. For the scan rate given above, a typical time constant of 3 s was used. The fine tuning of the chopping frequency and the phase of the lock-in was done by setting the laser frequency on an intense transition and maximize the acoustic signal before each scan. The two signals are recorded independently by a Macintosh Plus.

Sample cells based on the the concentric double-tubing design [9] have been employed. Basically, the cell is composed of two tubes with different diameters; the smaller one is housed concentrically in the larger one. The inner tube is open ended leading to pressure nodes near the ends so that the microphone is mounted in the middle of the tube. All the other appendages,

such as fingers for the drying agent, gas valve, microphone signal outlet and the optical windows, are attached to the outer tube. Pyrex glass tubings with different diameters were used for the construction of the cells. The inner tube has an i.d. of 4 mm and length of 200 mm, and outer tube has an i.d. of 15 mm and length of 280 mm including the windows. The outer tube has two pieces jointed by a 3/4 in. Cajon Ultra-torr connector. A 1/4 in. and 1/8 in. Cajon Ultra-torr connectors are used for the dry agent finger and the microphone connection, respectively. Optical windows (micro cover glass, VWR Scientific Inc. No. 1¹/₂) are glued to the outer tube at the Brewster angle with epoxy.

The sample cells were evacuated on a vacuum line pumped by an oil diffusion pump with a typical background pressure of several millitorrs. ¹³CO₂ (Cambridge Isotopic laboratories Inc., 99% ¹³C) and ¹²CO₂ (Matheson Gas Products, >99.8% bone dry) gases were then introduced to the sample cell. A mechanical pressure gauge (Omega) was used to monitor the sample pressure with an accuracy of 5%. One atm total pressure was used without any buffer gas. P₂O₅ was stored in the cell finger before the cell was evacuated. After the sample was prepared, P₂O₅ could be introduced to the outer tubing by simply rotating the cell with an appropriate angle. According to the different volumes of the cell, it may take three days to a week to reduce the water density to the minimum level. The water molecular density in equilibrium with P₂O₅ is about 8x10¹¹ molecules cm⁻³ based on the data given in the CRC handbook [10].

For the Venus bands of ¹³CO₂, wavelength was calibrated against water transitions in the same spectrum since the Venus bands have similar intensities to water transitions under certain conditions (very low water concentration). This was done by recording a spectrum of the sample with a little water in the same cell and then the step numbers of the birefringent

filter which corresponding to water lines are obtained from the spectrum. A third order least square fitting program is then used to convert step numbers to wavenumbers.

For the much weaker transitions of the $5\nu_3+(2\nu_1, \nu_1+2\nu_2, 4\nu_2)$ triad, two identical sample cells were used for the wavelength calibration. One cell is filled with CO_2 and the drying agent P_2O_5 , and the other is filled with CO_2 and a little water (about 10 torr) with a total pressure of one atm. The spectrum of CO_2 is taken from the cell with the drying agent which is placed in the laser cavity and the water spectrum is taken from the other cell placed outside of the laser cavity. In order to satisfy acoustic resonant conditions in both cells, they have to be filled with about the same components. To increase the output power of the laser, the stock output coupler is installed (95% reflectivity), since the water spectrum is taken outside of the laser cavity. The same least square fitting program is used for the conversion from step numbers to wavenumbers.

Intensity calibration was carried out by using water and phenol transitions in the spectral range. Water is placed in one finger of the sample cell and spectrum is taken after equilibrium reached at certain temperature. In order to use phenol as a standard for intensity calibration, drying agent has to be used for the same sample. This is performed by placing the drying agent between the tubes of the cell and phenol in a finger.

VI-3 Results and Discussion

(A) $^{12}\text{CO}_2$ Transitions

(1) The Venus bands. Three vibrational bands of $^{12}\text{CO}_2$ were observed at positions 11496, 12672, and 12774 cm^{-1} for the transitions of $5\nu_3$, $5\nu_3+(\nu_1$,

2v₂), respectively, as shown in Figure VI-1 and Figure VI-2. These transitions were previously studied in laboratory by Herzberg and Herzberg [3] using the long absorbing pathlength apparatus [11]. All these bands show well-defined rotational structure. Due to the improvement in the overall performances of our photoacoustic apparatus [9], the spectrum of the diad has much higher quality than that of our previous study [8]. The hot band which belongs to the 5v₃ transition was also observed and the position of this band was determined by Herzberg and Herzberg [3]. Figure VI-3 shows this hot band in the P-branch region of the 5v₃ band. Due to the serious jitter in the frequency scan and the power fluctuation of the laser caused by birefringent effect during data acquisition for the short wavelength region, it is too difficult to identify the hot bands associated with the 5v₃+(v₁, 2v₂) transitions.

The transition cross section of the 5v₃ band was estimated by comparing the integrated band intensity to that of the nearby water bands by the following relation given by Gutow, Davidsson and Zare [12]

$$\frac{\sigma_u}{\sigma_s} = \frac{A_u \rho_s \nu_s}{A_s \rho_u \nu_u}$$

where the subscript u and s refer to the unknown sample and the standard, respectively, σ is the absorption cross section, A is the integrated band area, ν is the transition energy in wavenumber, and ρ is the molecular density (assuming ideal gas).

The absorption cross section of the 5v₃ band was determined to be 4.8x10⁻²⁵ cm⁻¹ cm² molecule⁻¹. This value is two times larger than that determined by Rank et al. [4]. The absorption cross sections of the diad were estimated in our previous investigation [8] and we reexamined these values by using the phenol overtone (4 - 0) transition at 13611 cm⁻¹ as a new

standard. By taking the partial pressure of phenol as 0.308 Torr [13] and absorption cross section of $1.2 \times 10^{-25} \text{ cm}^2 \text{ molecule}^{-1}$ [14], we determined that the absorption cross sections to be 7.6×10^{-26} and 1.8×10^{-25} for the $2\nu_2+5\nu_3$ and $\nu_1+5\nu_3$ transitions, respectively. The cross section for the stronger component of the diad measured this time is consistent with our previous studies [8]. However the cross section of the weaker component measured this time is two times smaller than the previous result. This discrepancy is obvious due to the fact that the weaker component was seriously affected by water interference in our previous measurement which made the cross section larger than the true value. The spectra used for these cross section calibrations are given in Figure VI-4 and Figure VI-5 for the $5\nu_3$ and $5\nu_3+(\nu_1, 2\nu_2)$ transitions, respectively.

Comparing these cross section measurements with the results obtained by Rank and co-workers [4], our photoacoustic measurements are larger than theirs by a factor of two and three for the $5\nu_3$ and $\nu_1+5\nu_3$ transitions, respectively. However, the relative intensities of these transitions are very close to the values obtained by Herzberg [3] and Young [6,7]. We estimate that the uncertainties for the cross section measurements are a factor of three and those for the relative intensity are a factor of 0.5. The transition cross sections and relative intensities of these Venus bands for $^{12}\text{CO}_2$ from different sources are given in Table VI-1.

(2) Transitions beyond the Venus Bands. The highest overtone transitions which were detected in the Venus spectrum are the $5\nu_3+(\nu_1, 2\nu_2)$ Fermi diad. The stronger component has a transition energy of 12775 cm^{-1} and the weaker one has a transition energy of 12672 cm^{-1} . In 1953, Herzberg and Herzberg reproduced the Venus bands by using the long absorbing path

apparatus [3]. In their investigation on these weak overtone transitions, an extremely weak band head which belongs to the strongest component of the $5\nu_3+(2\nu_1, \nu_1+2\nu_2, 4\nu_2)$ triad located at 13966 cm^{-1} was detected. The position of the head agreed well with the prediction made by Herman [15] in 1948. The detection of this faint band head required a path length of 5500 meters and a $^{12}\text{CO}_2$ pressure of 10 atm. Due to the weakness of the band, the authors could not determine the origin of the transition. The intensity of this band was estimated to be about two percent of the intensity of the $5\nu_3$ band by Herzberg and Herzberg [3]. A rough estimate indicates that the intensity of this transition is on the order of $10^{-27}\text{ cm}^2\text{ molecule}^{-1}\text{ cm}^{-1}$.

In our previous investigations on the $5\nu_3+(\nu_1, 2\nu_2)$ Venus bands [8], we did not observe any trace of the $5\nu_3+(2\nu_1, \nu_1+2\nu_2, 4\nu_2)$ triad. The reasons for this came from two aspects. First, the detection sensitivity of our previous apparatus was not high enough and second, the water interference in the spectral range of the $5\nu_3+(2\nu_1, \nu_1+2\nu_2, 4\nu_2)$ triad was too strong so that the bands could be totally masked. By employing the new photoacoustic sample cell described in the experimental section, the transitions of the $5\nu_3+(2\nu_1, \nu_1+2\nu_2, 4\nu_2)$ triad have been recorded with sufficient signal to noise ratio. The spectrum is shown in Figure VI-6.

The positions of the band heads of this triad were determined by using the water transitions in the same spectral range. This calibration was performed by taking spectra from two sample cells with identical dimensions to maintain the same resonant frequency, one filled with pure $^{12}\text{CO}_2$ and the other with $^{12}\text{CO}_2$ and saturated water vapor. The pure $^{12}\text{CO}_2$ cell is placed in the laser cavity and the other is placed out of the laser cavity. Although both of the cells were filled with $^{12}\text{CO}_2$ gas with pressures close to one atm, the spectrum taken outside of the laser cavity did not provide any vestige of the

$5\nu_3+(2\nu_1, \nu_1+ 2\nu_2, 4\nu_2)$ triad. Figure VI-7 shows the spectra of water and the triad of $^{12}\text{CO}_2$ from the same scan.

In addition to the $5\nu_3+(2\nu_1, \nu_1+ 2\nu_2, 4\nu_2)$ triad, the even weaker transitions of the $3\nu_3+(4\nu_1, 3\nu_1+2\nu_2, 2\nu_1+4\nu_2, \nu_1+6\nu_2, 8\nu_2)$ pentad located near 12000 cm^{-1} have been observed by using the same sample cell as in the case of the triad. Since the intensities of components are so weak and they also differ very much, only the three stronger bands have been recorded. Figure VI-8 shows the spectrum of these three bands. Difficulties were encountered when attempts were made to determine the position of these transitions. First, the transitions of the pentad are so weak and there is interference by the water transitions in the same region even though drying agent (P_2O_5) was used. Second, the same method used for determining the positions of the triad could not be used here, because the high reflector had to be used to increase the intracavity laser power to record the $^{12}\text{CO}_2$ spectrum and this made the output power too small to record the water spectrum. In view of these reasons, the bandhead positions of the transitions were determined by using the head positions of the $5\nu_3+(\nu_1, 2\nu_2)$ diad of $^{13}\text{CO}_2$ (natural abundance) in the same spectrum (see Figure VI-5). Due to these factors, the accuracy of the positions for those components of the pentad is much lower than that for the triad. The uncertainty is estimated to be two cm^{-1} .

To confirm the identities of these new observed transitions, calculations of the origin positions for the $5\nu_3+(2\nu_1, \nu_1+2\nu_2, 4\nu_2)$ triad and the $3\nu_3+(4\nu_1, 3\nu_1+2\nu_2, 2\nu_1+4\nu_2, \nu_1+6\nu_2, 8\nu_2)$ pentad have been performed by employing the molecular parameters from the work of Courtoy [16] and a list of the molecular parameters are given in Table VI-2. Then the Hamiltonian matrix for a given Fermi polyad was diagonalized to give the eigenvalues relative to the ground state and the eigenvectors. These eigenvectors

represent the fractional contributions of the unperturbed states to the perturbed states. A detailed explanation of the calculation is given in Appendix VI-A and a list of the computer program for the energy calculations can be found at the end of this chapter.

From the eigenvectors obtained from the calculation, the relative transition intensities within the Fermi polyad can be estimated. In order to do this, an assumption has to be made that the dominant transition within the Fermi polyad should be the one which has the lowest quantum number change (see Appendix VI-A for detailed explanation). The other transitions between the ground state and the unperturbed final states are very weak so that their intensities are ignored. For example, in the case of the $5\nu_3+(2\nu_1, \nu_1+2\nu_2, 4\nu_2)$ triad, the dominant transition is the $(2\ 0\ 5) - (0\ 0\ 0)$ transition. The intensities of the $(1\ 2\ 5) - (0\ 0\ 0)$ and $(0\ 4\ 5) - (0\ 0\ 0)$ transitions are ignored. With this assumption, the normalized transition intensity for a given component in the Fermi polyad is equal to the fractional contribution from the unperturbed $(2\ 0\ 5)$ state to the perturbed eigenstates within the polyad.

In order to determine the origins of the transitions from bandhead positions which were measured experimentally, a simulation program was used to reproduce the rotational structures of the bands. The molecular parameters for the simulations are also from the work of Courtoy [16] and they are listed in Table VI-2. Figure VI-9 is the rotational structure simulation for the central component of the $5\nu_3+(2\nu_1, \nu_1+2\nu_2, 4\nu_2)$ triad, and Figure VI-10 is a simulation for the central band of the pentad. From the simulations, band head positions relative to the origin are determined. Then these head positions relative to the origin are subtracted from the corresponding measured head positions to obtain the band origins.

Rotational constants for these simulations were calculated following the procedures described by Courtoy [16] and other authors [3, 17].

First the rotational constants for the unperturbed vibrational states is given by

$$B^0 = B_{000} - \sum_i \alpha_i v_i + \sum_{i \leq j} \gamma_{ij} v_i v_j$$

where B^0 is the rotational constant for an unperturbed vibrational state, B_{000} is the rotational constant for the ground state, α_i 's and γ_{ij} 's are parameters obtained from the best fit of the observed levels. Then the rotational constants for the perturbed states for a given Fermi polyad can be obtained by taking the perturbation into account, thus

$$B_i^p = \sum_{j=1}^n a_{ij}^2 B_j^0$$

where B_i^p is the rotational constant for an individual perturbed state within the polyad, a_{ij} 's are the eigenvectors from the unperturbed states to the i th perturbed state, and B_j^0 's are rotational constants for the unperturbed states within the polyad. The coefficients a_{ij} 's are obtained from the energy calculations mentioned above. These coefficients for the $2\nu_1+5\nu_3$ triad and $4\nu_1+3\nu_3$ pentad are shown in Table VI-3. Note that both the unperturbed and the perturbed states are labelled by the same notation and the first column is for the perturbed states. Calculated rotational constants and some of the measured values for highly excited states are given in Table VI-4.

After the determinations of the head positions relative to the origins, the band origins of the transitions for the $5\nu_3+(2\nu_1, \nu_1+2\nu_2, 4\nu_2)$ triad and the

$3\nu_3+(4\nu_1, 3\nu_1+2\nu_2, 2\nu_1+4\nu_2, \nu_1+6\nu_2, 8\nu_2)$ pentad are obtained. Those origins and other related values are given in Table VI-5, Table VI-6, for the triad and Table VI-7, Table VI-8 for the pentad, respectively. Note that in Table VI-5 the position of the $2\nu_1+5\nu_3$ component differs greatly from the calculated value. The reason is that the water lines used for the wavelength calibration do not cover this component (see Figure VI-7) and resulted in a large deviation in the least square fitting for the calibration.

It is interesting to compare the relative intensities and relative positions of the components within the same type of polyads with different energies, such as the $\nu_3+(2\nu_1, \nu_1+ 2\nu_2, 4\nu_2)$, $3\nu_3+(2\nu_1, \nu_1+ 2\nu_2, 4\nu_2)$ and $5\nu_3+(2\nu_1, \nu_1+ 2\nu_2, 4\nu_2)$ triads. These polyads only differ in the number of quanta of excitation in ν_3 . The relative intensities and positions of these triads are given in Table VI-9. The relative intensity variation of these triads are also depicted in Figure VI-11.

From these values, it is clear that when the excitation energy increases, the relative intensity of the component with the lowest transition energy in the triad decreases, and that with the highest transition energy increases. The relative intensity of the middle component stays about the same. If we examine the energy splitting within the triads, the change in the energy splitting with increasing transition energy is consistent with the relative intensity change. When the transition energy increases, the spacing between the component with the lowest transition energy and the middle component increases, and that between the component with the highest transition energy and the middle component decreases. This phenomenon conforms fully to the quantum mechanics explanations.

Note that the assignments or the labelling of the CO_2 overtone transitions are adopted from the early conventions according to which the

unperturbed ν_1 state is higher in energy than the $2\nu_2$ state. The ordering of these unperturbed states for $^{12}\text{CO}_2$ in different phases has been discussed in many studies and it has been firmly established that for $^{12}\text{CO}_2$ in the gas phase the unperturbed $2\nu_2$ state is higher in energy than the ν_1 state [18-26]. However, this discussion does not concern the present work much based on the following considerations.

First, no matter which level is higher in energy for the unperturbed states, the final or the perturbed states are always mixtures of the unperturbed states. The difference lies only in which final state contains the ν_1 or $2\nu_2$ unperturbed state more than the other or vice versa. From this point of view, the identity of each component within one Fermi polyad is not so important as long as the energy is considered since each component state contains different portions of every unperturbed state. In another words, using these normal mode assignment for the perturbed state is only partially correct. Second, the present work contains investigations on both $^{12}\text{CO}_2$ and $^{13}\text{CO}_2$, and it is convenient to use the same labelling on both of them for comparison because the ordering of these unperturbed states for $^{13}\text{CO}_2$ are reversed from that for $^{12}\text{CO}_2$.

(B). $^{13}\text{CO}_2$ Transitions

(1) The Venus Bands. To the best of our knowledge, the highest transitions which have been observed for $^{13}\text{CO}_2$ are the $3\nu_3+(\nu_1, 2\nu_2)$ diad [3, 16, 27-28]. Due to the large sample size required for the long pathlength experiments, there have been few high-energy overtone studies on isotopic species. In addition, water interference in the near infrared for heavy-atom overtones could be very serious [8,9]. As a matter of fact, the $5\nu_3+(\nu_1, 2\nu_2)$ diad of $^{13}\text{CO}_2$ is overlapped by much stronger water transitions, especially for

the weaker components. By using the photoacoustic method, sample size is not an important factor that affects the sensitivity of the detection, since the signal is not strongly dependent on the pathlength. As a matter of fact, the photoacoustic signal is inversely proportional to the volume of the sample cell [28]. By properly using a strong drying agent P_2O_5 , water interference has been minimized to a satisfactory level.

Three of the Venus bands located at head positions; 11192.4, 12351.4, and 12463.5 cm^{-1} for the $5\nu_3$ and the $5\nu_3+(\nu_1, 2\nu_2)$ diad, respectively, have been recorded in this investigation. The spectra are shown in Figure VI-12 and Figure VI-13 for the $5\nu_3$ and $5\nu_3+(\nu_1, 2\nu_2)$ transitions, respectively. All three bands show well-defined rotational structure as expected for a linear molecule. The P-branches of these transitions even show more regular progressions than those for the corresponding bands in the $^{12}CO_2$ case since the laser scans more smoothly in the range from 800 to 900 nm. The band head positions were determined by using the water lines as wavelength standards in the same spectrum with an uncertainty of one wavenumber.

In order to confirm the identities of these transitions, the same procedure is used to carry out the energy calculations as that performed in the $^{12}CO_2$ case. The molecular parameters are from the work of Chedin [22] and they are listed in Table VI-10. From the calculations, the eigenvalues and eigenvectors for a given Fermi polyad are obtained. The calculated energies in this work are consistent with those of another source [30]. In order to determine the band origins, rotational structures are simulated in the same way as for $^{12}CO_2$. The molecular parameters for the simulations are also from the work of Chedin [22] and they can be found in Table VI-10.

The intensities of these transitions are estimated by the following procedures. As mentioned before, the intensity of the $5\nu_3$ band for $^{12}CO_2$ is

determined by calibrating against the nearby water transitions. We simply assume that the intensity of the $5\nu_3$ band for $^{13}\text{CO}_2$ is the same as $^{12}\text{CO}_2$, because the difference in intensities between these two species for the $5\nu_3$ band is probably much smaller than the experimental uncertainty. Then the intensities of the other transitions are calibrated against that of the $5\nu_3$ band. We determined that the weaker component has a absorption cross section of 4.6×10^{-26} and that for the stronger one is $2.4 \times 10^{-25} \text{ cm}^2 \text{ molecule}^{-1} \text{ cm}^{-1}$. The transition cross sections and the relative intensity ratios for both the measured and the calculated for these three Venus bands are given in Table VI-11.

It is worth pointing out that the magnitude in Fermi interaction in $^{13}\text{CO}_2$ is much different from that in $^{12}\text{CO}_2$. This is due to the fact that the energy difference between unperturbed states $2\nu_2$ and ν_1 in $^{13}\text{CO}_2$ is much bigger than that in $^{12}\text{CO}_2$. Consequently, the Fermi interaction in $^{13}\text{CO}_2$ is much smaller. The energy levels for the lowest Fermi diad of both the unperturbed and the perturbed states for the two species are depicted in Figure VI-14.

Due to the different magnitudes in Fermi resonance in the two species, the relative intensities of the $5\nu_3 + (\nu_1, 2\nu_2)$ diad for $^{13}\text{CO}_2$ differs much from that of $^{12}\text{CO}_2$. According to Gray, Schorn, and Barker [5], the intensity ratio of the $5\nu_3 + (\nu_1, 2\nu_2)$ diad of $^{12}\text{CO}_2$ is about two. From our measurement the intensity ratio of the $5\nu_3 + (\nu_1, 2\nu_2)$ diad of $^{13}\text{CO}_2$ is about five. The absorption cross sections and the relative intensities of these Venus bands for both $^{12}\text{CO}_2$ and $^{13}\text{CO}_2$ are given in Table VI-12.

(2) Hot Band Transitions. Because of the smoother scan of the infrared laser in the middle wavelength (800-900 nm) range, three hot bands associated

with the three Venus transitions have also been identified. An enlargement of the $5\nu_3$ hot band spectrum is shown in Figures VI-15. The hot bands associated with the diad are shown in the insets of Figure VI-13. The positions of these hot bands are determined by using the positions of the $5\nu_3$, $5\nu_3+(\nu_1, 2\nu_2)$ transitions of $^{13}\text{CO}_2$ and the $5\nu_3$ transition of $^{12}\text{CO}_2$ (which is an impurity in the $^{13}\text{CO}_2$ sample) as standards in the same spectrum. The uncertainty of these positions is estimated to be two wavenumbers.

The calculated hot band positions are determined by taking the difference between the upper and lower perturbed levels. These measured and calculated positions for the hot bands are given in Table VI-13.

(3) Transitions beyond the Venus Bands. Just like that for $^{12}\text{CO}_2$, the $2\nu_1+5\nu_3$ triad has been observed for $^{13}\text{CO}_2$ located at bandhead positions of 13510, 13639, and 13738 cm^{-1} for the $5\nu_3+2\nu_1$, $5\nu_3+\nu_1+2\nu_2$, $5\nu_3+4\nu_2$ transitions, respectively. The spectrum is shown in Figure VI-17. These head positions were determined by using the water overtone lines in the same spectral region. Both the $^{13}\text{CO}_2$ and water spectra were taken from the same scan by placing the $^{13}\text{CO}_2$ cell inside the laser cavity and the water cell outside the laser cavity. The uncertainty of the positions is estimated to be one cm^{-1} . The spectra of $^{13}\text{CO}_2$ and water are shown in Figure VI-17. The same energy calculations on the energy levels of this triad were also performed. The measured and calculated for this triad are given in Table VI-14. Note this time that the position of the $4\nu_2+5\nu_3$ component measured this way resulted in a considerable deviation compared with the calculated value, since the water bands do not cover this component.

Due to the mass difference between $^{13}\text{CO}_2$ and $^{12}\text{CO}_2$, the energy differences of unperturbed states are different from those of $^{12}\text{CO}_2$ and this

results in differences in the Fermi interaction. Consequently, the relative intensities and positions are different from those for $^{12}\text{CO}_2$. It is interesting to compare the energy splitting and relative intensities of this triad for $^{12}\text{CO}_2$ and $^{13}\text{CO}_2$ to see the overall effect of the Fermi interactions. Those values for both of the two species are given in Table VI-15. From these values, it can be seen that the first spacing in the triad for $^{13}\text{CO}_2$ is larger than that for $^{12}\text{CO}_2$ resulting in a smaller absorption cross section for the $4\nu_2+5\nu_3$ component of $^{13}\text{CO}_2$. The second spacing in the triad for $^{13}\text{CO}_2$ is smaller than that for $^{12}\text{CO}_2$ leading to a larger absorption cross section for the $2\nu_1+5\nu_3$ component of $^{13}\text{CO}_2$. Due to this intensity shift in $^{13}\text{CO}_2$, the first component band in the same type of triads for the higher energy range could be totally vanished for this isotopic species.

Only two of the strongest components for the $4\nu_1+3\nu_3$ pentad have been observed for $^{13}\text{CO}_2$ compared with three for $^{12}\text{CO}_2$. The spectrum of these two bands is shown in Figure VI-18. The band head positions of these two bands are determined by using the positions of the $5\nu_3$, $5\nu_3+(\nu_1, 2\nu_2)$ transitions of $^{13}\text{CO}_2$ and the $5\nu_3$ transition of $^{12}\text{CO}_2$ (which is a impurity in the $^{13}\text{CO}_2$ sample) in the same spectrum. The uncertainty of these positions is estimated to be 2 cm^{-1} .

The same energy calculations and rotational structure simulations as those performed on the Venus bands have also been carried out for the $4\nu_1+5\nu_3$ pentad for $^{13}\text{CO}_2$. From these calculations and simulations, the band origins and the relative intensities for a given polyad can be obtained. These calculated and measured values are given in Table VI-16 and Table VI-17 for this pentad of $^{13}\text{CO}_2$.

After the observation of the three components for the $^{12}\text{CO}_2$ pentad, a great effort was made to detect the third band for the pentad of $^{13}\text{CO}_2$ without

any success. The calculated results on relative intensities for the components of the pentad clearly show that only two component transitions can be observed under our experimental conditions. The estimated relative intensities of these two components are consistent with the calculated values.

VI-4 Conclusions

Overtone transitions of $^{12}\text{CO}_2$ and $^{13}\text{CO}_2$ in the near infrared have been studied by means of laser photoacoustic spectroscopy. By employing an improved photoacoustic sample cell, the sensitivity has been increased to an order of 10^{-10} cm^{-1} and the water interference in the spectral range has been minimized to a level of satisfaction. A total of twenty one transitions of $^{12}\text{CO}_2$ and $^{13}\text{CO}_2$ have been identified including the hot bands in the spectral range from 10000 to 14000 cm^{-1} and seventeen of them were observed for the first time. In addition, theoretical calculations on the energy levels and eigenvectors were performed and good agreements have been obtained between the experimental results and the calculated values. It can be seen that in this energy range, the Fermi resonance is still the dominant interaction in CO_2 molecule.

It is obvious that in our spectral range, the overtone and combination bands of CO_2 follow exactly the pattern as expected. However, due to the difference in Fermi interaction for different energy levels, intensity shifts have been observed and for higher degeneracy polyads in higher energy range, some of the component bands are totally missing under our experimental conditions. Unfortunately, our infrared laser does not scan

smoothly enough to permit rotational analysis on these new observed transitions.

APPENDIX VI-A

THE HAMILTONIAN MATRIX DIAGONALIZATION OF CARBON DIOXIDE

The most distinguishing characteristic of vibrational spectra of carbon dioxide is the Fermi resonance. Due to the fact that the fundamental ν_1 has about the same energy and symmetry as that of the first overtone $2\nu_2$, strong interaction between the two occurs. Consequently, all the vibrational transitions with energies equal or greater than ν_1 belong to different Fermi polyads with degeneracy of ν_1+1 , i.e. diads, triads, tetrads, etc. For example, if there is a state with $\nu_1=1$, there is always another state with $\nu_2=2$ which has approximately the same energy as the $\nu_1=1$ state and they interact with each other to form two perturbed states. Consequently, the transition will be a diad. If there is a state with $\nu_1=2$, there are always two other states with $\nu_1=1$, $\nu_2=2$ and $\nu_2=4$ to interact with each other to form three perturbed states. In this case, the transition will be a triad.

In order to calculate the energy levels, Courtoy determined the spectroscopic constants for several isotopic species of this molecule [16, 26], and very good agreement between the observed energy levels and the calculated energy levels was obtained. In his calculation, the only interactions that were taken into account are the Fermi resonance and the l-type doubling for the P-state. In 1979, Chedin derived spectroscopic constants for ten isotopic species of carbon dioxide by considering five more interactions other than the two for Courtoy's treatment. For our experimental accuracy, we have found that only the Fermi interaction needs to be taken into account.

When only the Fermi interaction is considered, the Hamiltonian matrix will have only two types of elements. The diagonal element will have the form of

$$G_0(v_1 v_2 v_3 l) = \sum_i \omega_i^0 v_i + \sum_{i \leq j} x_{ij}^0 v_i v_j + g_{22} l^2 + \sum_{i \leq j \leq k} y_{ijk} v_i v_j v_k$$

and the off-diagonal term caused by the Fermi interaction is of the form

$$W' = \frac{1}{2} (W_0 - \lambda_1 v_1 - \lambda_2 v_2 - \lambda_3 l - \lambda_3 v_3) [(v_2 + 2)^2 - l^2]^{1/2} v_1^{1/2}$$

where v_1 , v_2 , and v_3 are the vibrational quantum numbers, and all the parameters are from the work of Courtoy [16]. Then the Hamiltonian matrix is constructed and diagonalized. Eigenvalues and eigenvectors are obtained.

From the eigenvectors for each Fermi polyad, the relative transition intensities can be estimated. In order to do this, an assumption that has to be made is that the total transition intensity of the polyad comes from the component transition that has the smallest vibrational quantum number change. Take the $2v_1 + 3v_3$ triad as an example. This means that the total intensity of the triad is the same as that of the transition from the ground state to the unperturbed (2 0 3) state. The intensities of the other transitions can be ignored due to the fact that they have larger quantum number changes. This assumption can be explained by the following mathematical treatment.

The observed intensities within the Fermi polyad can be expressed by the following equations

$$I_i = \sum_{j=1}^n a_{ij}^2 \mu_j^2$$

where a_{ij} is the eigenvector obtained from the energy calculation mentioned above, μ_j is the transition dipole moment from the ground state to the j th unperturbed state, and n is the degeneracy of the polyad. The intensity contributions from different transitions within the polyad can then be obtained by solving this equation. For the $2\nu_1+3\nu_3$ triad, 99% of the total intensity of the polyad is from the transition with the smallest quantum number change, i.e. from the ground state to the (2 0 3) unperturbed state.

REFERENCES

- [1]. W. S. Adams and T. Dunham, *Publ. Astron. Soc. Pacific.*, **44** (1932) 243
- [2]. A. Adel and V. M. Slipher, *Phys. Rev.*, **46** (1934) 240
- [3]. G. Herzberg and L. Herzberg, *J. Opt. Soc. Am.*, **43** (1953) 1037
- [4]. D. H. Rank, U. Fink, J. V. Foltz, and T. A. Wiggins, *Astrophys. J.*, **140** (1964) 366
- [5]. L. D. Gray, R. A. Schorn, and E. S. Barker, *Appl. Opt.*, **8** (1969) 241
- [6]. L. D. Gray Young, *Appl. Opt.*, **10** (1971) 662
- [7]. L. D. Gray, R. A. Schorn, E. S. Barker and A. Woszczyk, *Acta Astronomica*, **21**, (1971) 329
- [8]. X. Yang, C. Petrillo and C. Noda, *Chem. Phys. Lett.* , **214** (1993) 536
- [9]. X. Yang and C. Noda, *J. Phys. Chem.*, Submitted for publication
- [10]. D. R. Lide, *CRC Handbook of Chemistry and Physics*, 73rd Ed. 1992-1993, p. 15-21
- [11]. H. J. Bernstein and G. Herzberg, *J. Chem. Phys.*, **16** (1948) 30
- [12]. J. H. Gutow, J. Davidsson and R. N. Zare, *Chem. Phys. Lett.*, **185** (1991) 120
- [13]. E. W. Balson, *Trans. Faraday Soc.*, **43** (1947) 48
- [14]. J. Davidsson, J. H. Gutow and R. N. Zare, *J. Phys. Chem.*, **94** (1990) 4069
- [15]. R. C. Herman, *Astrophys. J.*, **107** (1948) 386
- [16]. C. P. Courtoy, *Can. J. Phys.*, **35** (1957) 608
- [17]. A. Del and D. M. Dennison, *Phys. Rev.*, **44** (1933) 99
- [18]. G. Amet and M. Pimbert. *J. Mol. Spectrosc.*, **16** (1965) 278
- [19]. H. R. Gordon and T. K. McCubbin, *J. Mol. Spectrosc.*, **19** (1966) 137
- [20]. H. E. Howard-Lock and B. P. Stoicheff, *J. Mol. Spectrosc.*, **37** (1971) 321

- [21]. Z. Cihla and A. Chedin, *J. Mol. Spectrosc.*, **40** (1971) 337
- [22]. A. Chedin, *J. Mol. Spectrosc.*, **76** (1979) 430
- [23]. S. Montero, *J. Chem. Phys.*, **79** (1983) 4091
- [24]. N. Papineau and M. Pealat, *J. Chem. Phys.*, **79** (1983) 5758
- [25]. N. Papineau and M. Pealat, *Appl. Opt.*, **24** (1985) 3002
- [26]. Y. Garrabos, M. A. Echargui and F. Marsault-Herail, *J. Chem. Phys.*, **91** (1989) 5869
- [27]. C. P. Courtoy, *Ann. Soc. Sci. Bruxelles, Serie 1* (1959) 5
- [28]. D. Burch, D. A. Gryvnak, and R. R. Patty, *J. Opt. Soc. Am.*, **58** (1968) 335
- [29]. J. Davidsson, J. H. Gutow, and R. N. Zare, *J. Phys. Chem.*, **94** (1990) 4069
- [30]. L. S. Rothman, R. L. Hawkins, R. B. Wattson, and R. R. Gamache, *J. Quant. Spectrosc. Radiat. Transfer*, **48** (1992) 537
- [31]. L. S. Rothman, R. R. Gamache, R. H. Tipping, C. P. Rinsland, M. A. H. Smith, D. C. Benner, V. M. Devi, J. M. Flaud, C. Camy-Peyret, A. Perrin, A. Goldman, S. T. Massie, L. R. Brown and R. A. Toth, *J. Quant. Spectrosc. Radiat. Transfer*, **48** (1992) 469

LIST OF COMPUTER PROGRAM FOR ENERGY CALCULATIONS OF $^{12}\text{CO}_2$

```

REM This program uses the molecular parameters from the work of Courtoy
DEFDBL a-z
DIM a(9,9), d(9), v(9,9), b(9), z(9)
f$=FILES$(0)
IF f$<>" " THEN
OPEN f$ FOR OUTPUT AS 1
PRINT #1, "CO2 vibrational energy levels"
PRINT #1, " "
END IF
CALL init
loop:
INPUT "Enter degeneracy (or 0 to quit) > ", deg
IF deg=0 THEN
CLOSE 1
END
END IF
PRINT "Denote the group by the largest v1 and smallest v2"
INPUT "Enter v1, v2, v3, L > ", v1, v2, v3, vam
FOR i = 1 TO deg: FOR j = 1 TO deg: a(i,j)=0:NEXT:NEXT
FOR i = 1 TO deg
CALL diag(v1-i+1, v2+2*i-2, v3, vam, a(i,i))
NEXT
IF deg > 1 THEN
FOR i = 1 TO deg-1
CALL offdiag(v1-i+1, v2+2*i-2, v3, vam, a(i,i+1))
a(i+1,i)=a(i,i+1)
NEXT
END IF
CALL jacobi(a(), deg, np, d(), v(), b(), z(), nrot)
REM print solution
PRINT "Eigenvalues"
FOR i = 1 TO deg
PRINT i, d(i)
NEXT
PRINT "Eigenvalues and eigenvectors"
FOR i = 1 TO deg
PRINT "Eigenvalue = ";d(i)
PRINT "Eigenvectors are...."
FORj = 1 TO deg
PRINT "(", v1-j+1; v2+2*j-2; v3; vam; ")", v(j, i)
NEXT
NEXT
IF f$<>" " THEN
PRINT#1, "Eigenvalues for (v1, v2, v3, L) = "; v1;v2; v3; vam
FOR i = 1 TO deg: PRINT#1, i, d(i): NEXT
PRINT #1, " "
PRINT#1, "Eigenvalues and eigenvectors"
FOR i = 1 TO deg
PRINT#1, "Eigenvalue = ";d(i)

```

```

PRINT#1, "Eigenvectors are...."
FOR j = 1 TO deg
PRINT#1, " ("; v1-j+1; v2+2*j-2; v3; vam; ")", v(j, i), v(j,i)^2
NEXT
NEXT
PRINT #1, " "
END IF
GOTO loop
END
SUB offdiag(v1, v2, v3, vam, wp) STATIC
SHARED w0, lam1, lam2, lam3, lam1
wp=(w0-lam1*v1-lam2*v2-lam3*v3-lam1*vam)
wp=wp*.5*SQR((v2+2)^2-vam^2)*SQR(v1)
END SUB
SUB diag(v1, v2, v3, vam, g0) STATIC
SHARED om1, om2, om3
SHARED x11, x12, x13, x22, x23, x33, g22
SHARED y111, y112, y113, y123, y222, y122, y223, y333, y133, y233
g0=om1*v1+om2*v2+om3*v3+g22*vam^2
g0=g0+x11*v1^2+x12*v1*v2+x13*v1*v3+x22*v2^2+x23*v2*v3
g0=g0+x33*v3^2+y111*v1^3+y222*v2^3+y333*v3^3
g0=g0+y112*v1^2*v2+y113*v1^2*v3+y123*v1*v2*v3
g0=g0+y122*v1*v2^2+y223*v2^2*v3+y133*v1*v3^2+y233*v2*v3^2
END SUB

SUB init STATIC
SHARED om1, om2, om3
SHARED x11, x12, x13, x22, x23, x33, g22
SHARED y111, y112, y113, y123, y222, y122, y223, y333, y133, y233
SHARED w0, lam1, lam2, lam3, lam1
om1=1345.04
om2=667.25
om3=2361.71
x11=-3.63
x12=3.44
x22=-.635
x13=-19.28
x23=-12.51
x33=-12.56
y111=.13
y112=-.08
y113=0
y123=.02
y222=.01
y122=-.07
y223=0
y333=.015
y133=.07
y233=.01
g22=.775
w0=51.31
lam1=.15
lam2=.41
lam3=.78

```

```

laml=0
END SUB
SUB jacobi(a(), n, np, d(), v(), b(), z(), nrot) STATIC
REM eigenvalue solver using JACOBI method
REM translated from Fortran (Numerical Recipes)
FOR ip = 1 TO n
FOR iq = 1 TO n
v(ip, iq) = 0
NEXT
v(ip,ip)=1
b(ip)=a(ip,ip)
d(ip)=b(ip)
z(ip)=0
NEXT
nrot = 0
FOR i = 1 TO 50
sm = 0!
FOR ip = 1 TO n-1
FOR iq = ip+1 TO n
sm=sm+ABS(a(ip,iq))
NEXT
NEXT
IF (sm = 0!) THEN EXIT SUB
IF (i < 4) THEN
tresh = .2 * sm /n^2
ELSE
tresh = 0
END IF
FOR ip = 1 TO n-1
FOR iq = ip+1 TO n
g=100!*ABS(a(ip, iq))
IF ((i > 4) AND (ABS(d(ip))+g = ABS(d(ip))) AND (ABS(d(iq))+g = ABS(d(iq)))) THEN
a(ip,iq)=0
ELSEIF(ABS(a(ip, iq)) > tresh) THEN
h=d(iq)-d(ip)
IF (ABS(h)+g = ABS(h)) THEN
t = a(ip,iq)/h
ELSE
theta=.5*h/a(ip, iq)
t = 1!/(ABS(theta)+SQR(1+theta^2))
IF (theta < 0) THEN t=-t
END IF
c=1!/SQR(1+t^2)
s=t*c
tau=s/(1+c)
h=t*a(ip,iq)
z(ip)=z(ip)-h
z(iq)=z(iq)+h
d(ip)=d(ip)-h
d(iq)=d(iq)+h
a(ip,iq)=0
FOR j=1 TO ip-1
g=a(j,ip)
h=a(j,iq)

```

```

a(j,ip)=g-s*(h+g*tau)
a(j,iq)=h+s*(g-h*tau)
NEXT
FOR j=ip+1 TO iq-1
g=a(ip,j)
h=a(j,iq)
a(ip,j)=g-s*(h+g*tau)
a(j,iq)=h+s*(g-h*tau)
NEXT
FOR j=iq+1 TO n
g=a(ip,j)
h=a(iq,j)
a(ip,j)=g-s*(h+g*tau)
a(iq,j)=h+s*(g-h*tau)
NEXT
FOR j = 1 TO n
g=v(j,ip)
h=v(j,iq)
v(j,ip)=g-s*(h+g*tau)
v(j,iq)=h+s*(g-h*tau)
NEXT
nrot=nrot+1
END IF
NEXT
NEXT
FOR ip=1 TO n
b(ip)=b(ip)+z(ip)
d(ip)=b(ip)
z(ip)=0
NEXT
NEXT
END SUB

```

LIST OF COMPUTER PROGRAM FOR ROTATIONAL SIMULATIONS OF $^{12}\text{CO}_2$

REM this is the simulation program of the CO2 rotational structure
 REM the molecular constants are from the work of Courtoy

```

INPUT "Enter FWHM ", fwhm
jmax =100
nshape = fwhm*12/interval
nshape2 = nshape/2
DIM eu(jmax), el(jmax)
INPUT "Enter v1 ", v1
INPUT "Enter v2 ", v2
INPUT "Enter v3 ", v3
INPUT "the transition energy: "; energy
n=v1+1
DIM b(n),a(n)
FOR i=0 TO n-1
INPUT "the contribution coef. ";a(i)
NEXT
v2=0
FOR i=0 TO n-1
v1=n-1-i
v2=2*i
CALL calparm(v1,v2,v3, bv, dv, hv)
CALL calparm(0!, 0!, 0!, b000,d000,h000)
PRINT "transition energu= "; energy
PRINT "Bv= ", bv
REM PRINT "B0= ", b000
b(i)=bv
v1=v1
v2=v2
NEXT
b=0
d=0
FOR i=0 TO n-1
b=b+a(i)^2*b(i)
d=d+a(i)^2*d(i)
NEXT
PRINT"rotational constant for the upper level"
PRINT b
jmin=0
FOR j=jmin TO jmax
fj=j*(j+1)
eu(j)=b*fj-dv*fj*fj+hv*fj*fj*fj
el(j)=b000*fj-d000*fj*fj+h000*fj*fj*fj
NEXT
npeak=2*jmax
DIM position(npeak), intensity(npeak), shape(nshape)
FOR i=2 TO jmax STEP 2
position(i)=eu(i)-el(i-1)
position(i+jmax)=eu(i-1)-el(i)

```



```

intensity(i)=(2*i+1)*EXP(-el(i)/208)
intensity(i+jmax)=intensity(i)
NEXT
minpos=1E+10
maxpos=-1E+10
FOR i=1 TO npeak
IF minpos>position(i) THEN minpos=position(i)
IF maxpos<position(i) THEN maxpos=position(i)
NEXT
numpoints=(maxpos-minpos)/interval+fwhm/interval*20
minpos=minpos-fwhm*10
DIM x(numpoints), y(numpoints)
parm=fwhm^2/4
FOR i=0 TO nshape
z=i*interval - fwhm*6
shape(i) = 1/(z*z+parm)
NEXT
FOR i=0 TO numpoints
x(i)=minpos + i*interval
y(i)=0
NEXT
FOR j=1 TO npeak
peakcenter=(position(j)-minpos)/interval
peakwidth = fwhm/interval
intj=intensity(j)
IF (peakcenter - nshape2<0) THEN GOTO skippeak
IF (peakcenter + nshape2 > numpoints) THEN GOTO skippeak
FOR i=peakcenter-nshape2 TO peakcenter+nshape2
y(i)=y(i)+intj*shape(i-peakcenter+nshape2)
NEXT
skippeak:
NEXT
REM Band head position
peakmax=0
FOR i=1 TO numpoints
IF (peakmax<y(i)) THEN
peakmax=y(i)
index=i
END IF
NEXT
CALL printfile(x(),y(), numpoints)
INPUT h$
END

SUB calparm(v1,v2,v3,b,d,h) STATIC
b0=.39021
alpha1=.00126
alpha2=-.00076#
alpha3=.0030875
gamma11=0!
gamma12=.000035
gamma13=.000014
gamma22=0!
gamma23=.00001

```

```

gamma33=.0000035
lq=0
b=b0-alpha1*v1-alpha2*v2-alpha3*v3+gamma11*v1^2+gamma12*v1*v2
b=b+gamma13*v1*v3+gamma22*v2^2+gamma23*v2*v3+gamma33*v3^2
END SUB

```

```

SUB printfile(x(),y(), numpoints) STATIC
SHARED fwhm, v1,v2,v3,b000,d000,h000,b,energy,index
f$="CO2 "+STR$(fwhm)+" v"+STR$(energy)+"v3"+STR$(v3)
OPEN f$ FOR OUTPUT AS 1
OPEN f$+".info" FOR OUTPUT AS 2
PRINT #2, "FWHM= ", fwhm
PRINT #2, "Energy= "; energy
PRINT #2, "Bv,Dv,Hv= "; b
PRINT #2, "Bandhead at "; x(index)
CLOSE 2
FOR i=1 TO numpoints
WRITE#1, x(i),y(i)
NEXT
CLOSE 1
END SUB

```

Table VI-1 Absorption cross sections and relative intensities of the Venus bands for $^{12}\text{CO}_2$

Transition	Transition cross section ($\text{cm}^{-1} \text{ cm}^2 \text{ molecule}^{-1}$)		Relative intensity		
	This work	Rank	This work	Rank	Herzberg
$5\nu_3$	4.8×10^{-25}	2.4×10^{-25}	1.0	1.0	1.0
$\nu_1 + 5\nu_3$	1.8×10^{-25}	5.8×10^{-26}	0.38	0.24	0.3
$2\nu_2 + 5\nu_3$	7.6×10^{-26}	3.0×10^{-26} *	0.16	0.13	0.1

* From Ref. 7

Table VI-2 Molecular parameters from Ref. 16 for the energy calculations and rotational simulations of $^{12}\text{CO}_2$

ω°_1 134504	ω°_2 667.25	ω°_3 2361.71	x°_{11} -3.63
x°_{22} -0.635	x°_{33} -12.56	x°_{12} 3.44	x°_{13} -19.28
x°_{23} -12.51	y_{111} 0.13	y_{222} 0.01	y_{333} 0.015
y_{112} -0.08	y_{122} -0.07	y_{133} 0.07	y_{113} 0
y_{223} 0	y_{233} 0.01	y_{123} 0.02	g_{22} 0.775
B_{000} 0.39021	B_e 0.391625	α_1 126-e05	α_2 -76-e05
α_3 308.75-e05	γ_{11} 0	γ_{22} 0	γ_{33} 0.35-e05
γ_{12} -3.5-e05	γ_{13} 1.4-e05	γ_{23} 1-e05	

Table VI-3 Coefficients for the rotational simulations of different polyads for $^{12}\text{CO}_2^*$

Triad	2 0 5	1 2 5	0 4 5		
2 0 5	0.5472	0.7070	0.4129		
1 2 5	0.7738	0.3041	0.5556		
0 4 5	0.2627	0.6385	0.7217		
Pentad	4 0 3	3 2 3	2 4 3	1 6 3	0 8 3
4 0 3	0.1519	0.4412	0.6383	0.5501	0.2687
3 2 3	-0.5249	-0.5836	-0.0419	0.4596	0.4234
2 4 3	0.7508	-0.1793	-0.4051	0.1848	0.4538
1 6 3	-0.3635	0.6029	-0.4042	-0.1847	0.5539
0 8 3	0.0746	-0.2630	0.5131	-0.6464	0.4941

* Note that the first number is the quantum number for ν_1 and the second for ν_2 and the third for ν_3

Table VI-4 Rotational constants of $^{12}\text{CO}_2$ in cm^{-1} for some of the highly excited states*

Vib. States	B_0	B_p	$B_{\text{exp.}}$
0 4 3	0.3841	0.3823	0.3823
1 2 3	0.3814	0.3804	0.3804
2 0 3	0.3785	0.3812	0.3812
0 8 3	0.3873	0.3842	
1 6 3	0.3847	0.3818	
2 4 3	0.3820	0.3798	
3 2 3	0.3791	0.3809	
4 0 3	0.3761	0.3825	
0 0 5	0.3748	0.3748	0.3748
0 2 5	0.3765	0.3756	0.3756
1 0 5	0.3737	0.3745	0.3745
0 4 5	0.3781	0.3765	
1 2 5	0.3754	0.3744	
2 0 5	0.3725	0.3749	

* B_0 is for the unperturbed state, B_p is for perturbed state and $B_{\text{exp.}}$ is from the work of Herzberg and Herzberg in Ref. 3

Table VI-5 Measured and calculated band origins for the $4\nu_2+5\nu_3$ triad of $^{12}\text{CO}_2$

Component	Meas. origin [cm ⁻¹]	Cal. origin [cm ⁻¹]	Meas.-Cal. [cm ⁻¹]
$4\nu_2+5\nu_3$	13825.1	13824.5	0.6
$\nu_1+2\nu_2+5\nu_3$	13955.7	13957.5	-1.8
$2\nu_1+5\nu_3$	14063.2	14065.7	-2.5

Table VI-6 Spacings and relative intensities for the $5\nu_3+(2\nu_1, \nu_1+2\nu_2, 4\nu_2)$ triad of $^{12}\text{CO}_2$

Component transitions	Spacing between transitions* [cm-1]			Relative intensity		
	Exp.	Cal.	Exp.-Cal.	Exp.	Cal.	Exp.-Cal.
$4\nu_2+5\nu_3$	130.6	133.0	0.6	0.09	0.07	0.02
$\nu_1+2\nu_2+5\nu_3$	0	0	0	0.62	0.60	0.02
$2\nu_1+5\nu_3$	107.5	108.2	-0.7	0.29	0.33	0.04

* Relative to the central component

Table VI-7 Measured and calculated origins of the $4\nu_1+3\nu_3$ pentad for $^{12}\text{CO}_2$

Component	Meas. origin [cm ⁻¹]	Cal. origin [cm ⁻¹]	Meas.-Cal. [cm ⁻¹]
$8\nu_2+3\nu_3$	*	11732.8	
$\nu_1+6\nu_2+3\nu_3$	11914.0	11913.6	0.4
$2\nu_1+4\nu_2+3\nu_3$	12050.6	12051.0	-0.4
$3\nu_1+2\nu_2+3\nu_3$	12179.9	12181.6	-1.7
$4\nu_1+3\nu_3$	*	12355.0	

* Too weak to be measured

Table VI-8 Spacings and relative intensities for the $4\nu_1+3\nu_3$ pentad of $^{12}\text{CO}_2$

Component transitions	Spacing between transitions* [cm ⁻¹]			Relative intensity		
	Exp.	Cal.	Exp.-Cal.	Exp.	Cal.	Exp.-Cal.
$8\nu_2+3\nu_3$		180.8			0.00006	
$\nu_1+6\nu_2+3\nu_3$	136.6	137.4	-0.8	0.20	0.13	0.07
$2\nu_1+\nu_2+3\nu_3$	0	0	0	0.51	0.56	-0.05
$3\nu_1+2\nu_2+3\nu_3$	129.3	130.6	-1.3	0.29	0.28	0.01
$4\nu_1+3\nu_3$		173.4			0.02	

* Spacing between adjacent bands, and this for the central component is zero

Table VI-9 The relative intensities and the relative positions to the central component of different triads for $^{12}\text{CO}_2$

Transitions	Relative intensity *		Relative position to the central band [cm^{-1}]	
	Measured	Calculated	Measured	Calculated
$4\nu_2 + \nu_3$	0.15	0.13	124.2	124.0
$4\nu_2 + 3\nu_3$	0.10	0.10	128.0	128.0
$4\nu_2 + 5\nu_3$	0.09	0.07	130.6	133.0
$\nu_1 + 2\nu_2 + \nu_3$	0.65	0.66	0	0
$\nu_1 + 2\nu_2 + 3\nu_3$	0.66	0.64	0	0
$\nu_1 + 2\nu_2 + 5\nu_3$	0.62	0.60	0	0
$2\nu_1 + \nu_3$	0.20	0.21	121.8	121.9
$2\nu_1 + 3\nu_3$	0.23	0.26	114.4	114.3
$2\nu_1 + 5\nu_3$	0.29	0.33	107.5	108.2

* The relative intensities and positions of the $2\nu_1+\nu_3$ and $2\nu_1+3\nu_3$ triads are obtained from the HITRAN database (see Ref. 30)

Table VI-10 Molecular parameters from Ref. 22 for the energy calculations and rotational structure simulations of $^{13}\text{CO}_2$

ω°_1 1336.28711	ω°_2 648.341797	ω°_3 2295.23877	x°_{11} -3.00017262
x°_{22} 1.49001026	x°_{33} -11.7358589	x°_{12} -5.10998726	x°_{13} -18.674469
x°_{23} -11.7563066	y_{111} 0.0242212862	y_{222} -4.22580913e-03	y_{333} 5.62079996e-03
y_{112} 6.81840815e-04	y_{122} -4.48305979e-02	y_{133} 6.22764491e-02	y_{113} -7.71441e-02
y_{223} -2.02638209e-02	y_{233} 1.70341805e-02	y_{123} 8.88499618e-02	g_{22} 1.49001026
B_{000} 0.390239716	α_1 1.20363291e-03	α_2 6.94377115e-04	α_3 3.00088781e-03
D_0 1.33225114e-07	γ_{11} -1.63962886e-06	γ_{22} -9.40911923e-06	γ_{33} 8.31453508e-06
γ_{12} 1.14343729e-05	γ_{13} 1.43563311e-05	γ_{23} 9.70381097e-06	β_1 9.66982605e-11
β_2 2.21335705e-09	β_3 3.2178837e-10		

Table VI-11 Band Origins and absorption Cross Sections for the Venus bands of $^{13}\text{CO}_2$

Transition	Meas. origin [cm ⁻¹]	Cal. origin [cm ⁻¹]	Meas.-Cal [cm ⁻¹]	Cross section [cm ² cm ⁻¹ mol ⁻¹]
5v ₃	11182.3	11183.5	-1.2	4.8x10 ⁻²⁵
2v ₂ +5v ₃	12341.4	12341.1	0.3	4.6x10 ⁻²⁶
v ₁ +5v ₃	12452.9	12452.5	0.4	2.4x10 ⁻²⁵

Table VI-12 Absorption cross sections and relative intensities of the Venus bands for both $^{12}\text{CO}_2$ and $^{13}\text{CO}_2$

Transitions	Absorption cross section [$\text{cm}^2\text{cm}^{-1}\text{molecule}^{-1}$]		Relative intensity	
	$^{12}\text{CO}_2$	$^{13}\text{CO}_2$	$^{12}\text{CO}_2$	$^{13}\text{CO}_2$
$5\nu_3$	4.8×10^{-25}	4.8×10^{-25}	1.0	1.0
$2\nu_2+5\nu_3$	7.6×10^{-26}	4.6×10^{-26}	0.16	0.10
$\nu_1+5\nu_3$	1.8×10^{-25}	2.4×10^{-25}	0.38	0.50

Table VI-13 Hot band positions associated with the Venus bands for $^{13}\text{CO}_2$

Transitions	Head position [cm ⁻¹]	Band origin [cm ⁻¹]	Calculated origin	Meas.-Cal.
$\nu_2+5\nu_3-\nu_2$	11133.9	11123.9	11125.0	-1.1
$3\nu_2+5\nu_3-\nu_2$	12277.0	12266.5	12267.6	-1.1
$\nu_1+\nu_2+5\nu_3-\nu_2$	12419.6	12409.7	12409.8	-0.1

Table VI-14 Measured and calculated band origins for the $4\nu_2+5\nu_3$ triad of $^{13}\text{CO}_2$

Component	Meas. origin [cm ⁻¹]	Cal. origin [cm ⁻¹]	Meas.-Cal. [cm ⁻¹]
$4\nu_2+5\nu_3$	13481.3	13476.4	4.9
$\nu_1+2\nu_2+5\nu_3$	13624.5	13623.7	0.8
$2\nu_1+5\nu_3$	13725.6	13725.0	0.6

Table VI-15 Energy splitting and relative intensity of the $2\nu_1+5\nu_3$ triad for $^{12}\text{CO}_2$ and $^{13}\text{CO}_2$. The data shows that the larger the spacing from the central component, the weaker the relative intensity.

Transition	Spacing* [cm^{-1}]		Relative Intensity	
	$^{12}\text{CO}_2$	$^{13}\text{CO}_2$	$^{12}\text{CO}_2$	$^{13}\text{CO}_2$
$4\nu_2+5\nu_3$	130.6	143.3	0.09	0.05
$\nu_1+2\nu_2+5\nu_3$	0	0	0.62	0.52
$2\nu_1+5\nu_3$	107.5	101.1	0.29	0.43

* Relative to the central component

Table VI-16 Measured and calculated values of band origins and relative intensities for the $4\nu_1+3\nu_3$ pentad in $^{13}\text{CO}_2$

Component	Meas. origin [cm ⁻¹]	Cal. origin [cm ⁻¹]	Meas.-Cal. [cm ⁻¹]
$8\nu_2+3\nu_3$	*	11469.1	
$\nu_1+6\nu_2+3\nu_3$	*	11662.3	
$2\nu_1+4\nu_2+3\nu_3$	11814.1	11815.7	-1.6
$3\nu_1+2\nu_2+3\nu_3$	11927.9	11931.7	-3.8
$4\nu_1+3\nu_3$	*	12068.3	

* Too weak to be measured

Table VI-17 Spacing and relative intensities of the $4\nu_1+3\nu_3$ pentad for $^{13}\text{CO}_2$

Component transitions	Spacing between transitions * [cm ⁻¹]			Relative intensity		
	Exp.	Cal.	Exp.-Cal.	Exp.	Cal.	Exp.-Cal.
$8\nu_2+3\nu_3$	**	193.2			0.006	
$\nu_1+6\nu_2+3\nu_3$	**	153.4			0.09	
$2\nu_1+\nu_2+3\nu_3$	0	0	0	0.52	0.47	0.05
$3\nu_1+2\nu_2+3\nu_3$	113.8	116.0	-2.2	0.48	0.40	0.08
$4\nu_1+3\nu_3$	**	136.6			0.03	

* Spacings are relative to the central component

** Too weak to be measured

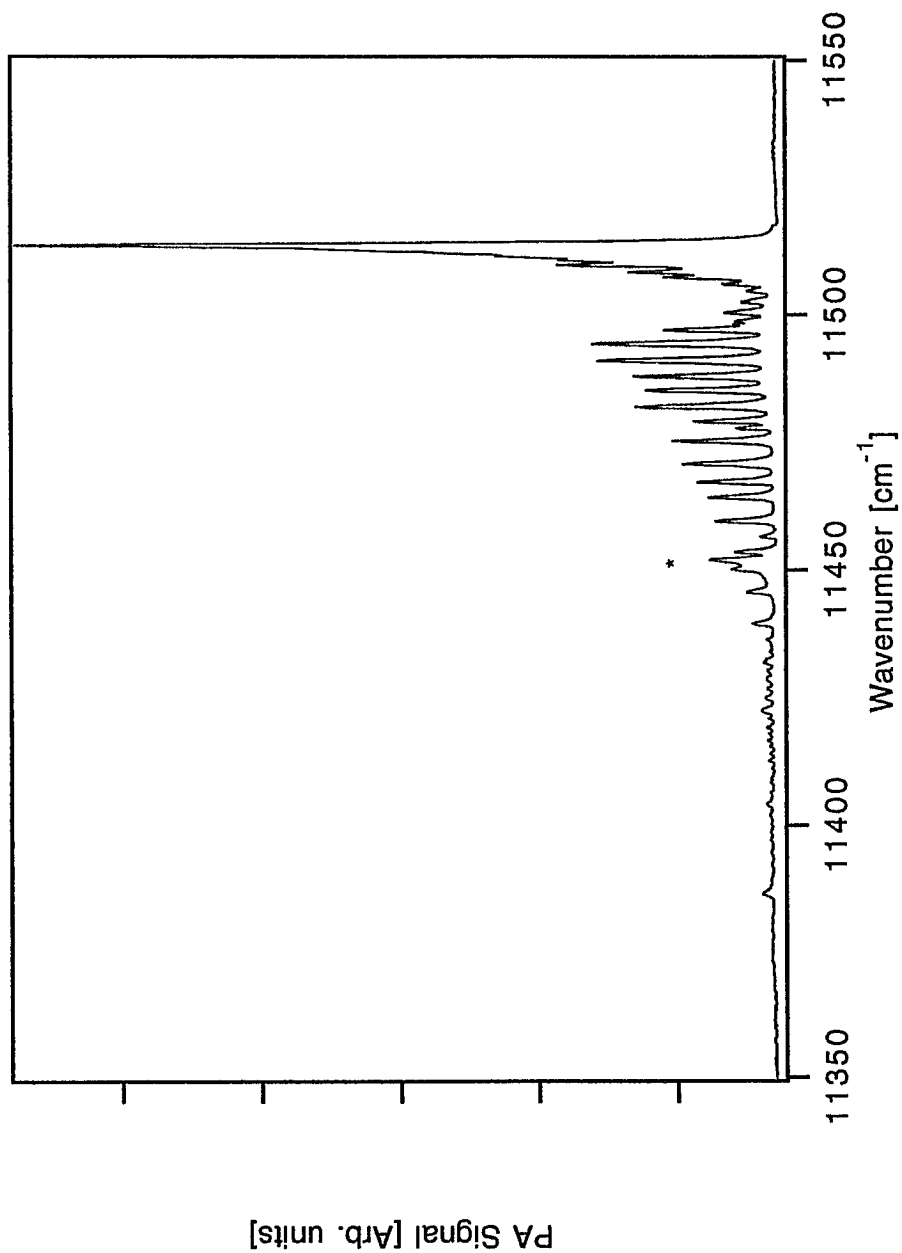


Figure VI-1 The $5\nu_3$ band of $^{12}\text{CO}_2$. The hot band is indicated by an asterisk.

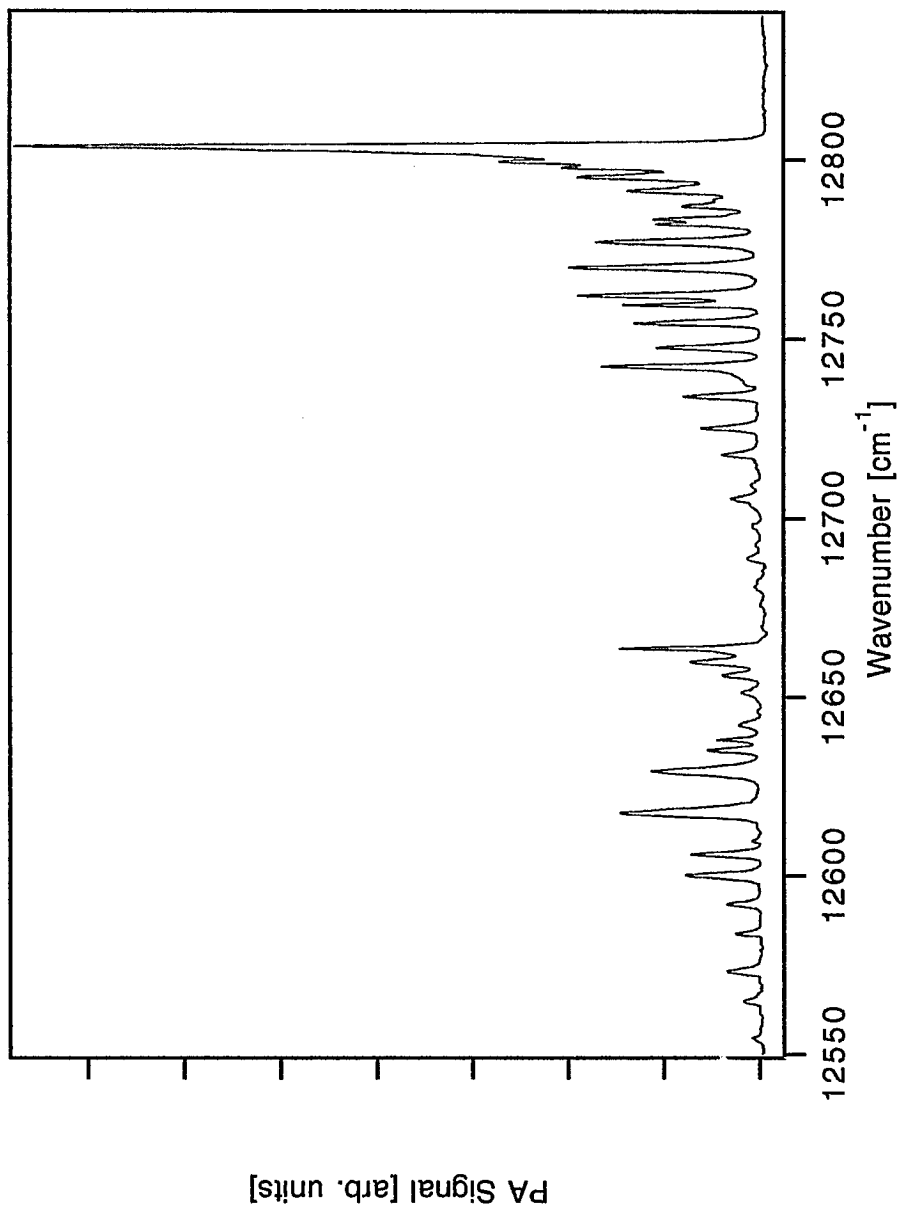


Figure VI-2. The $\nu_1+5\nu_3$ diad of $^{12}\text{CO}_2$

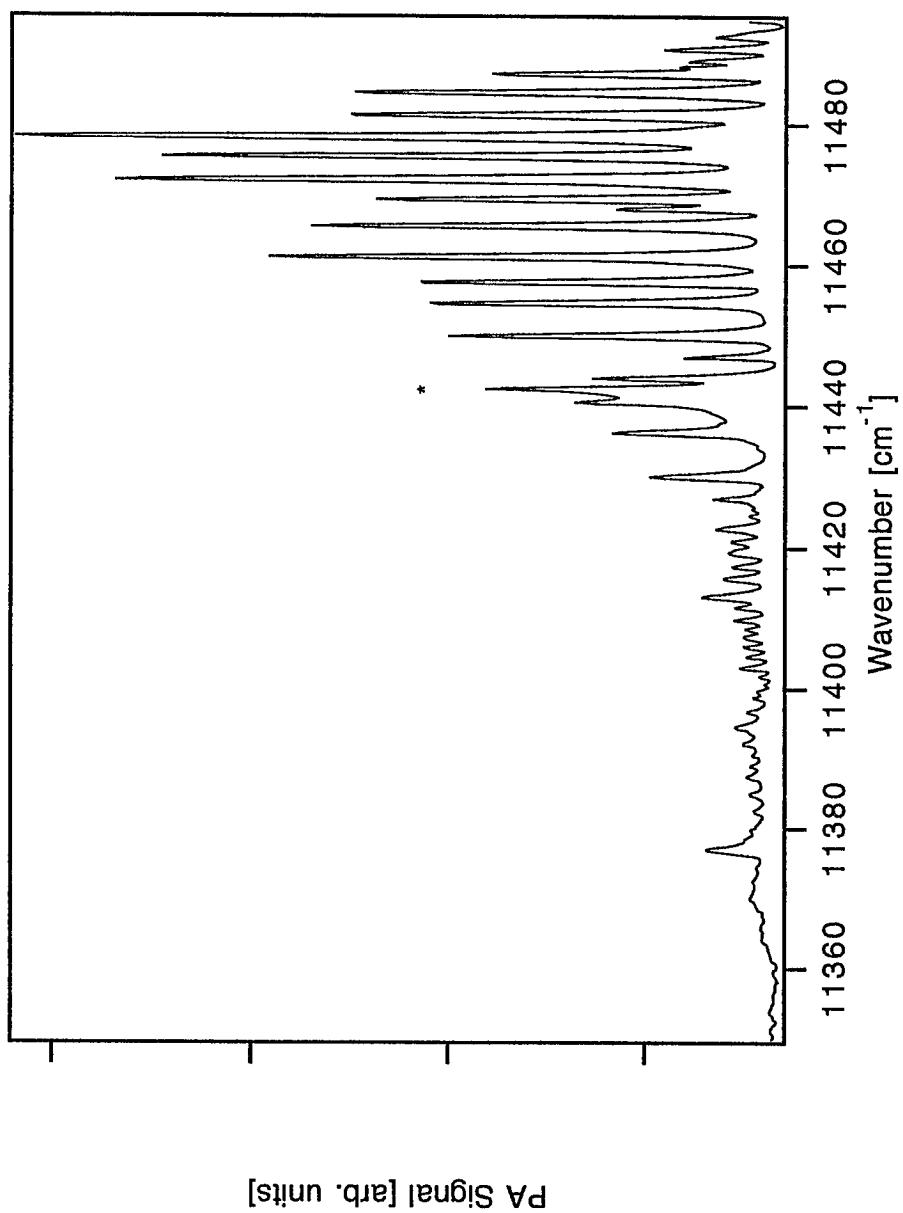


Figure VI-3. The hot band associated with $5\nu_3$ transition of $^{12}\text{CO}_2$. The head is in the P-branch region of the $5\nu_3$ band indicated by an asterisk.

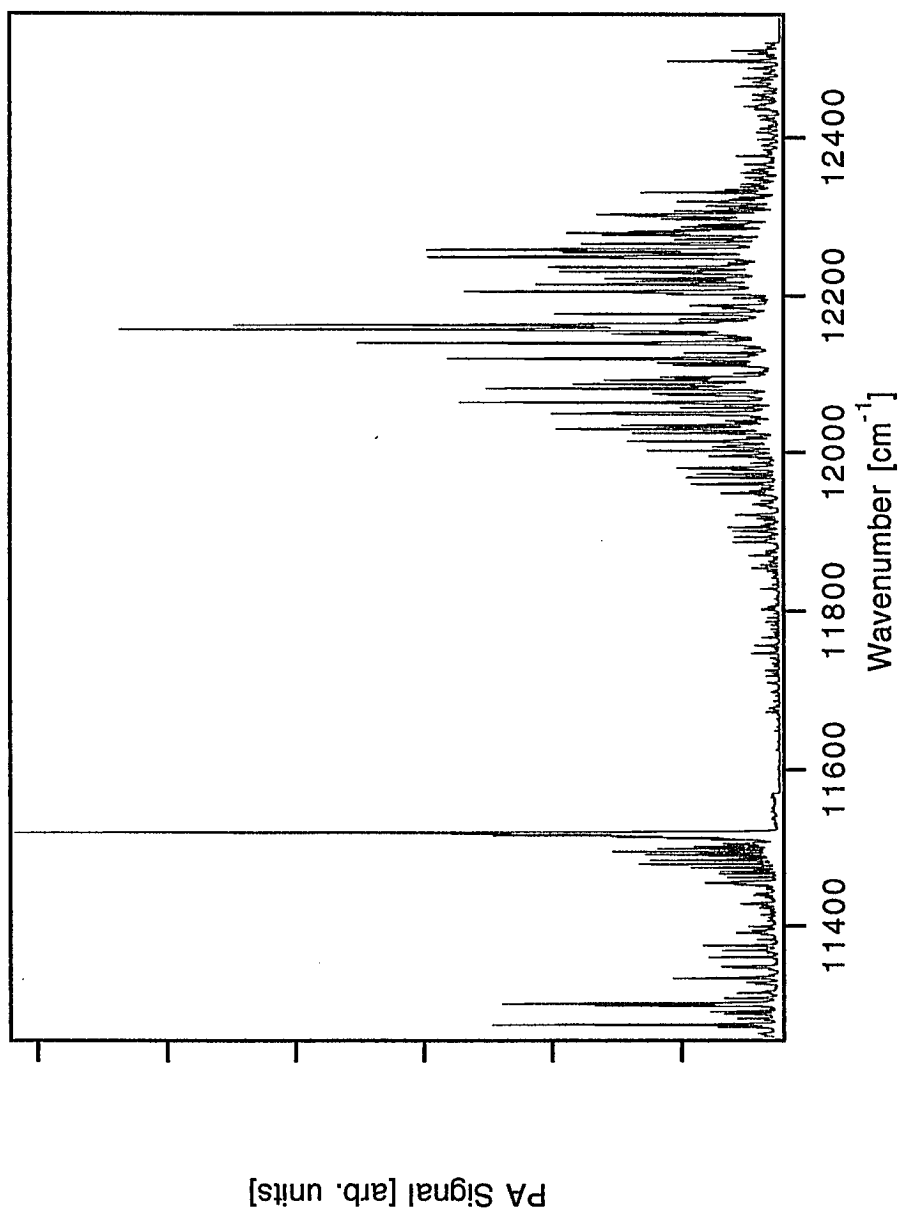


Figure VI-4. The $5\nu_3$ band of $^{12}\text{CO}_2$ near 11500 cm^{-1} and water overtone bands in the near infrared. Note that the sensitivity was changed by a factor of 10 near 11600 cm^{-1} .

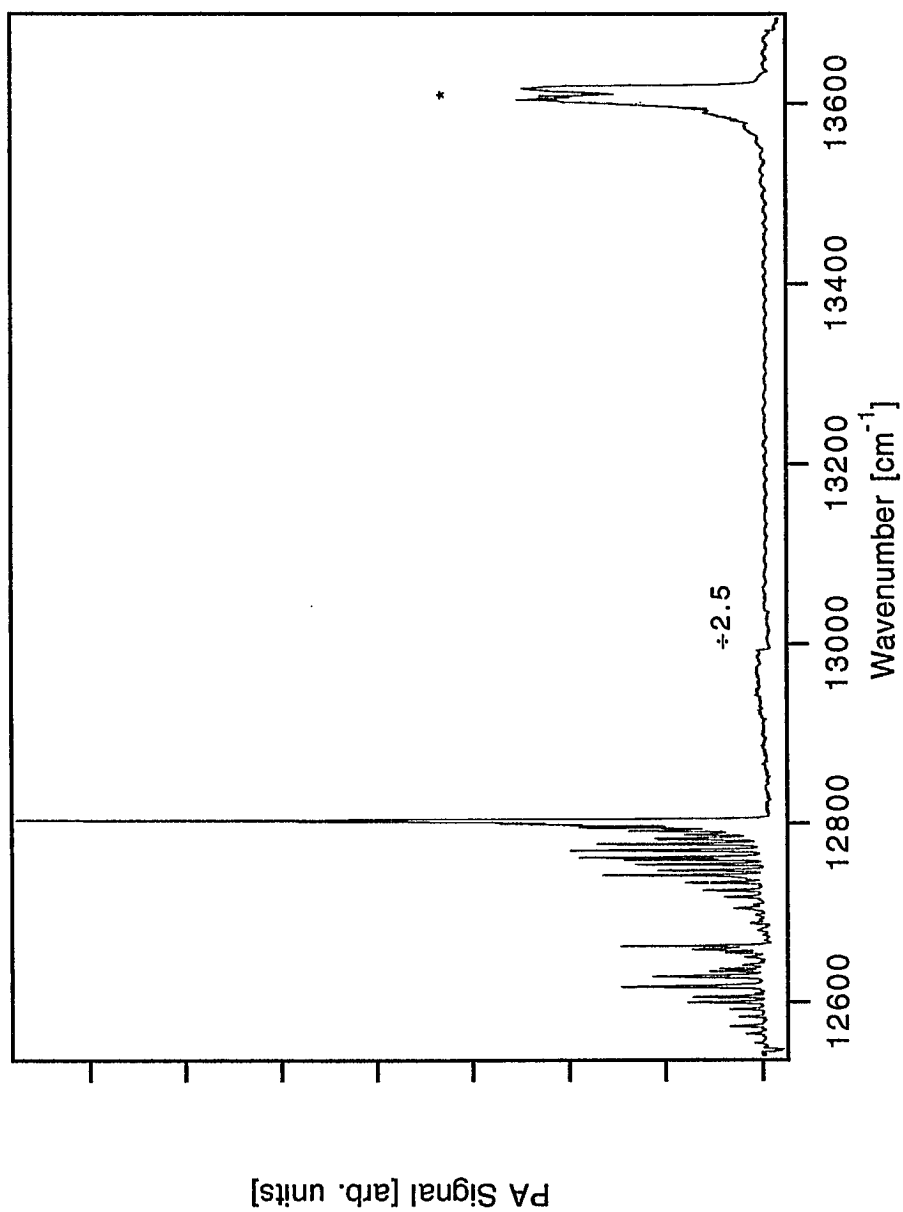


Figure VI-5. The $\nu_1+5\nu_3$ diad of $^{12}\text{CO}_2$ and the overtone band of phenol (indicated by an asterisk). The sensitivity was changed by a factor of 2.5 near 13000 cm^{-1} .

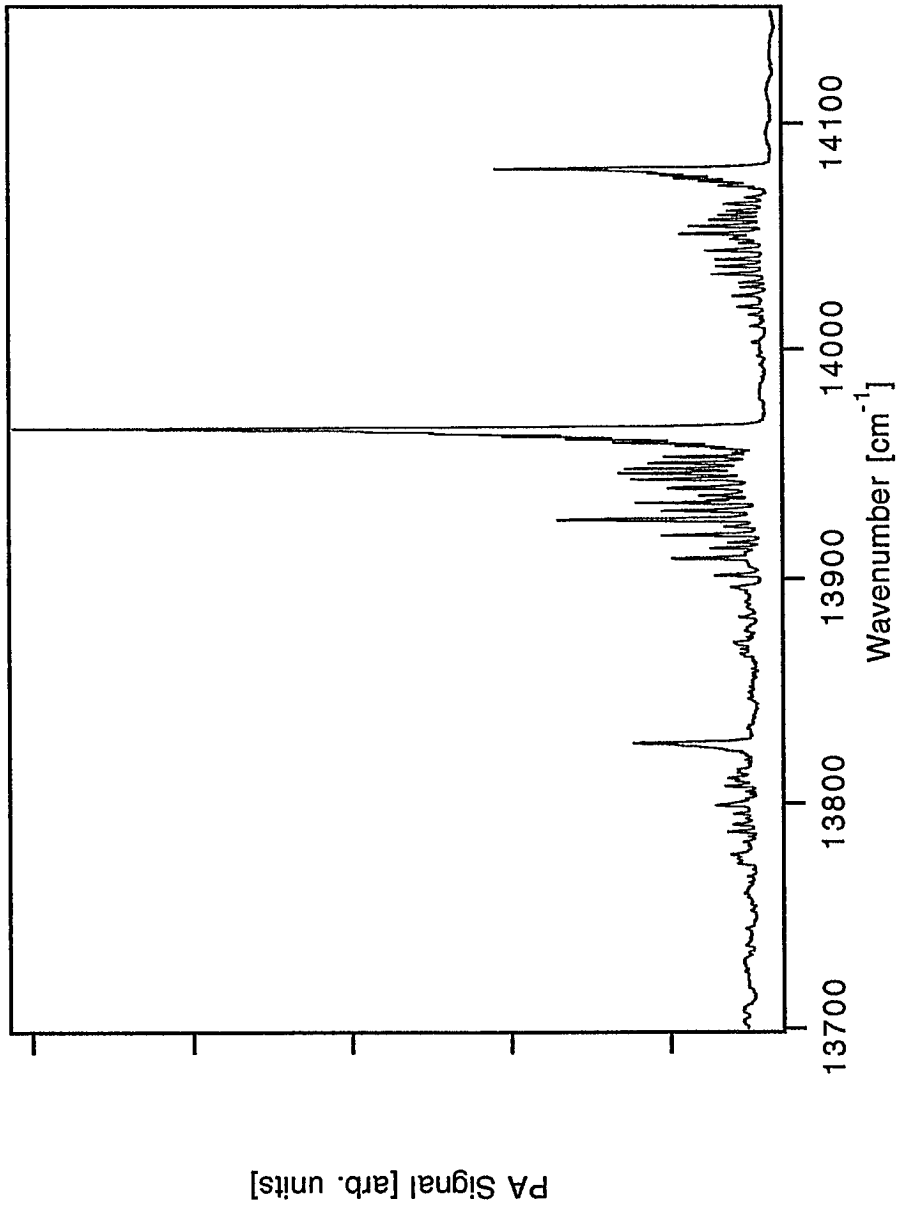


Figure VI-6. The spectrum of the $2\nu_1+5\nu_3$ triad for $^{12}\text{CO}_2$.

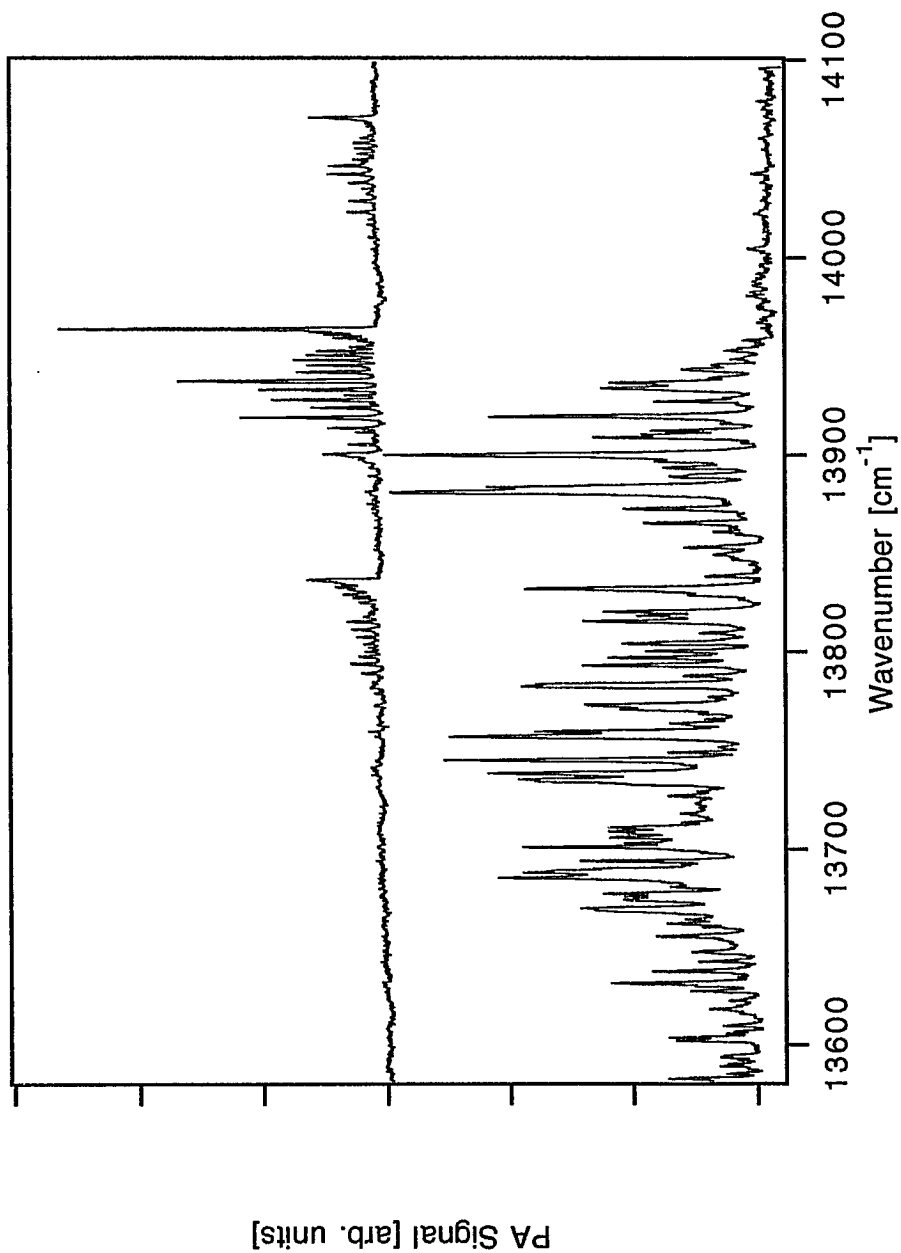


Figure VI-7. The spectra of water and the $2\nu_1+5\nu_3$ triad of $^{12}\text{CO}_2$ from the same scan. The top trace is the $^{12}\text{CO}_2$ triad and the bottom is the overtone bands of water. The water spectrum was taken outside of the laser cavity.

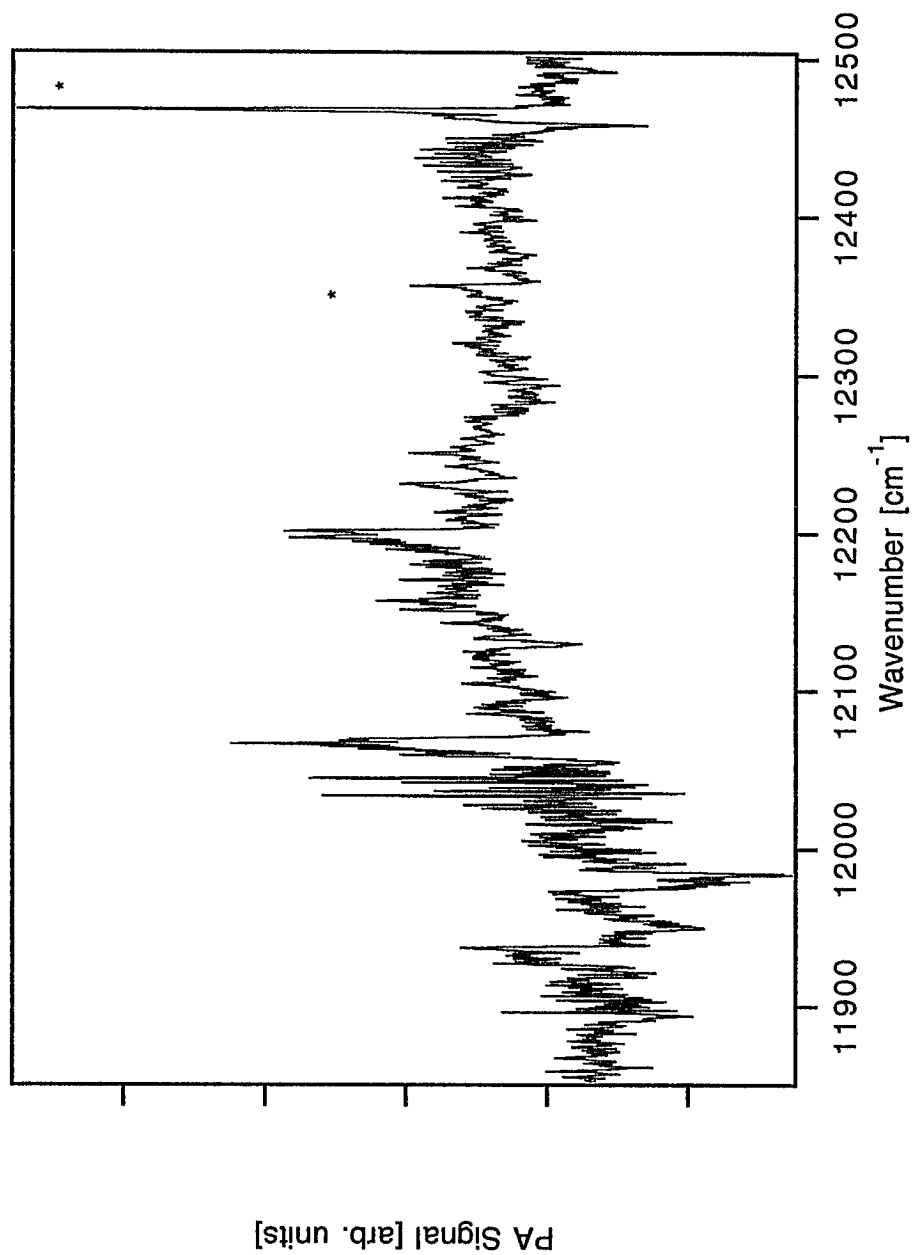


Figure VI-8. The three stronger components of the $4\nu_1+3\nu_3$ pentad of $^{13}\text{CO}_2$. The two bands indicated with asterisks on the right of the spectrum are the $\nu_1+5\nu_3$ diad of $^{13}\text{CO}_2$ with natural abundance in the sample.

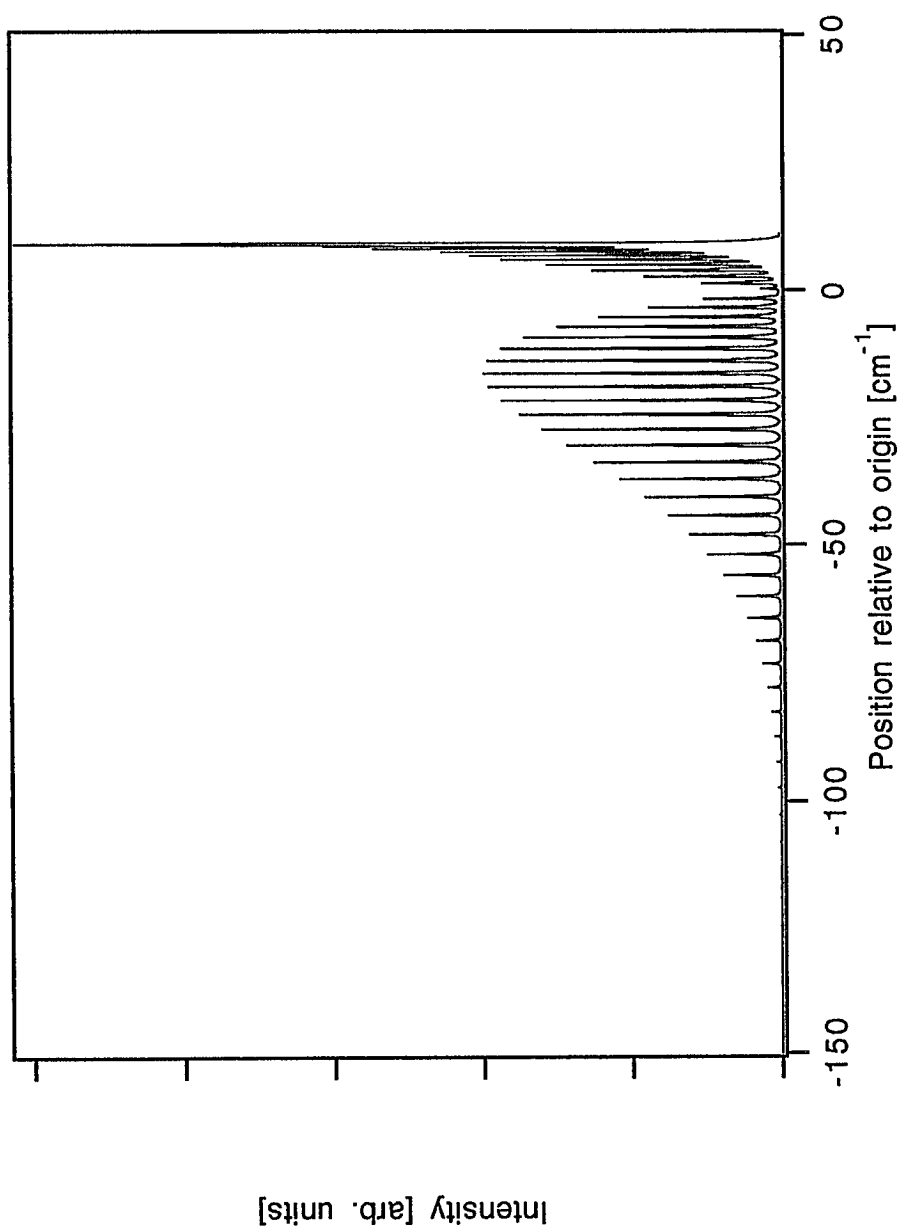


Figure VI-9. The rotational structure simulation for the central component of the $2\nu_1+5\nu_3$ triad.

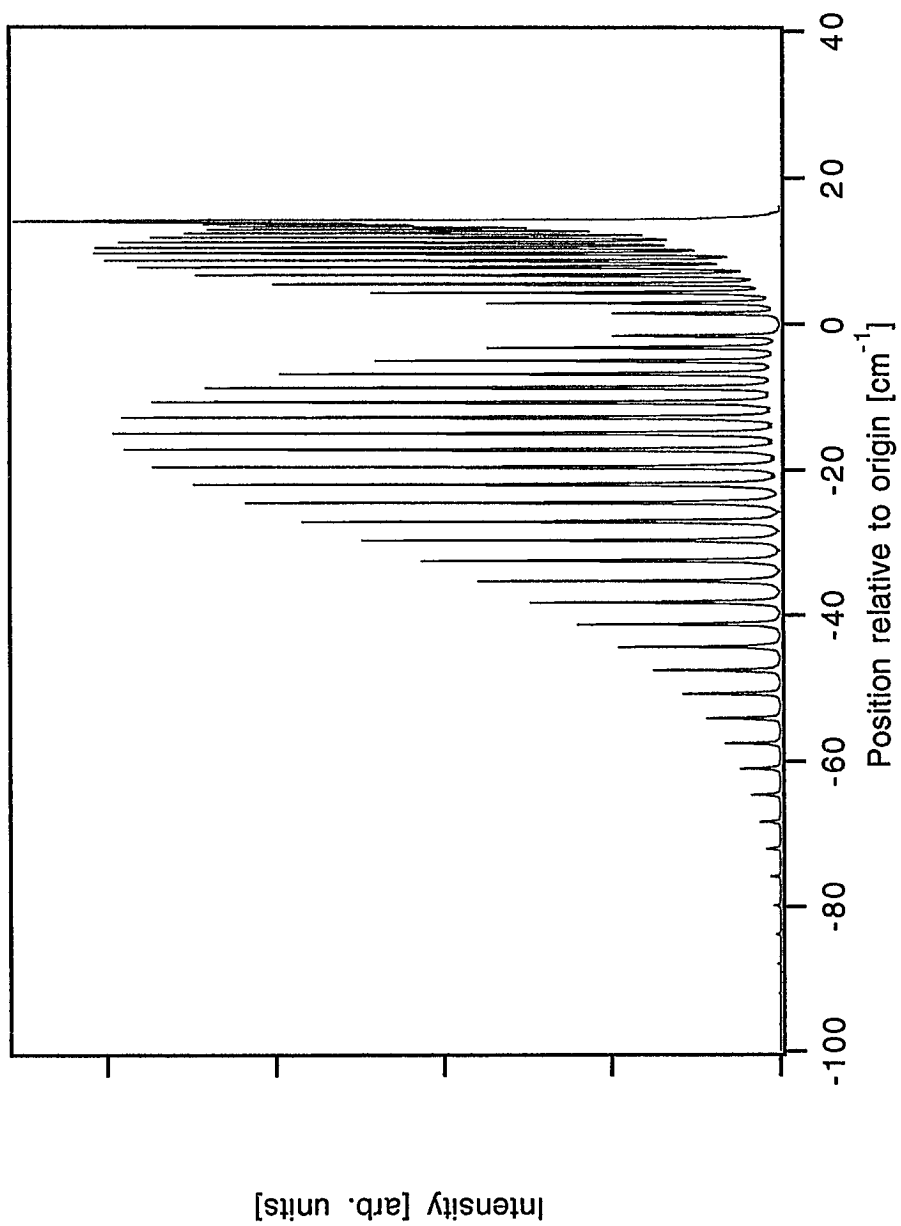


Figure VI-10. A simulation of the rotational structure of the central component for the $4\nu_1+3\nu_3$ pentad of $^{12}\text{CO}_2$.

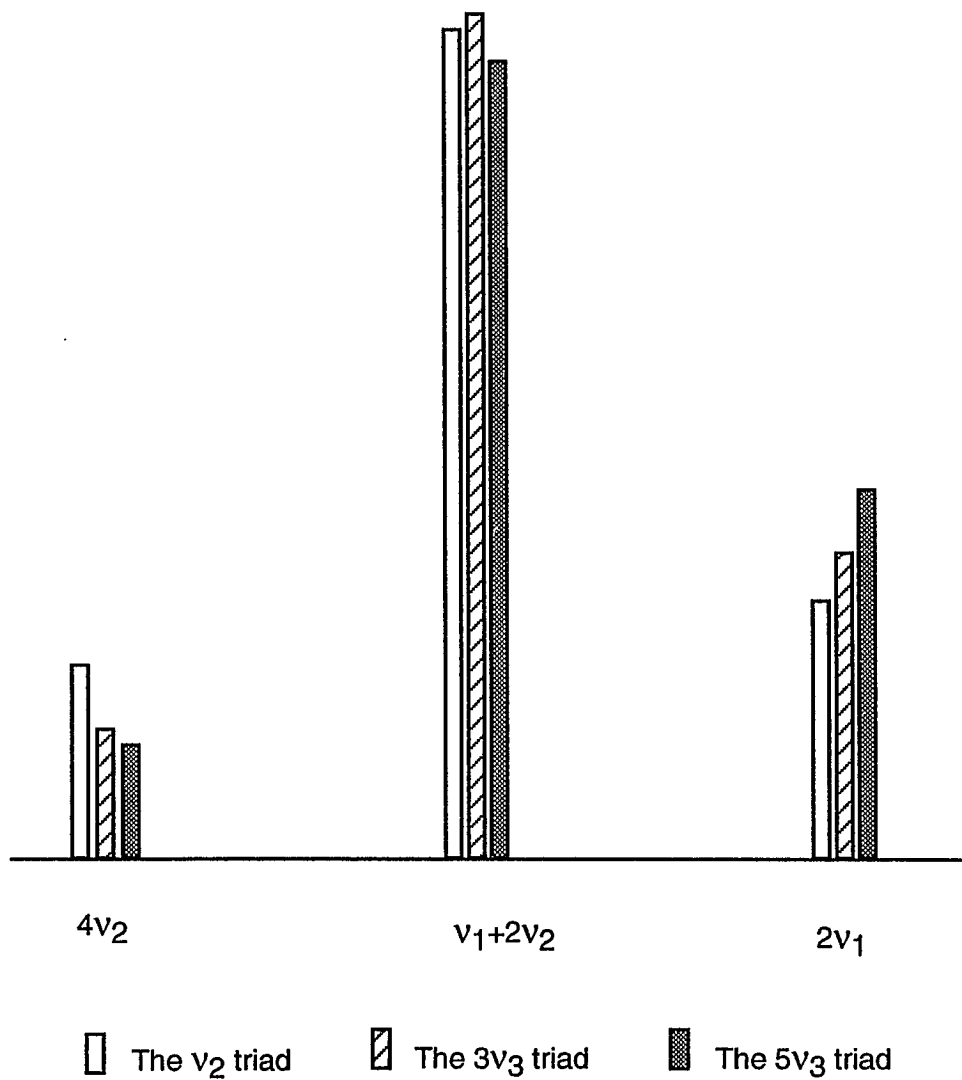


Figure VI-11. Relative intensities of different triads for $^{12}\text{CO}_2$.

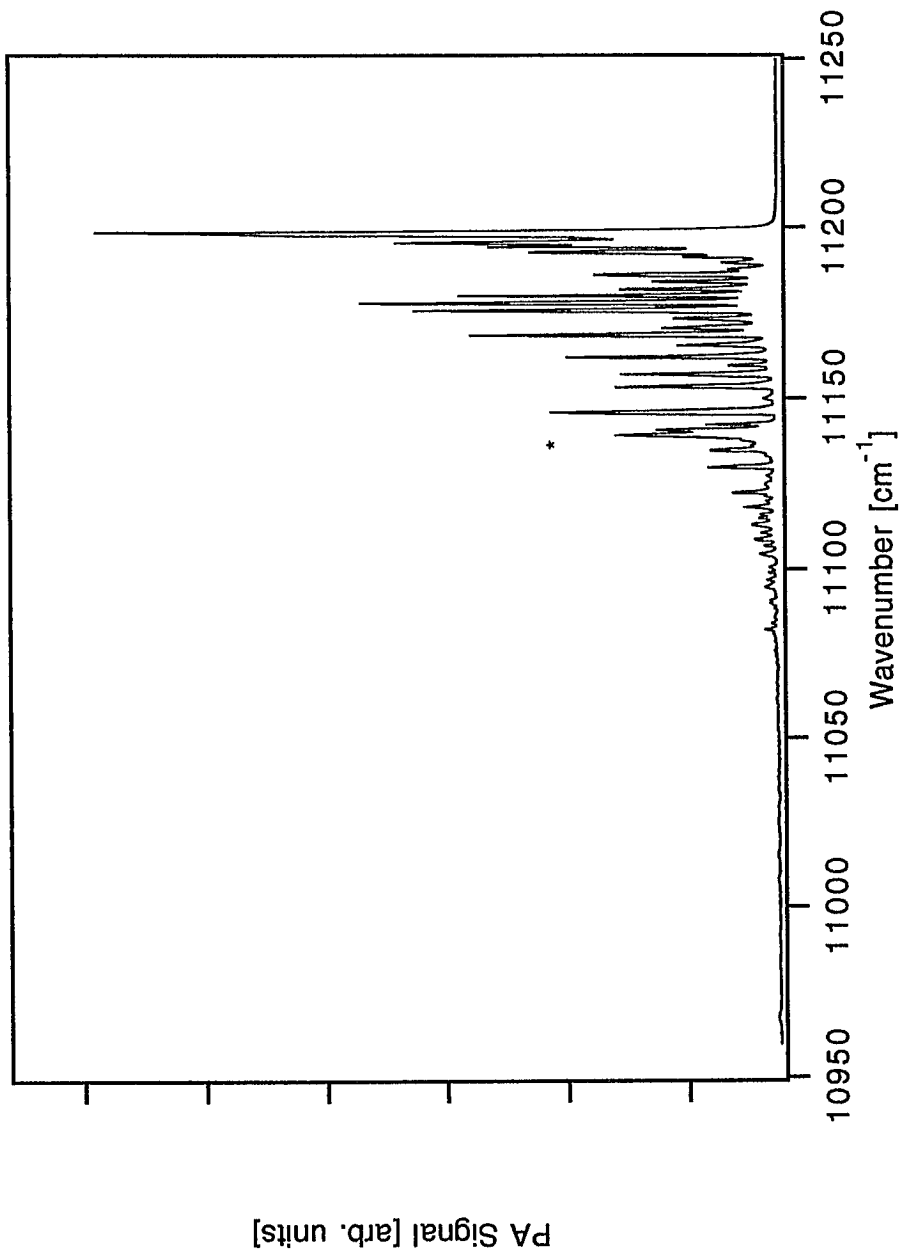


Figure VI-12. The 5v₃ transition of ¹³CO₂. The hot band associated with this transition is indicated by an asterisk.

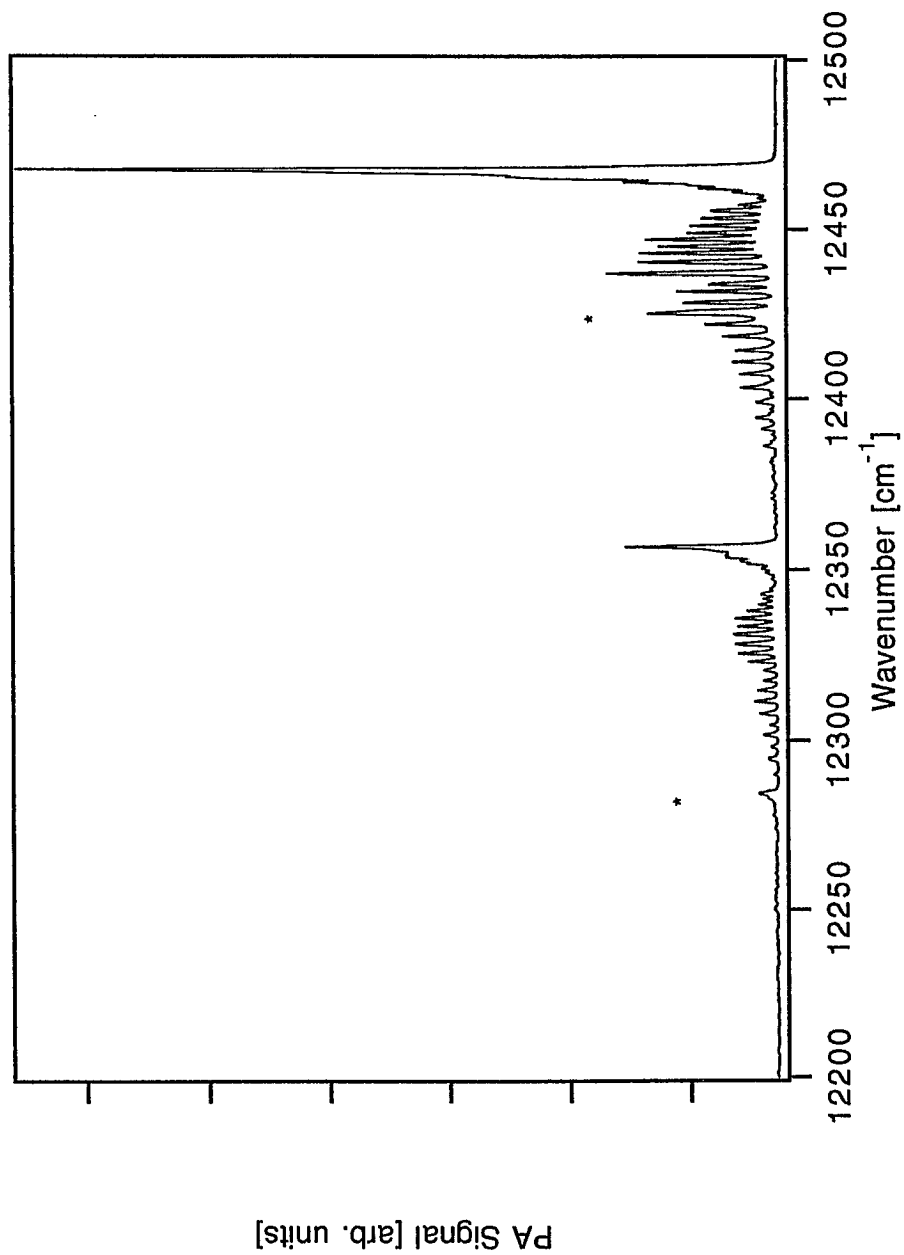


Figure VI-13. The $\nu_1+5\nu_3$ diad of $^{13}\text{CO}_2$. The hot bands associated with these transitions are indicated by asterisks.

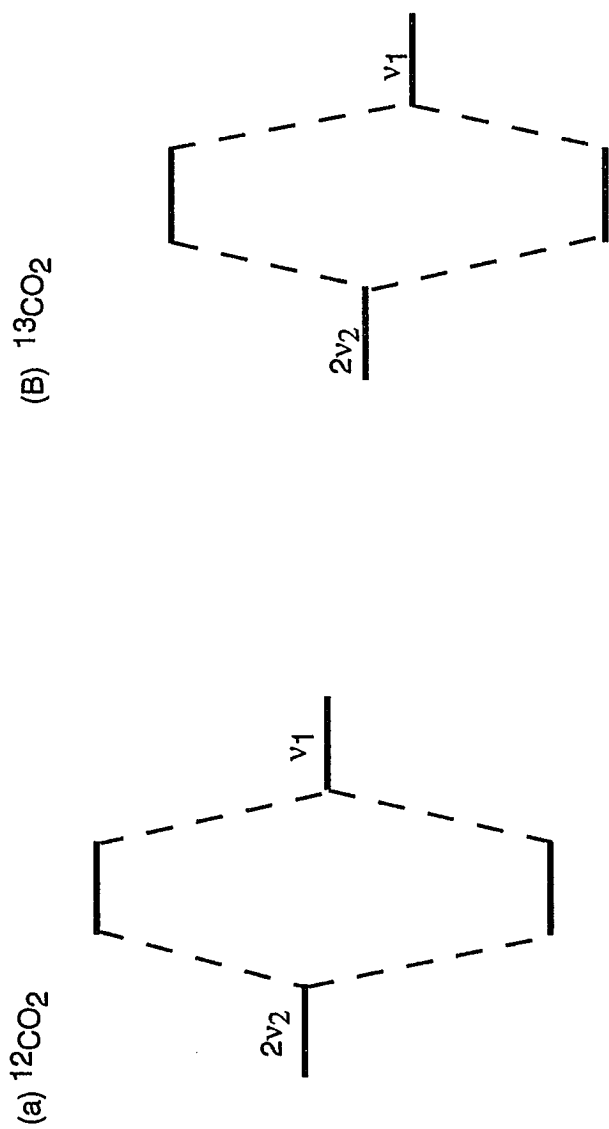


Figure VI-14. Fermi interaction in CO_2 . The energy difference between the unperturbed states for $^{12}\text{CO}_2$ is about 7 cm^{-1} and for $^{13}\text{CO}_2$, the difference is 30 cm^{-1} .

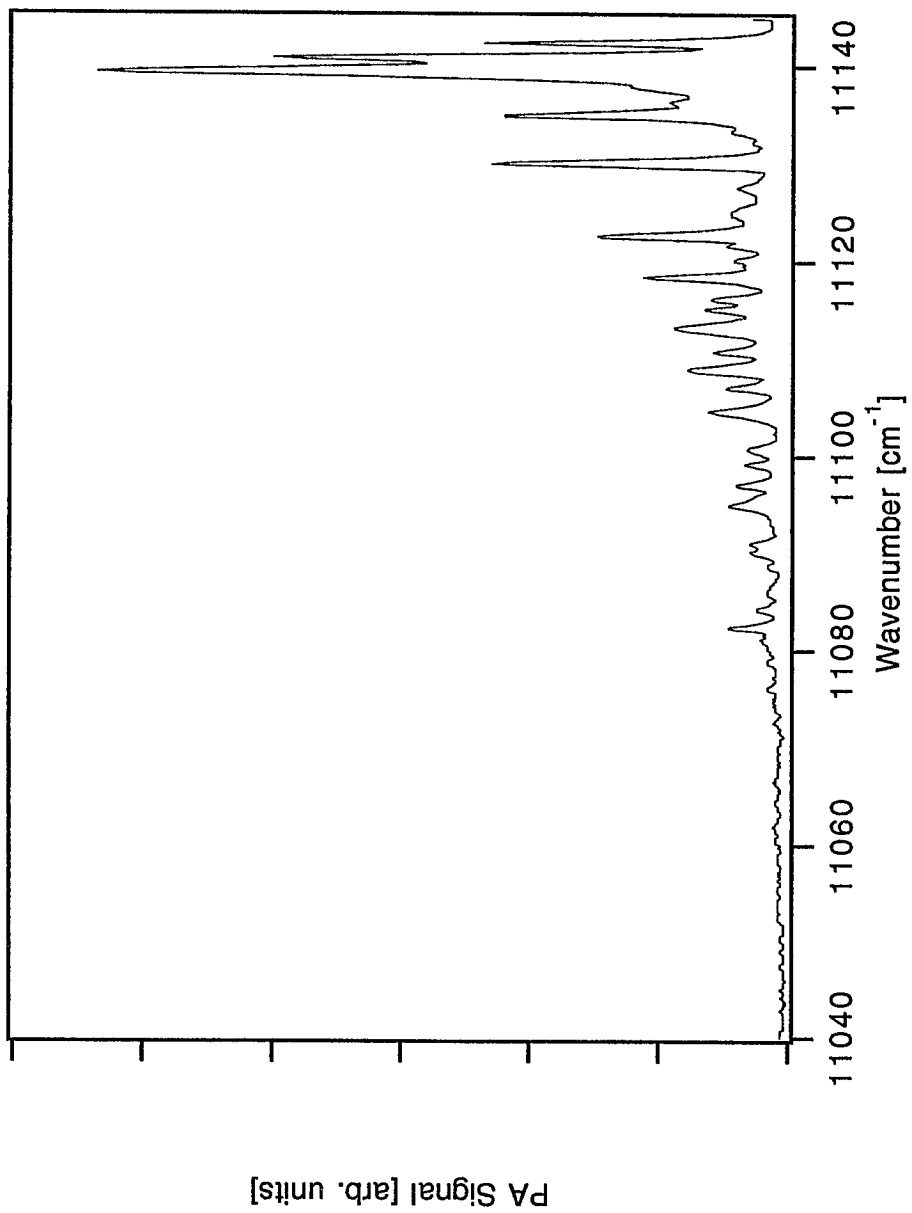


Figure VI-15. An enlargement of the $5\nu_3$ hot band.

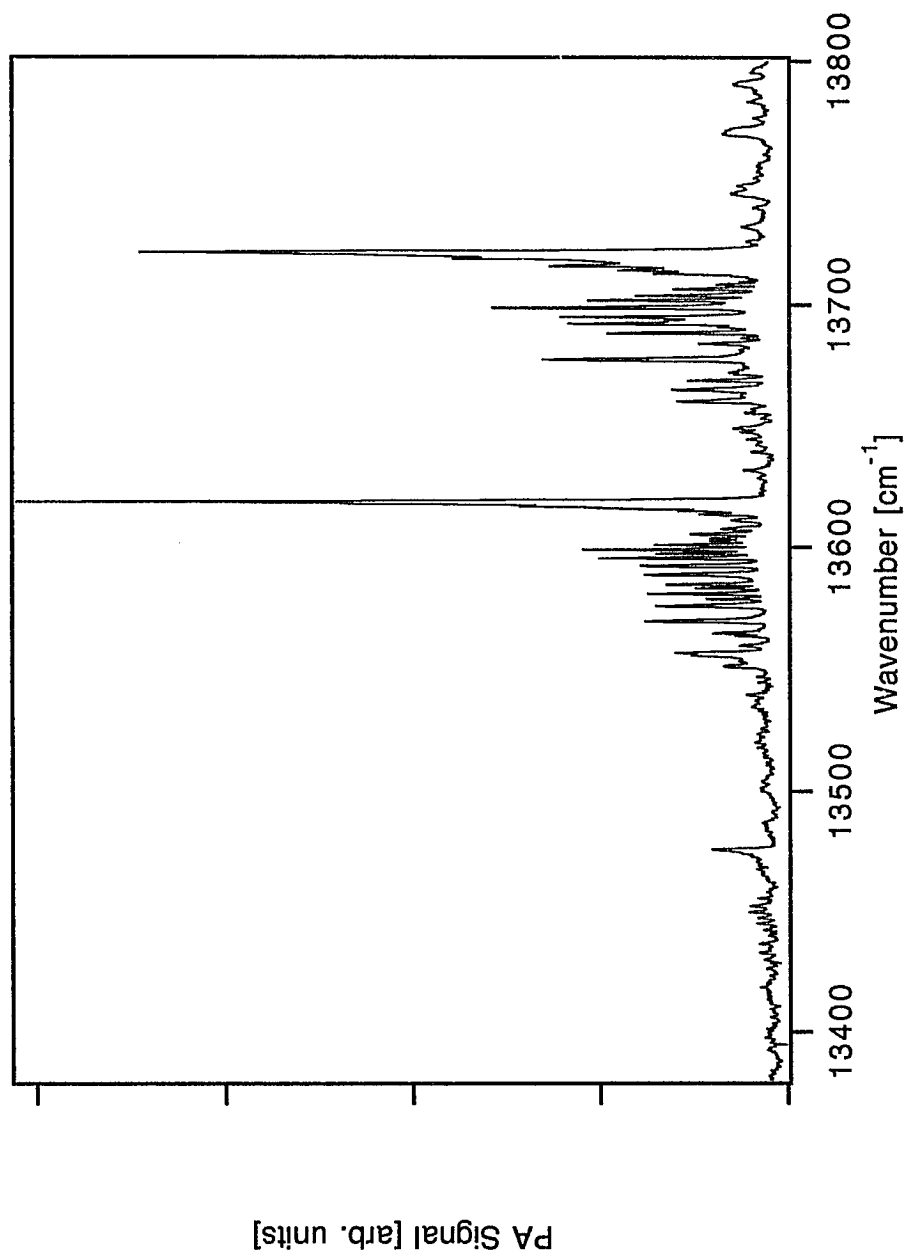


Figure VI-16. The spectrum of the $2\nu_1+5\nu_3$ triad for $^{13}\text{CO}_2$.

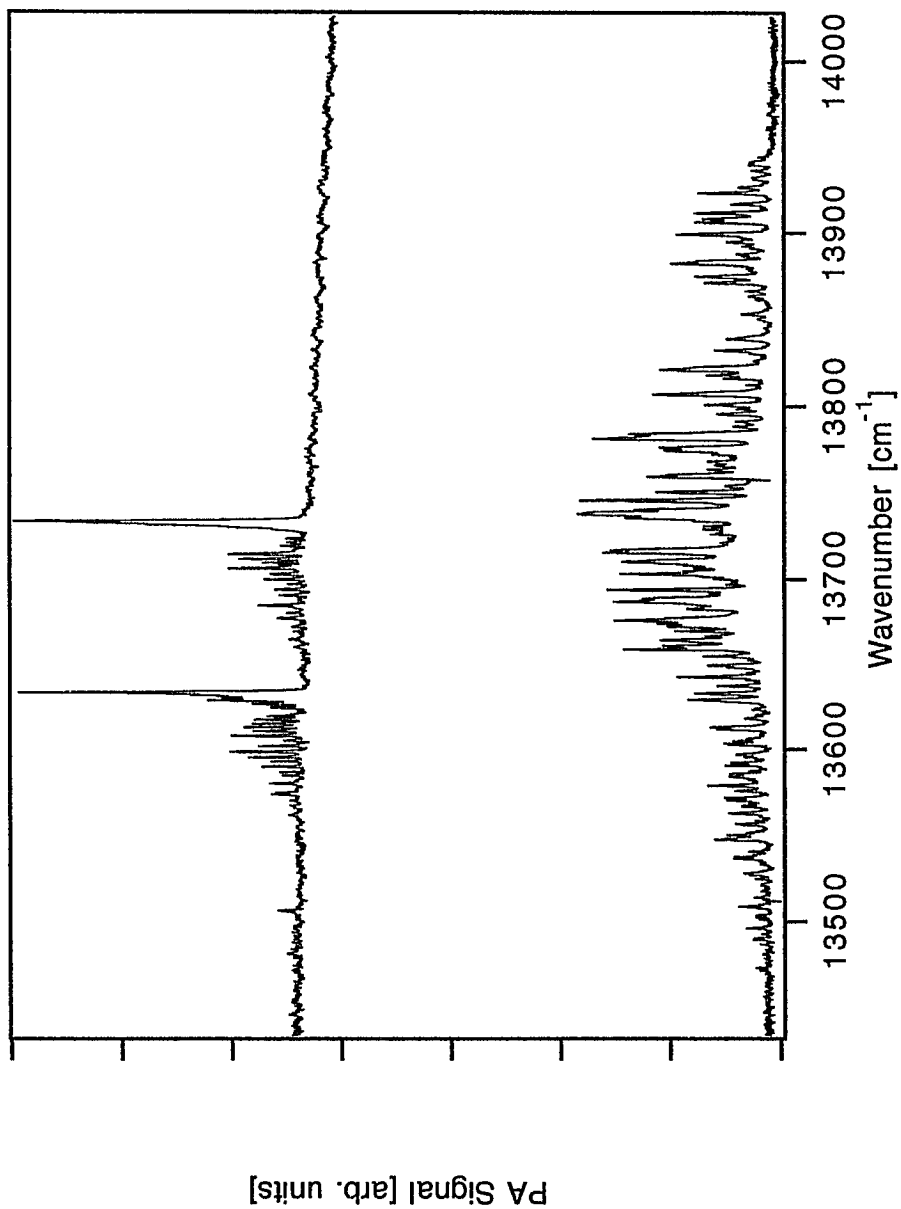


Figure VI-17. The spectra of the $2\nu_1+5_3$ triad for $^{13}\text{CO}_2$ and the overtone bands of water from the same scan. The top trace is the triad and the bottom is the water bands.

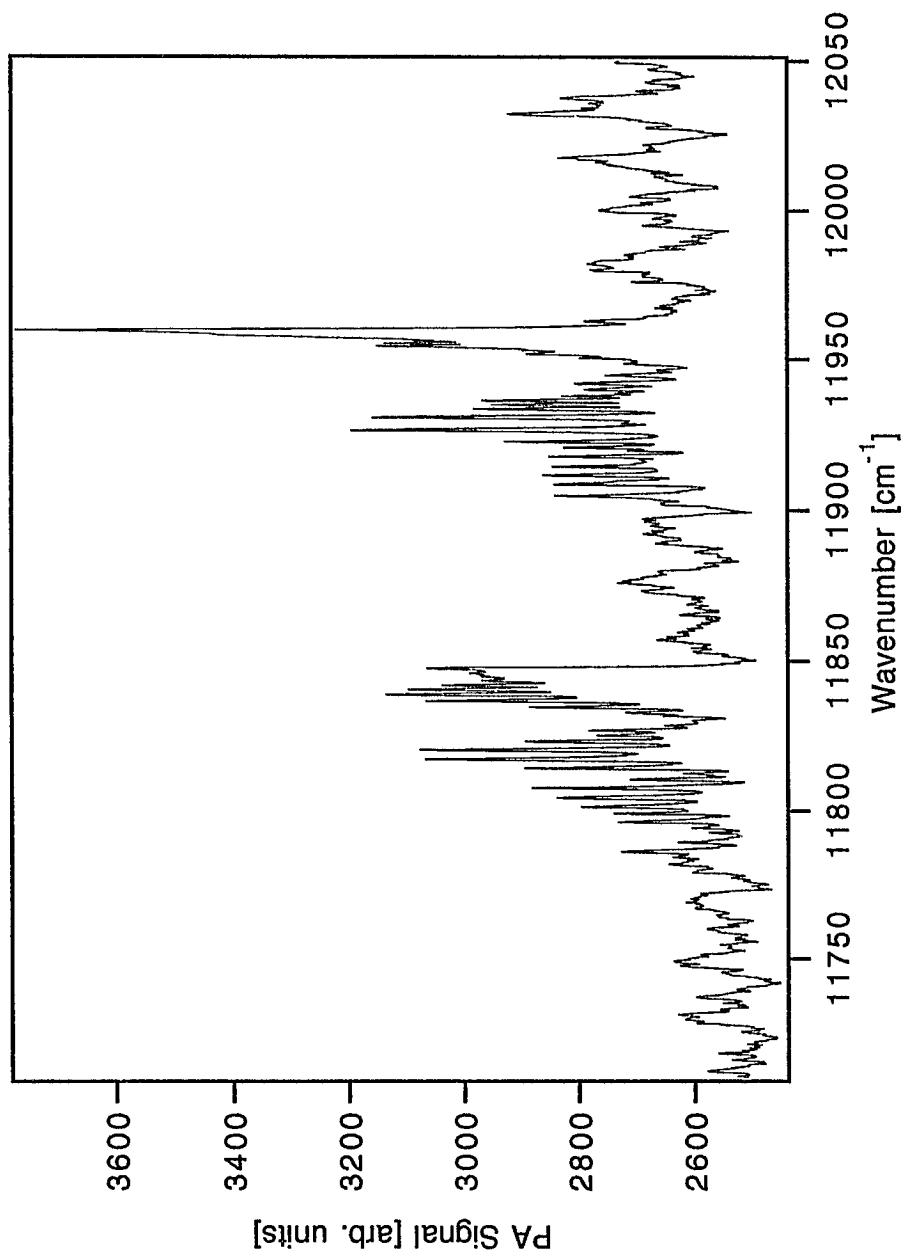


Figure VI-18. The two stronger components of the $4\nu_1+3\nu_3$ pentad of $^{13}\text{CO}_2$

CHAPTER VII

CONCLUSIONS

From this thesis work, the following conclusions can be drawn for both the experimental aspects of photoacoustic detection and the heavy-atom overtone studies.

VII-1 On the Experimental Aspects

Compared with the long absorbing path apparatus used for high energy overtone studies [1-11], photoacoustic spectroscopy has higher sensitivity, simpler experimental set-up, and uses much smaller sample sizes. These features make it a very attractive method for high energy overtone studies especially for isotopic species. By introducing the new photoacoustic cell design, our present apparatus possesses the following advantages and disadvantages:

The advantage of our apparatus lies mainly in the detection process of the photoacoustic signal. First, our sensitivity is high. The sensitivity of our apparatus is on the order of 10^{-10} cm⁻¹ under our experimental conditions, which is an equivalent of an optical path length about 1000 km atm for the detection of CO₂ overtone transitions. It can measure absorption cross section as small as 10^{-29} cm² molecule⁻¹ under one atm. Second, the apparatus has high immunity to background signals. The background signal presented in

our apparatus is estimated to be on the order of 10^{-11} cm^{-1} . This means that our detectability has not been limited by background signals. Third, the interference signal generated by water absorption is reduced to a very low level. By using the new cell, drying agents like P_2O_5 can be placed with the sample. The water molecular density is reduced to about $8 \times 10^{11} \text{ molecule cm}^{-3}$ [12] and this gives a water band absorptivity about $1 \times 10^{-9} \text{ cm}^{-1}$ in our spectral range.

The disadvantages of our apparatus mainly rest with the measurements of the band positions and absorption cross sections. Our accuracy on both the position and cross section measurements is rather poor. First, the position measurements depend on both the resolution of the laser and the method used. Using the water lines to calibrate the positions can introduce large uncertainty because the water lines do not cover the total spectral range. Due to its nature, photoacoustic spectroscopy is not the best method to perform intensity measurements. Besides, the laser is not scanned smoothly, this leads to irregular progressions in the rotational structure and some of the rotational bands were seriously affected, resulting in considerable uncertainty in the integration process.

In order to overcome these problems, first, an etalon may be used in the laser cavity to smooth the wavelength scan of the infrared laser and to increase the resolution. Second, more accurate methods are needed for the wavelength calibration: For example, to use a wavemeter to measure the wavelength. Third, new intensity calibration standard should be used on the cross section measurement, such as oxygen and HD.

VII-2 On the Heavy-Atom Overtone Studies

First, for these heavy-atom systems investigated in this thesis work, the most important conclusion can be reached is that heavy-atom overtone spectroscopy in the near infrared can be studied experimentally by employing the laser photoacoustic method. It opens a new research area for obtaining high energy spectroscopic information on heavy-atom molecules and may change the situation currently dominated by light-atom overtone spectroscopy in the high excitation energy range. From the observations on those overtone transitions, prediction can be made that some of the overtone transitions of these species in the visible region may be observed by using the same method.

Second, theoretical calculations on these systems are consistent with the observed values for both the positions and relative intensities and the normal mode model is still a good approximation for describing these systems in our spectral range.

Third, even in relatively high energy region, state mixing is heavily dependent on the symmetry properties of the systems. For example, heavier mixing has been observed in OCS than that in CO₂ due to the lower symmetry possessed by the former molecule.

Among these four systems, the most thoroughly studied ones are the ¹²CO₂ and ¹³CO₂ molecules. For these systems, the rotational analysis has not been performed due to the reasons mentioned before. If whenever conditions permit, the positions and the intensities of these new discovered transitions should be reexamined to obtain more accurate measurements. For N₂O, there are many transitions in our extended spectral range have not

been examined [6]. Transition cross sections of this molecule should also be measured. In addition, new overtone bands should be discovered by employing the new photoacoustic cell to eliminate water interference.

The work on OCS is also far from complete. First, the spectra of this molecule were taken by using the old photoacoustic cell for the early studies of the this thesis work. The water interferences are quite serious so that these overtone transitions need to be retaken by using the new cell to eliminate the water interferences. Second, transition intensities should be estimated by using a proper calibration standard.

REFERENCES

- [1] H. J. Bernstein and G. Herzberg, *J. Chem. Phys.* **16** (1948) 30
- [2] G. Herzberg and K. N. Rao, *J. Chem. Phys.* **17** (1949) 1099
- [3] S. P. Sinha, *J. Chem. Phys.* **18** (1950) 217
- [4] R. D. Cowan, G. Herzberg and S. P. Sinha, *J. Chem. Phys.* **18** (1950) 1538
- [5] C. Reid, *J. Chem. Phys.* **18** (1950) 1544
- [6] G. Herzberg and L. Herzberg, *J. Chem. Phys.* **18** (1950) 1551
- [7] B. D. Saksena, *J. Chem. Phys.* **20** (1952) 95
- [8] A. V. Jones, *J. Chem. Phys.* **20** (1952) 860
- [9] A. E. Douglas and D. Sharma, *J. Chem. Phys.* **21** (1953) 448
- [10] L. F. H. Bovey, *J. Chem. Phys.* **21** (1953) 830
- [11] G. Herzberg and L. Herzberg, *J. Opt. Soc. Am.* **43** (1953) 1037
- [12] D. R. Lide, *CRC Handbook of Chemistry and Physics*, 73rd Ed. 1992-1993, p. 15-21

APPENDIX

GENERAL INFORMATION ABOUT THE CARBON DIOXIDE MOLECULE

(1) Notations of vibrational states and transitions. Carbon dioxide is a linear molecule, and the two most abundant species, $^{12}\text{CO}_2$ and $^{13}\text{CO}_2$ studied in this thesis both belong to the point group $D_{\infty h}$. The molecule has four normal vibrational modes: Namely, the symmetric stretch, the asymmetric stretch and two bending vibrations. The two bending modes are degenerate and will have the same frequency.

Historically, there exist several different notations to indicate the vibrational states, and the vibrational transitions for this molecule, and they are quite confusing. For a triatomic linear molecule, one convention to label a vibrational state is to use the vibrational quantum number for each mode, in such an order that the position of the number indicates the vibrational mode, and the number itself indicates the energy of the state or the excitation. Usually, the vibrational quantum numbers are in parentheses, for example, (ν_1, ν_2, ν_3) . Here the convention is to assign the first number to the asymmetric stretch, the second to the bending and the third to the symmetric stretch. If a label reads like this, $(1, 2, 0)$ it means a vibrational state which has one quantum of excitation in the symmetric mode, two quanta in the bending mode and no excitation in the asymmetric mode. The vibrational ground state is $(0, 0, 0)$. Using this convention, any vibrational transition should be labeled with the upper and lower states, with the upper state written first. For example, the fundamental transition in the bending mode should read

(0, 1, 0)-(0, 0, 0) and first overtone (0, 2, 0)-(0, 0, 0).

However, there is another more convenient way used by spectroscopists to indicate both vibrational states and transitions. For a triatomic linear molecule, the Greek letter ν with subscripts 1, 2, and 3 is used to label the three frequencies and the modes. For example, ν_1 means the fundamental frequency for the symmetric mode, and ν_2 for the bending mode and ν_3 for the asymmetric mode. Besides, ν can be both a state and a transition. For example, ν_1 means the same state as (1, 0, 0) does, and ν_1 means the same transition as (1, 0, 0)-(0, 0, 0) does. For higher states or overtone and combination transitions, simply put the number of excitation in front of the corresponding ν 's and then take the summation of them to indicate the state or transition. For example, $2\nu_1+3\nu_3$ means the same state as (2, 0, 3) and is the same transition as (2, 0, 3)-(0, 0, 0).

For the $^{12}\text{CO}_2$ molecule, the fundamental frequencies for the symmetric, the bending and the asymmetric vibrational modes are 1388, 667, and 2349 cm^{-1} , respectively (see G. Herzberg, *Molecular Spectra and Molecular Structure, Vol. 2, Infrared and Raman Spectra of Polyatomic Molecules*, Krieger Publishing Company, Reprint Ed. 1991, p. 272), so that the first overtone vibration in the bending mode will have approximately the same energy as that of the symmetric fundamental vibration. In addition, these two vibrations have the same symmetry. Consequently, strong interaction between these two states occur which is called the Fermi resonance. Because of this inherent interaction, any vibrational states with $\nu_1 \neq 0$ will be interacting with other state or states. The total number of the states that are in the same interaction is ν_1+1 . For example, the state (1, 0, 3) or $\nu_1+3\nu_3$, will interact with state (0, 2, 3) or $2\nu_2+3\nu_3$, to form two new states which are usually called perturbed states. In the same manner, the state (2, 0, 3) or

$2\nu_1+3\nu_3$, will interact with states (1, 2, 3) and (0, 4, 3) or $\nu_1+2\nu_2+3\nu_3$ and $4\nu_2+3\nu_3$, to form three perturbed states. In consequence, vibrational transitions that involve those states mentioned above will show multiple structure. For instance, a transition which takes the $\nu_1+3\nu_3$ as the upper state will be a diad, and that which takes the $2\nu_1+3\nu_3$ as the upper state will be a triad, etc.

Sometimes, the notation like $5\nu_3+(2\nu_1, \nu_1+2\nu_2, 4\nu_2)$ is used to indicate a triad, and what it really shows are the three perturbed states within the triad. In this case, the three component states are $5\nu_3+2\nu_1$, $5\nu_3+\nu_1+2\nu_2$ and $5\nu_3+4\nu_2$. Any transition that takes this triad as the upper state will show three bands like the one observed in this thesis work. Frequently, the above notation is replaced with $2\nu_1+5\nu_3$ triad to mean the same state or transition.

Unfortunately, all those notations can not distinguish whether the state is perturbed or not. For example, $2\nu_1+3\nu_3$ could be a notation for both the unperturbed and the perturbed state. The reader has to decide according to the actual situation. However, all the states that are involved in observable vibrational transitions are the perturbed states unless there is no perturbation, since the unperturbed states only exist in the imagination or theoretical calculations. Note that the vibrational angular momentum quantum number l is ignored for simplicity in the above discussion.

(2) Transition selection rules and band features. This discussion will basically focus on the transitions studied in this work unless indicated otherwise. The ground state of CO_2 has the Σ_g^+ symmetry and excited states can have $\Sigma, \Pi, \Delta, \dots$ states depends on the vibrational angular momentum. The ro-vibrational transitions for CO_2 according to Herzberg (G. Herzberg, Molecular Spectra and Molecular Structure, Vol. 2, Infrared and Raman

Spectra of Polyatomic Molecules, Krieger Publishing Company, Reprint Ed.

1991) have the following selection rules:

Vibrationally, $\Delta l=0, \pm 1$, $\Sigma^- \rightarrow \Sigma^+$, $g \rightarrow g$, $u \rightarrow u$ are all forbidden,

Rotationally, $\Delta J=0, \pm 1$ with $J=0 \rightarrow J=0$ forbidden, $+ \rightarrow -$ is allowed, $s \rightarrow a$ is forbidden

where l is the vibrational angular momentum quantum number, J is the rotational quantum number, g , and u are the symmetry with respect to inversion, $+$ and $-$ are parity, and s and a are the symmetry with respect to an exchange of the identical nuclei.

Since the normal mode ν_1 , ν_2 and ν_3 have the symmetry of Σ_g^+ , Π_u and Σ_u^+ , all the states with even numbered ν_2 will have either Σ_u^+ or Σ_g^+ symmetry. This is the dominant situation in this thesis work because most of the transitions involve upper states with even numbered ν_2 . According to the selection rule above, the transitions with Σ_g^+ upper states are forbidden. The transitions with Σ_u^+ upper states are allowed.

Based on the direct product of the symmetry species of the three vibrations, only the odd numbered ν_3 will give a total symmetry of Σ_u^+ , i.e. the even numbered ν_3 transitions are forbidden. These selection rules are rigorously obeyed in the case of CO_2 . Since the allowed transitions are $\Sigma \rightarrow \Sigma$ transitions, or parallel transitions, the bands have only P ($\Delta J=-1$) and R ($\Delta J=+1$) branches. In the high excitation region, the R branch usually forms a bandhead due to the fact that the rotational constant for the upper state is smaller than that for the lower state. All the observations in this thesis work are consistent with these expectations.

COMPREHENSIVE LIST OF REFERENCES

- [1]. A. Adel and D. M. Dennison, *Phys. Rev.*, **43** (1933) 716.
- [2]. A. Adel and D. M. Dennison, *Phys. Rev.*, **44** (1933) 99
- [3]. A. Adel and V. M. Slipher, *Phys. Rev.*, **46** (1934) 240
- [4]. A. B. Wood, *A Textbook of Sound*, 3rd ed.; G. Bell and Sons: London, 1955; p. 246
- [5]. A. C. Tam, in *Ultrasensitive Laser Spectroscopy*, D. S. Kliger, Academic, New York, 1983
- [6]. A. Chedin, *J. Mol. Spectrosc.*, **76**, (1979) 430
- [7]. A. E. Douglas and D. Sharma, *J. Chem. Phys.* **21** (1953) 448
- [8]. A. Fayt, *Ann. Soc. Sci. Bruxelles*, **84** (1970) 69
- [9]. A. Fayt, *Ann. Soc. Sci. Bruxelles*, **86** (1972) 61
- [10]. A. Fayt, R. Vandenhoute, and J. G. Lahaye, *J. Mol. Spectrosc.* **119** (1986) 233
- [11]. A. G. Bell, *Am. J. Sci.* , **20** (1881) 305
- [12]. A. G. Bell, *Philos. Mag.* , **11** (1881) 510
- [13]. A. G. Maki, E. K. Plyer, and E. D. Tidwell, *J. Resear.*, the National Bureau of Standards, **66 A** (1962) 163
- [14]. A. G. Maki, W. B. Olson, and R. L. Sams, *J. Mol. Spectrosc.*, **81** (1980) 122
- [15]. A. Miklos and A. Lorincz, *Appl. Phys.* , **B 48** (1989) 213
- [16]. A. Rosencwaig, *Photoacoustics and Photoacoustic Spectroscopy*, In *Chemical Analysis*; Elving, P. J., Winefordner, J. D., Eds.; John Wiley and Sons: New York, 1980, Vol. 57
- [17]. A. V. Jones, *J. Chem. Phys.* **20** (1952) 860

- [18]. B. D. Saksena, *J. Chem. Phys.* **20** (1952) 95
- [19]. B. Henry, *Vibrational Spectra and Structure*, J. R. Durig, Ed., Vol. 10, Elsevier, New York, (1981)
- [20]. B. R. Henry and M. G. Sowa, *Prog. Analyt. Spectrosc.*, **12** (1989) 349
- [21]. C. F. Dewey Jr., *Opt. Eng.* , **13** (1974) 483
- [22]. C. K. N. Patel and R. J. Kerl, *Appl. Phys. Lett.*, **30** (1977) 578
- [23]. C. P. Courtoy, *Ann. Soc. Sci. Bruxelles, Seris 1*, (1959) 5
- [24]. C. P. Courtoy, *Can. J. Phys.*, **35** (1957) 608
- [25]. C. R. Bailey and A. B. D. Cassie, *Proc. Roy. Soc. London*, **135** (1932) 375
- [26]. C. R. Bailey and A. B. D. Cassie, *Proc. Roy. Soc. London*, **140** (1933) 605
- [27]. C. Reid, *J. Chem. Phys.* **18** (1950) 1544
- [28]. D. Burch, D. A. Gryvnak, and R. R. Patty, *J. Opt. Soc. Am.*, **58** (1968) 335
- [29]. D. H. Rank, U. Fink, J. V. Foltz, and T. A. Wiggins, *Astrophys. J.* , **140** (1964) 366
- [30]. D. J. Baniford, S. V. Filseth, M. F. Foltz, J. W. Hepburn, C. B. Moore, *J. Chem. Phys.*, **82** (1985) 3032
- [31]. D. R. Lide, *CRC Handbook of Chemistry and Physics*, 73rd Ed. 1992-1993, p. 15-21
- [32]. D. R. Preuss and J. L. Gole, *Appl. Opt.*, **19** (1980) 702
- [33]. Davidsson, J.; Gutow, J. H.; and Zare, R. N. *J. Phys. Chem.* , **94** (1990) 4069
- [34]. E. Kritchman, S. Shtrikman, and M. Slatkine, *J. Opt. Soc. Am.*, **68** (1978) 1257
- [35]. E. L. Kerr, and J. G. Atwood, *Appl. Opt.* , **7** (1968) 915
- [36]. E. Max and L. G Rosengren, *Opt. Commun.*, **11** (1974) 422
- [37]. E. W. Balson, *Trans. Faraday Soc.*, **43** (1947) 48

- [38]. F. Mayer-Bourbonneux, J. Dupre-Maquaire, and C. Mayer, *J. Mol. Spectrosc.*, **63** (1976) 288
- [39]. G. A West, J. J. Barrett, D. R. Siebert and K. V. Reddy, *Rev. Sci. Instrum.*, **54** (1983) 797
- [40]. G. Ametand M. Pimbert. *J. Mol. Spectrosc.*, **16** (1965) 278
- [41]. G. Herzberg and K. N. Rao, *J. Chem. Phys.* , **17** (1949) 1099
- [42]. G. Herzberg and L. Herzberg, *J. Chem. Phys.*, **18** (1950) 1551
- [43]. G. Herzberg and L. Herzberg, *J. Opt. Soc. Am.*, **43** (1953) 1037
- [44]. G. Herzberg, *Molecular Spectra and Molecular Structure, Vol. 2, Infrared and Raman Spectra of Polyatomic Molecules*, Reprint ed. Krieger: Malabar, 1991
- [45]. G. West, J. J. Barrett, D. R. Siebert, and K. V. Reddy, *Rev. Sci. Instrum.* , **54** (1983) 797
- [46]. H. E. Howard-lock and B. P. Stoicheff, *J. Mol. Spectrosc.*, **37** (1971) 321
- [47]. H. J. Bernstein and G. Herzberg, *J. Chem. Phys.*, **16** (1948) 30
- [48]. H. J. Callomon and H. W. Thompson, *Proc. Roy. Soc. A*, **222** (1954) 431
- [49]. H. L. Dai, R. W. Field, and J. L. Kinsey, *J. Chem. Phys.*, **82** (1985) 1606
- [50]. H. R. Gordon and T. K. McCubbin, *J. Mol. Spectrosc.*, **19** (1966) 137
- [51]. J. Davidsson, J. H. Gutow and R. N. Zare, *J. Phys. Chem.* , **94** (1990) 4069
- [52]. J. G. Lahaye, R. Vandenhoute, and A. Fayt, *J. Mol. Spectrosc.* **123** (1987) 48
- [53]. J. H. Gutow, J. Davidsson and R. N. Zare, *Chem. Phys. Lett.*, **185** (1991) 120
- [54]. J. M. Hollas, *Modern spectroscopy*, John Wiley and Sons, New York, (1990)
- [55]. J. Tyndall, *Proc. R. Soc. Lond.* , **31** (1881) 307

- [56]. J. Walrand, G. Blanquet, and C. P. Courtoy, *J. Mol. Spectrosc.*, **74** (1979) 165
- [57]. K. F. Luft, *Z. Tech. Phys.*, **24** (1943) 97
- [58]. K. K. Lehmann, G. J. Scherer and W. Klemperer, *J. Chem. Phys.*, **77** (1983) 2853
- [59]. K. V. Reddy and M. J. Berry, *Chem. Phys. Lett.*, **66** (1979) 223
- [60]. K. Veeken, N. Dam and J Reuss, *Infrared Phys.*, **25** (1985) 683
- [61]. L. B. Kreuzer, in *Optoacoustic Spectroscopy and Detection*, Yoh-Han Pao, Academic, New York, 1977
- [62]. L. B. Kreuzer, *J. Appl. Phys.*, **42** (1971) 2934
- [63]. L. D. G. Young, *ICARUS*, **17** (1972) 632
- [64]. L. D. Gray Young, *Appl. Opt.*, **10** (1971) 662
- [65]. L. D. Gray, R. A. Schorn, and E. Barker, *Appl. Opt.*, **8** (1969) 2087
- [66]. L. D. Gray, R. A. Schorn, and E. S. Barker, *Appl. Opt.*, **8** (1969) 241
- [67]. L. D. Gray, R. A. Schorn, E. S. Barker and A. Woszczyk, *Acta Astronomica*, **21** (1971) 329
- [68]. L. F. H. Bovey, *J. Chem. Phys.* **21** (1953) 830
- [69]. L. G. Rosengren, *Appl. Opt.*, **14** (1975) 1960
- [70]. L. G. Rosengren, *Infrared Phys.*, **13** (1973) 109
- [71]. L. J. Thomas III, M. J. Kelly and N. M. Amer, *Appl. Phys. Lett.*, **32** (1978) 736
- [72]. L. S. Masukidi, J. G. Lahaye, and A. Fayt, *J. Mol. Spectrosc.* **148** (1991) 281
- [73]. L. S. Masukidi, J. G. Lahaye, and A. Fayt, *J. Mol. Spectrosc.* **154** (1992) 137
- [74]. L. S. Rothman, R. L. Hawkins, R. B. Wattson, and R. R. Gamache, *J. Quant. Spectrosc. Radiat. Transfer*, **48** (1992) 537, and reference therein.
- [75]. L. S. Rothman, R. R. Gamache, A. Goldman, L. R. Brown, R. A. Toth, H. M. Pickett, R. L. Poynter, J.-M. Flaud, C. Camy-Peyret, A. Barbe, N.

- Husson, C. P. Rinsland, and m. A. H. Smith, *Appl. Opt.* , **26** (1987) 4058,
and references therein
- [76]. L. S. Rothman, R. R. Gamache, R. H. Tipping, C. P. Rinsland, M. A. H. Smith, D. C. Benner, V. M. Devi, J. M. Flaud, C. Camy-Peyret, A. Perrin, A. Goldman, S. T. Massie, L. R. Brown and R. A. Toth, *J. Quant. Spectrosc. Radiat. Transfer*, **48** (1992) 469
- [77]. M. E. Kellman, *J. Chem. Phys.* **93** (1990) 6630
- [78]. M. Huetz-Aubert, R. Tripodi, *J. Chem. Phys.*, **55** (1971) 5724
- [79]. M. L. Sage, Bond Mode, in Photoselective Chemistry, *Advances in Chemical physics, Volume XLVI*, John Wiley and Sons: New York, 1981 p293
- [80]. M. L. Viengerov, *Dokl. Akad. Nauk. SSSR* , **19** (1938) 678
- [81]. M. R. Da Silva, *Can. J. Phys.*, **64** (1986) 1098
- [82]. M. Sigrist, Environmental and Chemical Trace Gas Analysis by Photoacoustic Methods. In *Principles and Perspectives of Photothermal and Photoacoustic Phenomena*; Mandelis, A., Ed.; Elsevier: New York, 1992; Chapter III
- [83]. M. W. Sigrist, *J. Appl. Phys.*, **60** 7 (1986) R83
- [84]. M. Winnewiser, General discussion, *J. Chem. Soc. Farad. Trans. II*, **84** (1988) 1564
- [85]. N. Papineau and M. pealat, *Appl. Opt.*, **24** (1985) 3002
- [86]. N. Papineau and M. pealat, *J. Chem. Phys.*, **79** (1983) 5758
- [87]. P. F. Bartunek and E. F. Barker, *Phys. Rev.*, **48** (1935) 516
- [88]. P. F. Zittel and D. E. Masturzo, *J. Chem. Phys.*, **85** (1986) 4362
- [89]. P. Hess, *Topics in Curr. Chem.*, 111 (1983) 1
- [90]. P. L. Meyer and M. W. Sigrist, *Rev. Sci. Instrum.*, **61** (1990) 1779
- [91]. R. C. Herman, *Astrophys. J.*, **107** (1948) 386

- [92]. R. D. Cowan, G. Herzberg and S. P. Sinha, *J. Chem. Phys.* **18** (1950) 1538
- [93]. R. D. Kamm, *J. Appl. Phys.*, **47** (1976) 3550
- [94]. R. Schinke, V. Engel, P. Andresen, G. G. Balint-Kurti and D. Hauster, *Phys. Rev. Lett.*, **55** (1977) 111
- [95]. R. Tripodi, W. G. Vicenti, *J. Chem. Phys.*, **55** (1971) 2207
- [96]. R. V. Ambartzumian and V. S. Letokhov, Multiple Photon Infrared Laser Photochemistry, in Chemical and Biochemical Applications of Lasers, Vol. 3, C. B. Moore, Ed., Academic Press: New York, 1977
- [97]. S. Montero, *J. Chem. Phys.*, **79** (1983) 4091
- [98]. S. P. Sinha, *J. Chem. Phys.* **18** (1950) 217
- [99]. T. A. Holme and J. S. Hutchinson, *J. Chem. Phys.*, **84** (1986) 5455
- [100]. T. A. Holme, and J. S. Hutchinson, *Chem. Phys. Lett.* , **124** (1986) 181
- [101]. T. Dunham, in The Atmospheres of the Earth and Planets, G. P. Kuiper, Ed. University of Chicago Press, 2nd ed., (1952) Chap. XI
- [102]. T. F. Deaton, D. A. Depatie and T. W. Walker, *Appl. Phys. Lett.* , **26** (1975) 300
- [103]. T. F. Hunter and P. C. Turtle, in *Advances in Infrared and Raman Spectroscopy*, R. J. H. Clark, Vol. 7, Heyden, London, 1980
- [104]. T. L. Cottrell, J. C. McCoubrey, *Molecular Energy Transfer in Gases*, Butterworths, London, 1961
- [105]. V. P. Zharov and V. S. Letokhov, *Laser Photoacoustic Spectroscopy*. In *Springer Series in Optical Sciences*; Springer: Berlin, 1986, Vol. 37
- [106]. W. C. Roentgen, *Philos. Mag.* , **11** (1881) 308
- [107]. W. S. Adams and T. Dunham, *Publ. Astron. Soc. Pacific.*, **44**, (1932) 243
- [108]. X. Yang and C. Noda, in preparation
- [109]. X. Yang and C. Noda, *J. Phys. Chem.*, Submitted for publication
- [110]. X. Yang, C. Petrillo and C. Noda, *Chem. Phys. Lett.* , **214** (1993) 536

- [111]. Y. Garrabos, M. A. Echargui and F. Marsault-Herail, *J. Chem. Phys.*, **91**
(1989) 5869
- [112]. Z. Cihla and A. Chedin, *J. Mol. Spectrosc.*, **40** (1971) 337